TRANSITION METAL OXIDES SUPPORTED ON ACTIVATED CARBON FOR ADSORPTIVE DESULFURIZATION OF DIESEL FUELS

by

Thulisile Nombuso Nkomzwayo

submitted in accordance with the requirements for

the degree of

MASTER OF TECHNOLOGY

In

CHEMICAL ENGINEERING

at the

COLLEGE OF SCIENCE, ENGINEERING AND TECHNOLOGY

of

UNIVERSITY OF SOUTH AFRICA

SUPERVISOR:

Prof. Yali Yao

Co-SUPERVISOR

Prof. Diane Hildebrandt

Declaration

Name: ___Thulisile Nomuso Nkomzwayo_____

Student number: ___44565515_____

Degree: MTECH – Chemical Engineering_____

Exact wording of the title of the dissertation as appearing on the electronic copy submitted for examination:

TRANSITION METAL OXIDES SUPPORTED ON ACTIVATED CARBON FOR ADSORPTIVE DESULFURIZATION OF DIESEL FUELS

I declare that the above dissertation is my own work and that all the sources that I have used or quoted have been indicated and acknowledged by means of complete references.

I further declare that I submitted the dissertation to originality checking software and that it falls within the accepted requirements for originality.

I further declare that I have not previously submitted this work, or part of it, for examination at Unisa for another qualification or at any other higher education institution.

(The dissertation will not be examined unless this statement has been submitted.)

_____ __30 November 2020_____

SIGNATURE DATE

Dedication

Dedicated to:

To my amazing family, for their support throughout this journey.

And

In memory of my brother, Sihle Andy Ziqubu

Presentations and Publications

Conference Proceeding:

1. **T Nkomzwayo**, Y Yao, X Liu and D Hildebrandt, The deposition of metal oxides onto activated charcoal as a means of enhancing the reactive adsorption of thiophene compounds in diesel, International Workshop on Porous Materials and their Applications, CSIR Energy Centre conference, Council for Scientific and Industrial Research, Pretoria, South Africa, September 2018 (Oral Presentation).

2. **T Nkomzwayo**, Y Yao, X Liu and D Hildebrandt, The deposition of metal oxides onto activated charcoal as a means of enhancing the reactive adsorption of thiophene compounds in diesel, the Catalysis Society of South Africa (CATSA) conference Limpopo Province, South Africa, November 2018 (Oral Presentation).

3. **T Nkomzwayo**, Y Yao, X Liu and D Hildebrandt, Desulfurisation of model diesel via Zn and Cu oxides supported on activated carbon, the Catalysis Society of South Africa (CATSA) conference North West Province, South Africa, November 2017 (Poster Presentation).

4. Y Yao, **T Nkomzwayo**, Xinying Liu and Diane Hildebrandt, Desulfurization of diesel fuels using activated carbon loaded with different metal oxides, Advanced Nano and Energy Materials (ANEM) 2018, University of Western Australia, Perth, Australia, 12-14 December 2018.

5. Y Yao, **T Nkomzwayo**, L L Mguni, B Sempuga and Z Mthethwa, Gasification Char as a Potential Substitute of Activated Carbon in Adsorptive Desulfurization of Diesel Fuel, Advanced Energy Materials 2018 (AEM 2018), University of Surrey, Guildford, UK, 10-12 September 2018.

6. L Mguni, **T Nkomzwayo**, Y Yao, D Hildebrandt and D Glasser, Desulfurization of diesel fuels using metal oxide loaded activated charcoal and alumina, NULISTICE_2018 Conference and Expo, Maseru, Lesotho, 23-27 January, 2018.

Publications

1. L Mguni, Y Yao, **T Nkomzwayo**, Liu Xinying, Diane Hildebrandt, and David Glasser, Desulfurization of diesel fuels using intermediate Lewis acids loaded on activated charcoal and alumina, Chemical Engineering Communication, 2019, 206 (5), 572–580.

Acknowledgments

Firstly, I would like to convey sincere gratitude to everyone who contributed to the successful completion of this work. More importantly to the following individuals and institutions:

- To God Almighty, who makes all things possible through his grace and mercy.
- To my supervisors Prof. Yali Yao and Prof. Diane Hildebrandt for your invaluable guidance, continual support and patience.
- To Liberty Mguni my mentor, for always encouraging me to think beyond the norm.
- To Prof. Xinying Liu for his scientific contribution to this work, and instilling in me what it means to be a good researcher.
- To the staff member and my fellow colleagues in the Institute for the Development of Energy for African Sustainability (IDEAS), for helping in growing and developing my engineering and research skill.
- Special thank you to my family for all their support, motivation and belief in me.
- To the University of South Africa (UNISA) and National Research Foundation (NRF), in their funding of this work.

Abstract

In this study, period four transition metal oxides (Zn, Cr, Mn, Co, Fe, Cu, Ni), acting as intermediate Lewis acids, were supported on activated carbon (AC) and used in the adsorptive desulfurization (ADS) of model and commercial diesel in both batch-mode and fixed-bed applications. The Ni-oxide/AC had the highest desulfurization performance and removed 84.49 % of sulfur in model diesel and 95.17 % in commercial diesel at 30 °C. A trend in the ADS activity of period four transition metal oxides supported on AC was identified in both commercial and model diesel in the order of: Ni-oxide/AC > Cu-oxide/AC > Co-oxide/AC > Fe-oxide/AC > Mn-oxide/AC > Cr-oxide/AC > Zn-oxide/AC. The metal oxides/AC adsorbents had a higher selectivity for the sulfur compound, in the order of 4-E,6 -MDBT > 2,4,6 -TMDBT > 4,6-DMDBT, then the unmodified AC adsorbent.

There was no correlation between the Pearson hardness η metal oxide cation and the observed percentage of sulfur removal. However, a strong inverse linear relationship was observed sulfur removal decreased as the ionic covalent parameter (ICP) of the mixed metal oxide cations increased. Our findings suggested a novel concept in ADS of diesel fuel, i.e. that the ionic-covalent parameter (ICP) is a simple but more effective method of measuring the Lewis acidic strength of transition metal oxides. The adsorption kinetic of commercial diesel occurred via chemisorption in all the adsorbents used. Multi-component equilibrium isotherm modeling was used to identify how the competition interactions between sulfur compounds influenced the desulfurization performance. The results indicated that the incorporation of NiO onto AC significantly improved the synergistic interactions between the sulfur compounds and mitigated the competitive interaction between the more steric 4,6-DMDBT and 4-MDBT compounds.

Kinetic and thermodynamic process modeling suggested that adsorption occurred though chemisorption and became more favorable with an increase in temperature. Spent adsorbent analysis suggested that the high desulfurization performance of the $Ni_{(10\%)}O$/AC adsorbent was attributed to the increase in the adsorbents Lewis acidity upon loading with NiO, which led to an increase in Ni-S acid-base interactions, π-complexation interactions, and breakage in the aromatic rings of the sulfur compounds.

Keywords: adsorptive diesel desulfurization, period four transition metal oxides, activated carbon, Lewis acid strength, ionic-covalent parameter, multi-component isothermal modeling, synergistic adsorption

Table of Contents

Dedication ..... **II**

Presentations and Publications ..... **III**

Acknowledgments ..... **V**

Abstract ..... **VI**

Table of Contents ..... **VII**

List of Figures ..... **XI**

List of Tables ..... **XVI**

List of Abbreviations and Symbols ..... **XVIII**

Chapter 1: Introduction **1**

1.1 Background 1

1.2 Problem statement 2

1.3 Justification of the study 4

1.4 Key research questions 5

1.5 Research objectives 5

1.6 Thesis outline 6

Chapter 2: Literature Review **8**

2.1 Introduction 8

2.2 Developments in the hydrodesulfurization of diesel 9

2.3 Developments in oxidative desulfurization (ODS) of diesel 12

2.4 Developments in biological desulfurization of diesel 16

2.5 Developments in adsorptive desulfurization (ADS) 18

2.5.1 Application using AC and metal/metal oxide/AC composites 19

2.5.2 The π-complexation adsorbents 22

2.5.3 ADS of diesel using metal species and MOF 24

2.5.4 The effects of adsorbent acidity 26

2.6 Conclusion 28
Chapter 3: Experimental Procedure 29
3.1 Introduction 29
3.2 Materials 29
3.2.1 Diesel fuel 29
3.2.2 Adsorbent preparation 30
3.3 Adsorbent characterization 32
3.3.1 SEM/EDS analysis 32
3.3.2 HRTEM analysis 32
3.3.3. PXRD analysis 32
3.3.4 FTIR analysis 32
3.3.5 BET analysis 33
3.3.6 TGA/DTG analysis 33
3.3.7 Py-IR 33
3.4 Experimental Procedure 34
3.5 Treated diesel sulfur analysis 35
Chapter 4: Adsorptive desulfurization using period four transition metals oxide: A study of adsorbent Lewis acid strength derived from the metal oxide Ionic-Covalent Parameter ... 37
4.1 Introduction 37
4.2 Materials and methods 39
4.2.1 Adsorption procedure 39
4.2.2 Adsorption studies 40
4.3 Results and discussion 44
4.3.1 Adsorbent characterization 44
4.3.2 Adsorption evaluation of model diesel 56
4.3.3 Adsorption evaluation of commercial diesel 63
4.4 Conclusion 72

Chapter 5: An investigation into competitive adsorption in a multicomponent diesel system using Nickel Oxide /Activated Carbon 74

5.1 Introduction 74

5.2 Materials and methods 75

5.2.1 Adsorption procedure 76

5.2.2 Adsorption studies 76

5.3 Results and discussion 81

5.3.1 Adsorbent characterization 81

5.3.2 The effect of adsorbent metal loading 89

5.3.3 The effect of adsorbent dosage 90

5.3.4 The effect of adsorption temperature 91

5.3.5 A comparison of singular and multicomponent diesel ADS. 92

5.3.6 Multicomponent equilibrium isotherms 93

5.3.7 Adsorption kinetics 97

5.3.8 Adsorption thermodynamics 103

5.3.9 Analysis of spent adsorbents 105

5.4 Conclusion 106

Chapter 6: Conclusions and Recommendations 108

References 112

Appendices 131

A. Experimental design 131

A.1 Adsorbent metal loading 131

A.2 Experimental Layout Group 1: ADS of model and commercial diesel using AC loaded with metal oxides 131

A.3 Experimental Layout Group 2: ADS of model diesel carried out using highest performance metal oxide adsorbent. 133

B. Supplementary data: Chapter 4 137

C. Supplementary data: Chapter 5 141

List of Figures

Figure 1.1: Variations in sulfur specifications for diesel in different regions. Adopted from Reference [3] with the permission from Elsevier. 1

Figure 1.2: How HDS reaction rates decrease with an increase in the steric hindrance ability of sulfur compounds. Adopted from Reference [12] with the permission from Elsevier. 3

Figure 2.1: Various sulfur contaminants found in diesel. 9

Figure 2.2: Schematics of an HDS unit typically found in a refinery. Adopted from Reference [20] with the permission from John Wiley and Sons. 10

Figure 2.3: Schematic illustration of the sulfidation process of Mo_2Ni and $PMo_{11}Ni$ catalysts. Adopted from Reference [23] with the permission from Royal Society of Chemistry. 11

Figure 2.4: Illustration of the ODS process using a film-shear reactor. Adopted from Reference [2] with the permission from Elsevier. 13

Figure 2.5: Catalysis process of BF_3-CH_3COOH during sulfur oxidation using $K_2Cr_2O_7$. Adopted from Reference [44] with the permission from Elsevier. 15

Figure 2.6: Schematics of the aerobic pathways of DBT biodesulfurization. Adopted from Reference [48] with the permission from Elsevier. 17

Figure 2.7: The adsorption process using AC (the structure of AC was from [17]). 20

Figure 2.8: Adsorption mechanisms of DBT on MnO/AC adsorbent. Adopted from Reference [63] with the permission from Elsevier. 22

Figure 2.9: A π-complex formed between metal and π-electron cloud. Adopted from Reference [64] with the permission from Elsevier. 23

Figure 2.10: Thiophene molecules adsorbed via COP-27 MOF at a) cus-sites, and b) in the hexagonal unit channel of one unit. Adopted from Reference [73] with the permission from Royal Society of Chemistry. 25

Figure 2.11: Illustration on the adsorption of thiophene and benzene on Lewis and BrÖnsted acidic sites in HY zeolite. Adopted from Reference [78] with the permission from American Chemical Society. 27

Figure 3.1: GC-PFPD chromatogram of the sulfur content in commercial diesel used in this study 30

Figure 3.2: The synthesized metal oxide/AC adsorbents utilized in this study. 31

Figure 3.3: The a) batch mode and b) fixed-bed, experimental set-up used in this study. 34

Figure 4.1: The N_2 adsorption–desorption isotherms and resulting isotherm hysteresis loops obtained for AC loaded with metal (10 wt. %) oxides and unmodified AC…….....45

Figure 4.2: The PXRD patterns obtained for (a) AC, (b) Co-oxide/AC, (c) Cr-oxide/AC, (d) Cu-oxide/AC, (e) Fe-oxide/AC, (f) Mn-oxide/AC, (g) Ni-oxide/AC and (h) Zn-oxide/AC.. 47

Figure 4.3: TEM images and SAED patterns obtained for (a) AC, (b) Co-oxide or AC, (c) Cr-oxide or AC, (d) Cu-oxide or AC, (e) Fe-oxide or AC, (f) Mn-oxide or AC, (g) Ni-oxide or AC and (h) Zn-oxide or AC. 49

Figure 4.4: The SEM images and elemental mapping for (a) AC, (b) Co-oxide/AC, (c) Cr-oxide/AC, (d) Cu-oxide/AC, (e) Fe-oxide/AC, (f) Mn-oxide/AC, (g) Ni-oxide/AC and (h) Zn-oxide/AC. 51

Figure 4.5: The TGA/DTG plots observed for (a) AC, (b) Co-oxide/AC, (c) Cr-oxide/AC, (d) Cu-oxide/AC, (e) Fe-oxide/AC, (f) Mn-oxide/AC, (g) Ni-oxide/AC and (h) Zn-oxide/AC.. 53

Figure 4.6: The FTIR spectrum obtained for the metal oxide/AC adsorbents loaded with 10 wt. % metal. 54

Figure 4.7: The FT-IR spectrum obtained the metal oxide/AC adsorbents loaded after adsorption of pyridine in He, at 150 °C. 55

Figure 4.8: Experimental result curves showing how contact time affected the sulfur adsorption capacity of (a) DBT, (b) 4-MDBT and (c) 4,6-DMDBT, when using the various metal oxide/AC and unmodified AC adsorbents (10 wt. % metal loading, 30 g model diesel, 3 g adsorbent, at 30 °C for 3 hrs). 56

Figure 4.9: A comparison of the effect of temperature on total percentage sulfur removal at (a) 30 °C and (b) 60 °C desulfurization temperatures (10 wt. % metal loading, 30 g model diesel, 3 g adsorbent, for 3 hrs). 57

Figure 4.10: The effects of adsorbent Lewis acidity on sulfur removal performance in model diesel treated at high and low temperatures (10 wt. % metal loading, 30 g model diesel, 3 g adsorbent, for 3 hrs). 58

Figure 4.11: Linear relationship between percentage sulfur removal at (a) 30 °C and (b) 60 °C versus overall Pearson hardness (η), and (c) 30 °C and (d) 60 °C versus overall ionic-covalent parameter (ICP) of metal oxide cation (10 wt. % metal loading, 30 g model diesel, 3 g adsorbent, for 3 hrs). 62

Figure 4.12: A comparison of the reduction in concentrations of steric sulfur compounds (a) 4-MDBT, (b) 4,6-DMDBT, (c) 4-E,6-MDBT, (d) 1,4,6-TMDBT, (e) 2,4,6-TMDBT, (f) 3,4,6 –TMDBT (10wt. % metal loading, 30 g commercial diesel, 3 g adsorbent, at 30 °C for 3 hrs). 65

Figure 4.13: Comparison of the best fit straight lines for (a) pseudo-first order, (b) pseudo-second order (c) Elovich model, and (d) Weber–Morris plots obtained using metal oxide/AC adsorbents and unmodified AC (10 wt. % metal loading, 30 g commercial diesel, 3 g adsorbent, at 30 °C for 3 hrs). 68

Figure 4.14: Sulfur adsorption breakthrough curve of commercial diesel when using (a) unmodified AC, and (b) Ni-Oxide/AC adsorbents. Fitted model breakthrough curves of sulfur compounds in commercial diesel using (c) AC and (d) Ni-Oxide/AC. (10 wt. % metal loading, fuel LHSV of 0.31 h^{-1}, at ambient temperature for 7 hrs). 71

Figure 5.1: The N_2 adsorption-desorption isotherms obtained for unmodified AC and NiO/AC adsorbents with varying percentages of Ni loading……..... 82

Figure 5.2: The PXRD patterns of the $Ni_{(10\%)}O$/AC adsorbent..... 83

Figure 5.3: TEM images a) 50 nm, b) 100 nm and c) 5 nm and d) SAED pattern of the $Ni_{(10\%)}O$/AC adsorbent. 84

Figure 5.4: The a) SEM image, b) elemental mapping and c) EDS spectrum obtained for the $Ni_{(10\%)}O$/AC adsorbent. 85

Figure 5.5: The FT-IR spectrum of a) unmodified AC and the $Ni_{(10\%)}O$/AC adsorbent b) before and c) after calcination. 86

Figure 5.6: FTIR spectrum of pyridine adsorbed on a) $Ni_{(10\%)}O$/AC and b) unmodified AC , in He at 150 °C..... 87

Figure 5.7: The TGA/DTG plots observed for a) unmodified $Ni(CH_3CO_2)_2{\cdot}4H_2O$ and b) $Ni(CH_3CO_2)_2{\cdot}4H_2O$ loaded onto AC. 88

Figure 5.8: The effect of nickel loading on a) percentage sulfur removal and adsorption capacity of b) DBT c) 4-MDBT and d) 4,6-DMDBT (30 g model diesel: M1, 3 g adsorbent, at 30 °C for a 3 hrs duration). 90

Figure 5.9: The effect of $Ni_{(10\%)}O$/AC adsorbent dosage on desulfurization on a) percentage sulfur removal and adsorption amount of b) DBT c) 4-MDBT and d) 4,6-DMDBT (30 g model diesel: M1, at 30 °C for 3hrs)..... 91

Figure 5.10: A comparison of the effect of temperature on sulfur equilibrium adsorption capacity when a) AC and b) $Ni_{(10\%)}O$/AC adsorbents were used, and c) effect of temperature on total percentage sulfur removal (3 g adsorbent, 30 g model diesel M1)..... 92

Figure 5.11: A comparison of percentage sulfur removal performance of a) AC and b) $Ni_{(10\%)}O$/AC in the desulfurization of multicomponent (M1 and M2) and singular (M3,M4,M5) sulfur compounds model diesel (3 g adsorbent dosage, 30 g model diesel at 30 °C for 3 hrs).. 93

Figure 5.12: A comparison between the equilibrium isothermal results obtained through model prediction and experimental data for a) DBT, b) 4-MDBT, c) 4,6-DMDBT using unmodified AC adsorbent, and d) DBT, e) 4-MDBT f) 4,6-DMDBT using the $Ni_{(10\%)}O$/AC adsorbent. 95

Figure 5.13: Comparison of the best fit straight line (corresponding to the pseudo-first order model) versus experimental data at varying temperatures for a) DBT, b) 4-MDBT, c) 4,6-DMDBT using unmodified AC adsorbent, and d) DBT, e) 4-MDBT f) 4,6-DMDBT using the $Ni_{(10\%)}O$/AC adsorbent (3 g adsorbent and 30g model diesel M1). 98

Figure 5.14: Comparison of the best fit straight lines for pseudo-second order plots at varying temperatures for a) DBT, b) 4-MDBT, c) 4,6-DMDBT using unmodified AC adsorbent, and d) DBT, e) 4-MDBT f) 4,6-DMDBT using the $Ni_{(10\%)}O$/AC adsorbent (3 g adsorbent and 30 g model diesel M1)..... 100

Figure 5.15: Weber-Morris plots obtained at varying temperatures for a) DBT, b) 4-MDBT, c) 4,6-DMDBT using unmodified AC adsorbent, and d) DBT, e) 4-MDBT f) 4,6-DMDBT using the $Ni_{(10\%)}O$/AC adsorbent (3 g adsorbent and 30 g model diesel M1). 102

Figure 5.16: Arrhenius plots using pseudo-second order kinetic model constants using a) unmodified AC and b) $Ni_{(10\%)}O$/AC adsorbents (3 g adsorbent and 30 g model diesel M1). 103

Figure 5.17: Van't Hoff plots for sulfur compounds in model diesel M1 for a) unmodified AC and b) $Ni_{(10\%)}O$/AC. 104

Figure 5.18: FT-IR spectrum for a) $Ni_{(10\%)}O$/AC and b) AC, after adsorption experiments using (3 g adsorbent in 30 g of model diesel M2 at 30 °C). 106

Figure B.1: Lattice-fringe HRTEM images of obtained for (a) AC, (b) Co-oxide/AC, (c) Cr-oxide/AC, (d) Cu-oxide/AC, (e) Fe-oxide/AC, (f) Mn-oxide/AC, (g) Ni-oxide/AC and (h) Zn-oxide/AC……137

Figure B.2: The elemental analysis and EDS spectrum obtained for (a) AC, (b) Co-oxide/AC, (c) Cr-oxide/AC, (d) Cu-oxide/AC, (e) Fe-oxide/AC, (f) Mn-oxide/AC, (g) Ni-oxide/AC and (h) Zn-oxide/AC..... 138

List of Tables

Table 3.1: The composition of various model diesel used in this study. 30

Table 4.1: BET parameters obtained from N_2 physisorption.……...……44

Table 4.2: The composition, oxidation state, electronegativity, Pearson hardness parameter and ICP of adsorbents used in this study. 59

Table 4.3: Equilibrium adsorbent selectivity of metal-oxide/AC and AC adsorbents in ADS of commercial diesel, with 2,6/3,6-DMDBT as a reference compound. 66

Table 4.4: Kinetic parameters obtained for desulfurization of commercial diesel using various adsorbent at 30 °C. 69

Table 4.5: Parameters obtained for the breakthrough models using AC and Ni-oxide/AC adsorbents (10 wt. % metal loading, fuel LHSV of 0.31 h^{-1}, at ambient temperature and pressure for 7 hrs)..... 72

Table 5.1: BET parameters obtained from N_2 physisorption.……81

Table 5.2: Results of R^2 and error values obtained from the non-linear regression analysis of multiple component isotherm models when $Ni_{(10\%)}O$/AC and unmodified AC were used (model diesel M2 at 30°C). 96

Table 5.3: Equilibrium parameters obtained from the multiple component isotherm models when $Ni_{(10\%)}O$/AC and unmodified AC were used (model diesel M2 at 30°C). 96

Table 5.5: Thermodynamic parameters obtained in the ADS of 4,6-DMDBT, 4-MDBT and DBT using unmodified AC and the $Ni_{(10\%)}O$/AC adsorbent. 105

Table B.1: PXRD qualitative analysis results obtained for desulfurization adsorbents……139

Table B.2: Structural parameters of MeO/AC adsorbents. 139

Table B.3: The co-ordination number, spin state, ionic radius and atomic number corrective constant of the adsorbents used on this study. 140

Table C.1: Pseudo-first order parameters obtained for adsorption in model diesel M1 at varying temperatures…….141

Table C.2: Pseudo-second order kinetic parameters obtained for model diesel M1 adsorption at varying temperatures. 142

Table C.3: Intra-particle diffusion parameters obtained for adsorption using model diesel M1 at varying temperatures. 143

List of Abbreviations and Symbols

AC	Activated carbon
ADS	Adsorptive desulfurization
BET	Brunauer-Emmett-Teller
C	Constant related to the thickness of the boundary layer
$C_{ad,e}$	Concentration of sulfur adsorbed at equilibrium ($mg.kg^{-1}$)
C_b	Concentration of sulfur adsorbed at breakthrough ($mg.kg^{-1}$)
C_e	Concentration of sulfur in diesel at equilibrium ($mg.kg^{-1}$)
C_o	Concentration of sulfur initially in diesel ($mg.kg^{-1}$)
C_t	Concentration of sulfur in diesel at time, t ($mg.kg^{-1}$)
CN	Coordination number
CNT	Carbon nanotube
DBT	Dibenzothiophene
4,6-DMDBT	4, 6-Dimethyl-dibenzothiophene
1,4/1,6-DMDBT	1,4 or 1,6 -Dimethyl-dibenzothiophene
2,6/3,6-DMDBT	2,6 or 3,6 -Dimethyl-dibenzothiophene
E_a	Activation energy (kJ/mol)
4-EDBT	4-Ethyl-dibenzothiophene
4-E,6-MDBT	4-Ethyl, 6- methyl-dibenzothiophene
EF	Extended Freundlich isotherm model
EL	Extended Langmuir isotherm model
FTIR	Fourier Transform Infrared Spectroscopy

HSAB	Hard/soft acid/base
HDS	Hydro-desulfurization
ICP	Ionic-covalent parameter
k_f	Filtration rate constant (min^{-1})
k_i	Intra-particle diffusion rate constant ($mg.g^{-1}.min^{-0.5}$)
k_{Th}	Thomas rate constant ($ml.min^{-1}.mg^{-1}$)
k_{YN}	Yoon-Nelson rate constant (min^{-1})
k_1	Pseudo-first order rate constant (min^{-1})
k_2	Pseudo-second order rate constant ($g.mg^{-1}.min^{-1}$)
$K_{d,\ b}$	Adsorption distribution coefficient at fixed-bed breakthrough
$K_{d,\ e}$	Adsorption distribution coefficient at equilibrium
$K_{F,\ i}$	Freundlich constant of component i in single component model diesel ($mg.g^{-1}$)
$K_{L,\ i}$	Langmuir constant of component i in single component model diesel ($kg.mg^{-1}$)
L	Length of adsorbent bed (m)
M	Mass of adsorbent bed (g)
4-MDBT	4-Methyl-dibenzothiophene
NiO	Nickel oxide
ppmw	Parts per million weight
PXRD	Powder X-ray diffraction
Py-IR	Pyridine adsorption Fourier Transform Infrared Spectroscopy
Q	Diesel flowrate ($mL.min^{-1}$)
q_b	Amount of sulfur adsorbed per gram of adsorbent at breakthrough ($mg.g^{-1}$)

q_e	Amount of sulfur adsorbed per gram of adsorbent at equilibrium ($mg.g^{-1}$)
$q_{e,cal}$	Calculated amount of sulfur adsorbed per gram of adsorbent at equilibrium ($mg.g^{-1}$)
$q_{e,exp}$	Experimental amount of sulfur adsorbed per gram of adsorbent at equilibrium ($mg.g^{-1}$)
q_t	Amount of sulfur adsorbed per gram of adsorbent at time, t ($mg.g^{-1}$)
q_{Th}	Thomas maximum adsorption capacity ($mg.g^{-1}$)
q_{mi}	Adsorption capacity of component i in a binary model diesel ($mg.g^{-1}$)
q_{oi}	Adsorption capacity of component i in the single component model diesel ($mg.g^{-1}$)
r	Correlation coefficient
R	Universal gas constant (J/mol.K)
R^2	Squared regression correlation coefficient
r_i	Shannon ionic radius (Å)
R_{qi}	Ratio of adsorption capacities in singular and binary component model diesel
SEM/EDX	Scanning Electron Microscopy/Energy-dispersive X-ray spectroscopy
SRS	Sheindorf-Rebuhn-Sheintuch equation
SS	Spin state
SSE	Sum of squares error
t	Time (min)
T	Temperature (Kelvin)
TEM	Transmission electron microscopy
TGA/DTG	Thermogravimetric/Derivative thermogravimetry

1,4,6-TMDBT	1,4,6-Trimethyl-dibenzothiophene\
2,4,6-TMDBT	2,4,6-Trimethyl-dibenzothiophene
3,4,6-TMDBT	3,4,6-Trimethyl-dibenzothiophene
W	Mass of dry adsorbent (g)
wt %	Weight percentage
α	Corrective constant that is related to the atomic number
z	Oxidation state
η	Pearson cation hardness
τ	Time required to reach 50% linear breakthrough (min)
v	Advective velocity ($m.min^{-1}$)
χ	Electronegativity
ΔG	Change in Gibbs Free Energy ($kJ .mol^{-1}$)
ΔH	Change in Enthalpy ($kJ .mol^{-1}$)
ΔS	Change in Entropy ($kJ .mol^{-1}$)

Chapter 1

Introduction

1.1 Background

Sulfur compounds occur as natural contaminants in all primary fuel feedstock including natural gas, coal and crude oil. These sulfur compounds are released into the atmosphere as sulfurous oxides upon combustion [1]. Diesel is one of the most commonly used transportation fuels globally, while sulfur is the third most common element present in high concentrations in diesel. Combustion of the sulfur contaminants in diesel lead to the formation of sulfurous oxides (SO_x). In turn, these sulfurous oxides react with atmospheric moisture to produce sulfuric acid, which results in the formation acid-rain that is detrimental to natural eco-systems, and leads to the deformation of man-made structures. Additionally, long term exposure to SO_x gases can lead to respiratory failure in humans [2].

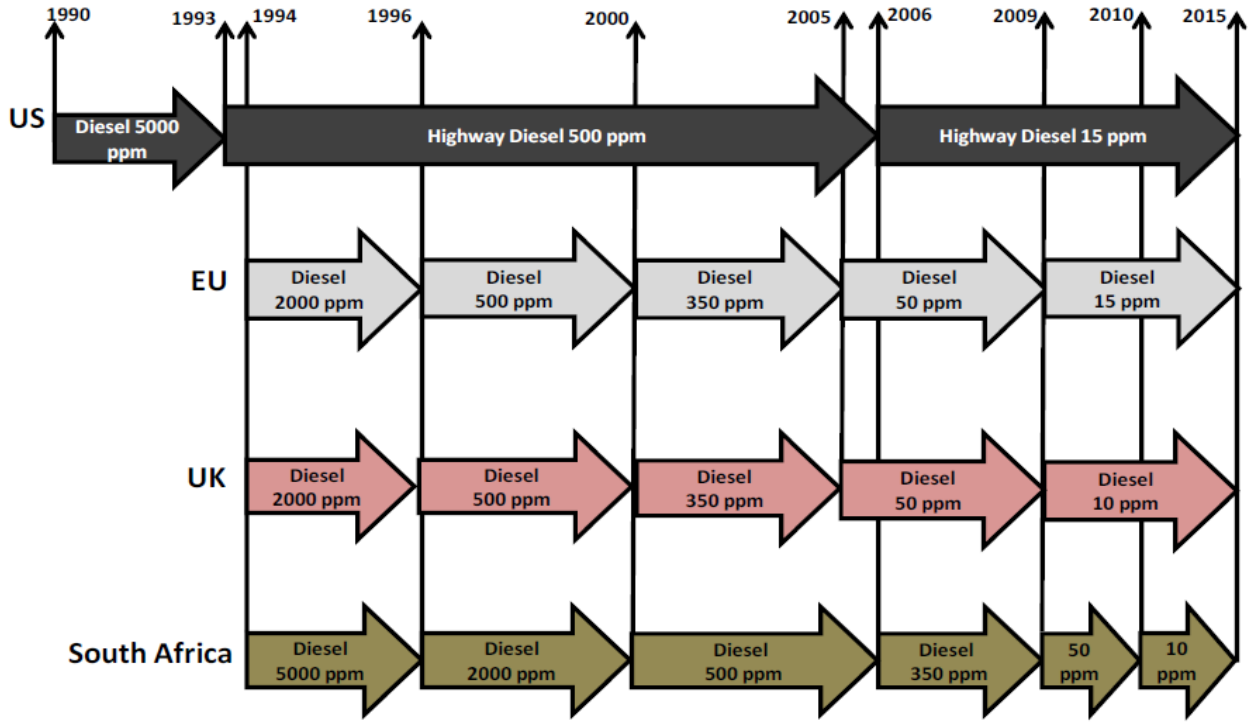

Figure 1.1: Variations in sulfur specifications for diesel in different regions. Adopted from Reference [3] with the permission from Elsevier.

Diesel combustion also leads to the emission of greenhouse gases, such as carbon dioxide and nitrous oxides, which are major contributors to global warming [1]. Due to increased scrutiny and public concerns about climate change and global warming, stringent legislation has been implemented to govern the concentration of sulfur in transportation fuels. The Euro 6 specifications require that the sulfur content of refinery diesel should be reduced to ≤ 10 ppm by 2015 [4]. The trend in the legislated sulfur content of diesel in different regions around the world, including South Africa is shown in **Figure 1.1**. Previous legislation passed by the South African Department of Minerals and Energy stipulated that the sulfur content in diesel should be ≤ 50 ppm. However, in 2017 the Clean Fuels 2 standard was implemented, which reduced the maximum sulfur content to ≤ 10 ppm [5].

1.2 Problem statement

Although several desulfurization processes have been proposed for use in industry, hydro-desulfurization (HDS) is the conventional industrial process used to treat diesel to remove sulfur compounds [6]. The HDS process causes diesel to react with hydrogen in the presence of a metal catalyst, and converts organic sulfur compounds into hydrogen sulfide (H_2S). Although HDS is a mature technology, it has several shortcomings, such as the expenses related to ensuring the high temperature and pressure required for the reaction, and the need for large quantities of hydrogen gas. The HDS process can effectively remove non-heterocycles sulfur compounds (such as thiols and sulphides), however, due to stereo hindrance, the process is ineffective in removing refractory heterocycles, such as complex derivatives of thiophenes (see **Figure 1.2**) [7]. Therefore, there is a need for the development and uptake of alternative processes, such as adsorption, extraction, oxidation and bioprocessing, especially for small-scale desulfurization. Among these options, adsorptive desulfurization (ADS) is considered to be one of the most promising alternatives, as the ADS process can be carried out at ambient conditions, and requires substantially lower capital and operational costs [8]. Moreover, studies have shown that regeneration of the spent adsorbent can be carried out using cost-effective technologies [9, 10 ,11] .

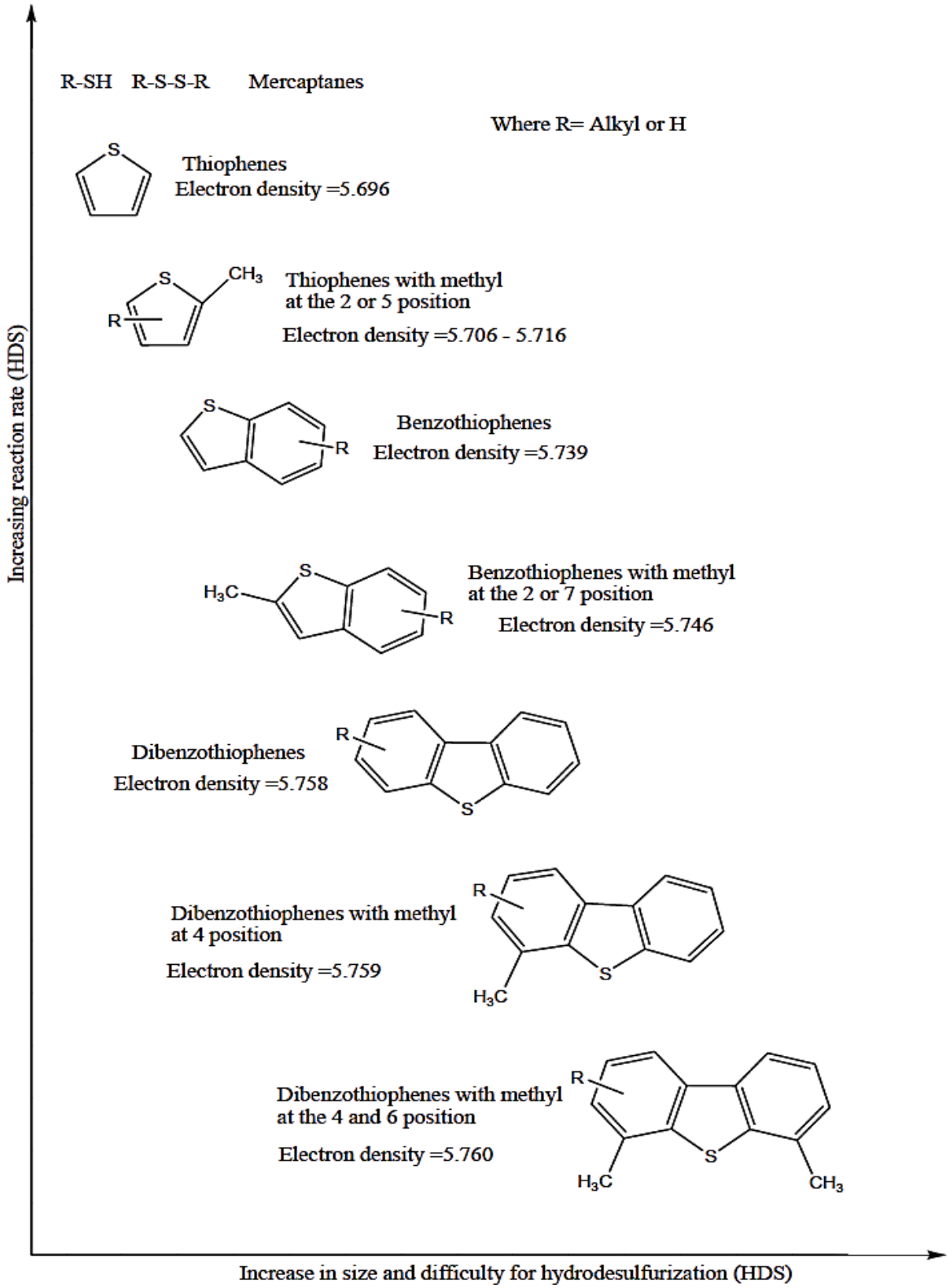

Figure 1.2: How HDS reaction rates decrease with an increase in the steric hindrance ability of sulfur compounds. Adopted from Reference [12] with the permission from Elsevier.

1.3 Justification of the study

Recently, numerous adsorbents with various physical and chemical properties have been developed, with the intention of studying their ability to remove sulfur compounds in fuels. Increasing attention is being given to carbon-based materials, such as activated carbon (AC) [13] and carbon nanotubes [7].

Increased consideration has been focused on AC because of its [1]: (1) high adsorption capacity; (2) large surface area that can be modified using a variety of chemical methods; (3) chemical and thermal stability; (4) low production cost which makes it economically suitable for large scale production processes; and (5) its broad structural variety. All these benefits make it ideal for use as an adsorbent for both gaseous and aromatic sulfur compounds.

The oxygen functional groups present on the AC surface significantly enhance the adsorption process. This is because their properties allow them to act as active centres that anchor catalyst precursors and metal ions [14]. When used in the synthesis of metal oxide composites, the AC acts as both metal oxide support, and active catalyst. The deposition of metal oxides onto the surface of carbon material enables sulfur compounds to be effectively captured via chemisorption, as metal-sulfur and π-electron interactions occur, which increase the adsorbent's sulfur removal capacity and selectivity [15].

ADS is a promising and cost-effective technology for the selective removal of organic sulfur compounds in commercial diesel. However, most of the research done using metal/metal oxide/activated carbon composites has been based on ADS of model diesel fuels and the ADS performance of these adsorbents in commercial diesels and proposed mechanisms are not elucidated. Although the physical and chemical characteristics of adsorbents containing transition metal oxides supported on AC and their desulfurization potential have been individually studied, not much work has been done to elucidate how the addition of these metal oxides affects the competitive interactions between the refractory sulfur compounds in the diesel. Various studies [16, 17] have suggested that the Lewis acid properties of the period four transition metal oxides were responsible for their enhanced desulfurization capabilities. However, they did not indicate if there was a trend in the desulfurization performance of the metal oxides across the period and how it correlated to their Lewis acid properties.

1.4 Key research questions

The key research questions are:

- Can period four transition metal oxides supported by AC effectively remove sulfur compounds in both commercial and model diesel fuels?
- Can the sulfur selectivity and adsorption capacity of AC be improved by depositing these metal oxides onto its surface?
- How does the incorporation of transition metal oxides onto AC affect the competitive interaction between sulfur compounds and other aromatics?
- Is there a trend in the desulfurization activity of period four transition metal oxides loaded onto AC?
- In what way does the Lewis acidity of period four transition metal oxides influence their desulfurization capability?
- Is there a correlation between the ionic-covalent parameter (ICP) of metal oxides/AC adsorbent and their desulfurization ability?

1.5 Research objectives

With the aim of seeking a method that is both effective and economically viable in removing sulfur from both model and commercial diesel fuel, this study focused on period four transition metal oxides incorporated onto AC in the ADS of diesel. The specific research objectives were as follows:

- To synthesize Me-oxide/AC adsorbents and characterize their physicochemical properties and morphology before and after desulfurization.
- To conduct adsorption experiments using lab-scale batch and continuous methods to investigate the effects of operational conditions on the desulfurization efficiency for model and commercial diesel fuel.
- To fit experimental data into various adsorption models for Me-oxide/AC adsorbents and correlate the adsorption activity to Me-oxide properties.

1.6 Thesis outline

The thesis is structured into six chapters, as follows:

- **Chapter 1: Introduction**

This chapter introduces the research topic, and provides the problem statement, the justification for the research, and the research objectives.

- **Chapter 2: Literature review**

This chapter provides a comprehensive literature review of conventional desulfurization methods currently being used for sulfur removal in both model and commercial diesel.

- **Chapter 3: Experimental**

This chapter provides the details of the experimental set-up, the adsorbent synthesis methods used, the operational parameters and procedures, and the adsorbent characterization methods used.

- **Chapter 4: Adsorptive desulfurization using period four transition metal oxides: A study of adsorbent Lewis acid strength derived from the cation Ionic-Covalent Parameter**

This chapter details the investigation into the desulfurization activity of period four transition metal oxides loaded onto AC, and how their activity correlates to the ICP and Lewis acid strength of metal oxide. Additionally, it details the investigation into the adsorption kinetics and selectivity involved in the desulfurization of both model diesel (containing DBT, 4-MDBT and 4,6-DMDBT) and conventional diesel was carried out in batch and fixed-bed applications.

- **Chapter 5: Isothermal, kinetic and thermodynamic study on the adsorptive desulfurization of model diesel fuels using Nickel Oxide /Activated Carbon**

This chapter reports on the desulfurization of model diesel fuel containing DBT, 4-MDBT and 4,6-DMDBT that was carried out at different temperatures, using NiO/AC adsorbents with varying dosages and adsorbent metal loading. The investigation focused on using extended isotherms for multi-component systems and empirical kinetic and thermodynamic models to investigate how sulfur compound interactions, adsorption kinetics and adsorption thermodynamics are affected by loading NiO onto the AC adsorbent.

- **Chapter 6: Conclusion and Recommendations**

The results and findings of the research work presented in the thesis are summarized here, and recommendations for future studies are proposed.

Chapter 2

Literature Review

In this chapter, diesel desulfurization technologies were reviewed and discussed, with an emphasis on current trends in techniques and adsorbents being used in ADS of both model and commercial diesel.

2.1 Introduction

Crude oil deposits found around the world contain significant amounts of sulfur compounds, which combust to form sulfur oxides [17]. Due to favourable atmospheric conditions, these sulfur oxides interact with water vapour and form acid rain, which is detrimental to infrastructure, crops, forests and aquatic life. Also, the sulfur compounds cause damage to the catalytic converter found in diesel engines, and reduce fuel economic efficacy [1]. To date, obtaining low sulfur fuels has been a challenge in the petroleum refinery industry, as sulfur is the third most abundant element in fossil fuels, and it is found in high concentrations in crude petroleum [2]. The predominant sulfur compounds found in middle distillates are benzothiophenes (BT) and its alkyl derivatives, whereas diesel fractions contain DBT and alkyl derivatives of DBT [18, 19] . Sulfur contaminants commonly found in diesel and middle distillate fractions are shown in **Figure 2.1**.

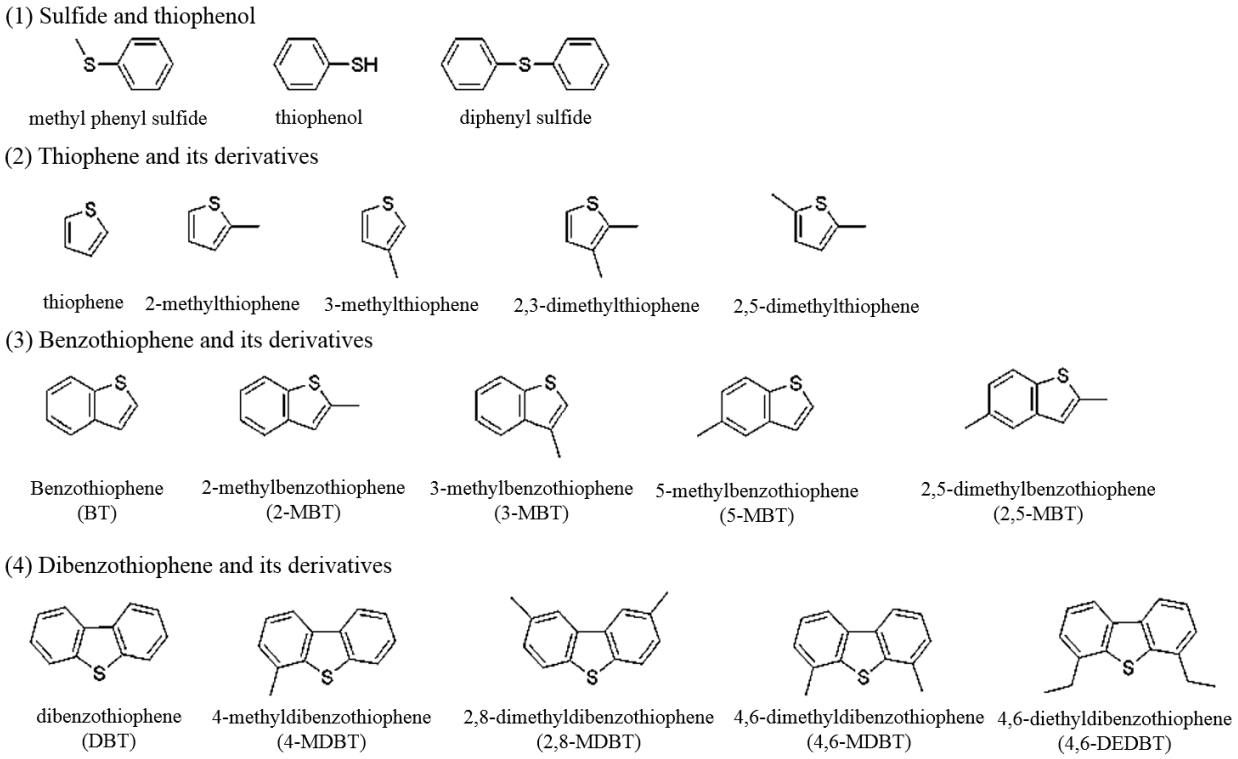

Figure 2.1: Various sulfur contaminants found in diesel [19].

2.2 Developments in the hydrodesulfurization of diesel

Hydrodesulfurization (HDS) is the conventional process used industrially to remove sulfur and nitrogen contaminants in petroleum fractions. These contaminants can be detrimental to the refinery process units and the catalyst, which has an adverse effect on product quality. During the process, the fuel feed is combined with hydrogen-rich gas, then it is preheated to temperatures varying from 260 °C to 427 °C (reactor inlet temperature). Typical HDS reactions are carried out at temperatures below 427 °C in fixed-bed reactors, so to mitigate fuel cracking. The oil and hydrogen were reacted over a metal oxide catalyst in the reactor to produce H_2S and other by-products (such as NH_3) [20]. The schematics of a typical HDS process is plotted in **Figure 2.2**. Cobalt and molybdenum (CoMo) supported on alumina supports are the most cost-effective catalysts for HDS, as they consume less hydrogen than other options, and the process is carried out at less severe operating conditions than the one using nickel-molybdenum catalyst. However,

if the removal of nitrogen is the main objective, Ni based catalysts consisting of nickel-cobalt-molybdenum or nickel-molybdenum are preferable [21].

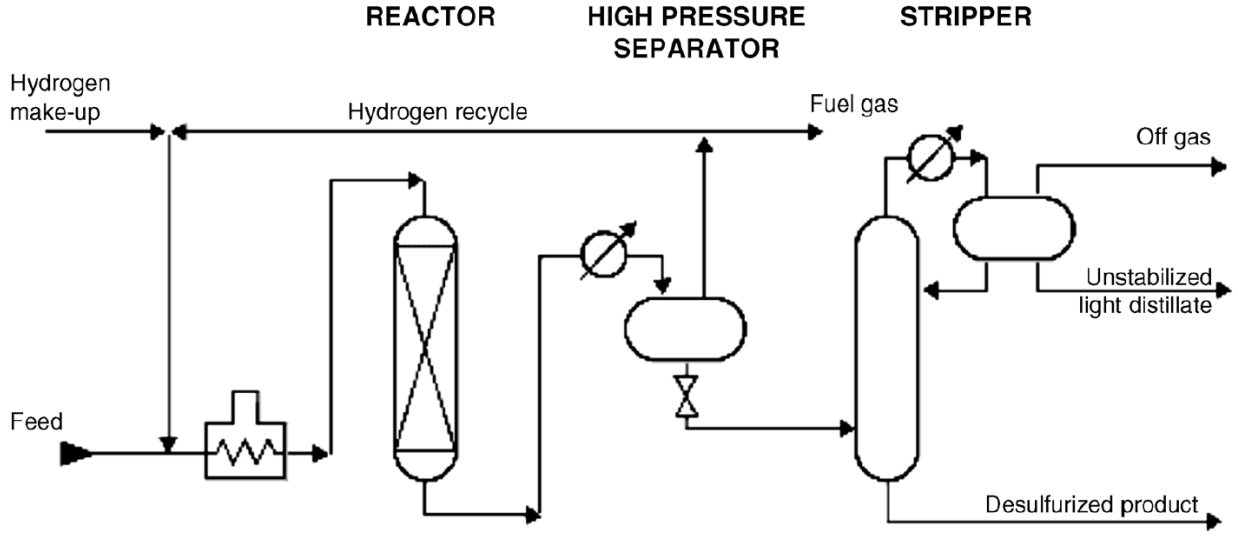

Figure 2.2: Schematics of an HDS unit typically found in a refinery. Adopted from Reference [20] with the permission from John Wiley and Sons.

Various HDS catalyst modifications have been studied and proposed to industry. For instance, a novel approach to synthesizing a highly active Ni/Mo/S catalyst for the desulfurization of dibenzothiophene was demonstrated [22]. The Ni/Mo/S catalysts were synthesized by sputtering, reactive gas aggregation and mass filtering, to modifying the orientation of the Ni/Mo/S catalysts into fullerene-like particles, flat-lying platelets and up-right oriented platelets. In doing so, different amounts of Ni/Mo/S active edge sites were obtained. The flat-lying platelets catalyst was twice as active as the fullerene-like catalyst, and the up-right oriented platelets showed six times higher activity than the fullerene-like catalyst [22]. Another example is to use crystalline polyoxometalates as a precursor in developing a Ni/Mo/S catalyst for the HDS of DBT [23]. Catalyst characterization showed that the use of the polyoxometalate led to direct active phase structural directing effects, which improved dispersion of the Ni/Mo/S and enhanced the HDS [23] (see **Figure 2.3)**. A third example is that of nickel supported using alumina and ZnO nanowires being used as a catalyst in HDS of diesel, kerosene and gasoline [24]. All three kinds of fuels contains approximately 200 ppm sulfur, and thiswas reduced to below 1 ppm, while the catalyst activity remained stable beyond a time on stream of 150 hours [24].

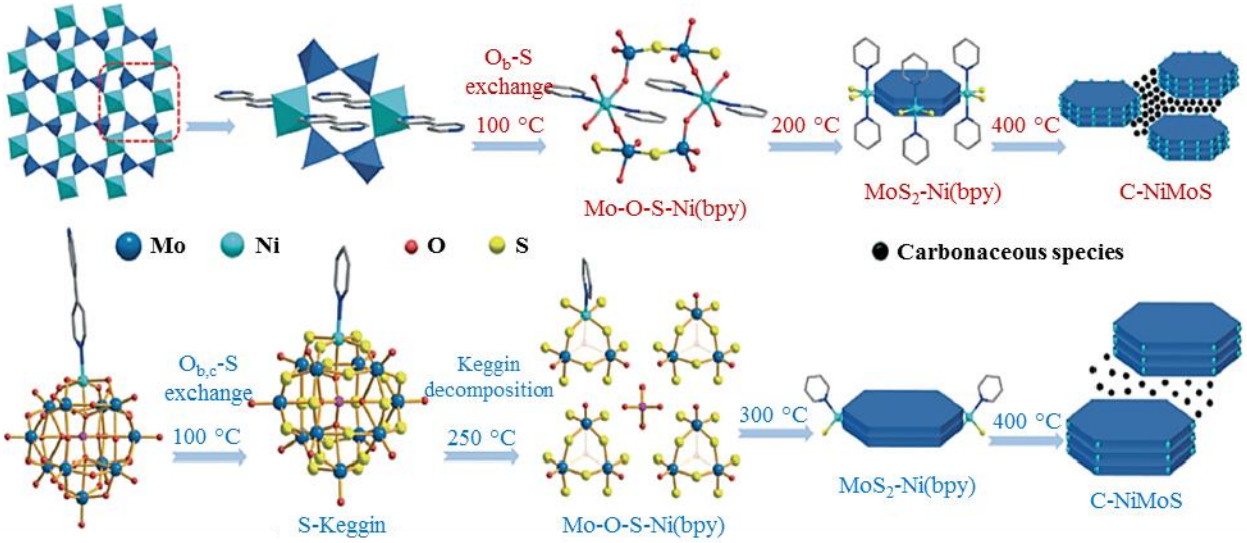

Figure 2.3: Schematic illustration of the sulfidation process of Mo_2Ni and $PMo_{11}Ni$ catalysts. Adopted from Reference [23] with the permission from Royal Society of Chemistry.

Another alternative is improving the design of the HDS process in order to overcome the low desulfurization activity seen with more steric thiophene compounds. For example, higher reactor reproducibility and a similar sulfur removal result to that obtained using a conventional fixed-bed reactor, was obtained when using a laboratory scale trickle-bed reactor loaded with a parallel single-pellet string commercial catalyst, under industrial HDS conditions [25]. DBT conversion and selectivity of 90 % and 80 %, respectively, were obtained using a micro trickle-bed reactor loaded with a Ni/Mo/S/γ-Al_2O_3 catalyst. The reaction was carried out at low temperature and hydrogen pressure conditions, similar to those used in reactive distillation. Moreover, the estimated activation energy obtained were substantially lower than previously reported when using conventional fixed-bed HDS [26]. It was found that the HDS of commercial diesel was more favourable when using a slurry reactor loaded with a Ni/Mo/S/Al_2O_3 catalyst, than when using a conventional fixed-bed reactor. This was due to: (1)even temperature distribution within the reactor; (2) online loading and removal of the catalyst; and (3) the higher catalyst efficiency obtained using the slurry bed system [27].

HDS is a well-established technology, however it has significant disadvantages, including high operational cost and the need for a large volume of feed gas. More importantly, HDS is ineffective in treating complex derivatives of thiophenes which are found in high concentrations in diesel [17].

2.3 Developments in oxidative desulfurization of diesel

Unlike HDS, hydrogen gas is not required in the oxidative desulfurization (ODS) process, and it is conducted at relatively mild operational conditions (101,325 kPa and 313-373 K). ODS of petroleum fuels results in the formation of highly polar sulfones and sulfoxides. The sulfones/sulfoxides are extracted from the oxidized fuels using polar solvents, such as methyl (or ethyl) alcohols and acetonitrile [28]. The liquid oxidant and polar solvent can be recovered from the liquid fuel using methods such as distillation or centrifugation [6].

Selection of a suitable oxidant is crucial in ensuring a high level of active oxygen while avoiding undesirable side reactions and products. Although various research studies have been conducted on ODS using a variety of oxidants (including, air, ozone, organic peroxides, nitrogen oxides and metal oxides), hydrogen peroxide (H_2O_2) has been found to be the most suitable option [7]. H_2O_2 is a powerful oxidizing agent but it is less corrosive than other organic peroxides, as it readily decomposes into oxygen and water in the presence of light, which makes it a more environmentally friendly alternative than the others. Moreover, the simple production methods used in manufacturing H_2O_2 and its world-wide commercial availability make it a good option for ODS [18]. In a study conducted using H_2O_2 and a formic acid catalyst, followed by fixed bed ADS using zeolite coated with carbon nanotubes to improve the zeolites adsorption capacity, ODS was found to be ideal in removing complex derivatives of thiophenes in diesel [7]. However, the authors deduced that ODS used as a stand-alone process has low efficacy in removing the derivatives of benzothiophene and DBT [7].

Numerous researchers have reported on experiments done utilizing O_2 as an oxidant in ODS of petroleum fuels, because of its abundance, cost effectiveness and environmental affability. Zhang et al. [29] obtained an oxidation reactivity of 4,6-DMDBT > DBT > BT in their work on the ODS of model fuel using an O_2 oxidant and carbon nanotubes (CNT) as a novel catalyst. Additionally, an increase in CNT graphitization led to increased catalyst activity, due to higher electric conductivity upon graphitization, which enhanced electron transfer occurring in the oxidation-

reduction reaction [29]. In another ODS study, 92 % oxidation conversion of DBT in tridecane was obtained using O_2 in the presence of carbon fibre-supported iron phthalocyanine, as the incorporation of carbon fibre drastically improved the iron phthalocyanine catalyst activity and enhanced catalyst regeneration [30]. Murata et al. [31] examined the ODS of model and commercial diesel using an O_2/aldehyde oxidant and cobalt salts (chloride or acetate) as the catalysts. In addition, Rao et al. [32] used an oxygen/aldehyde oxidant in the absence of a metal catalyst followed by solvent extraction in the ODS of model diesel and diesel that had previously been treated using HDS. The results obtained showed a reduction in diesel sulfur concentrations from 448 to 77 ppm [32].

Other studies have looked at drastically reducing the reaction time of the ODS process by using ultrasound and film-shear reactors instead of conventional stirring. For example, Fox [19] reported that the same desulfurization capacity obtained from hours of stirring at elevated temperatures could be achieved within minutes at below room temperature when using a film-shear reactor (see **Figure 2.4)**. Similarly, Cheng [18] used a modified ultrasound-assisted film-shear system and reported a desulfurization efficiency of 99 % for three sulfidation cycles. The incorporation of ultrasound significantly reduced reaction time in ultrasound-assisted ODS of commercial diesel [33].

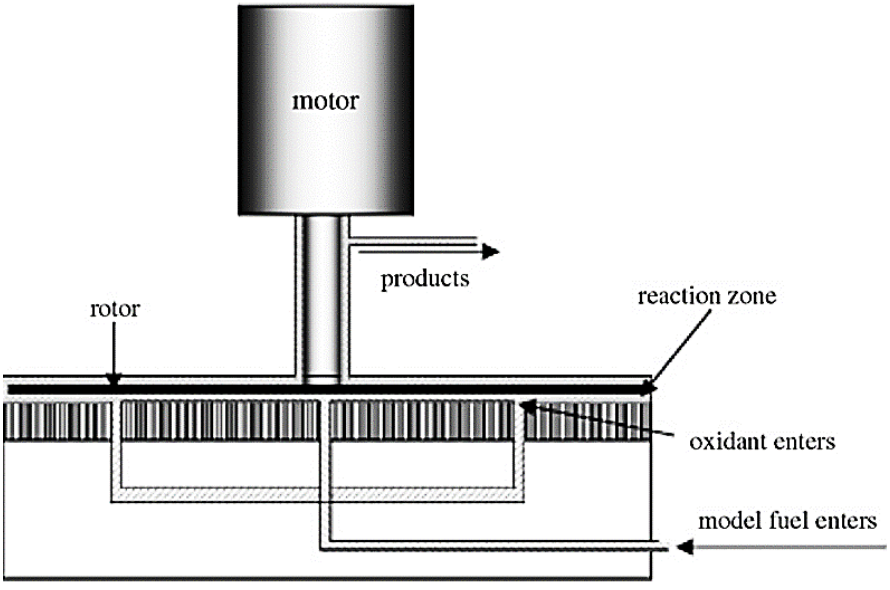

Figure 2.4: Illustration of the ODS process using a film-shear reactor. Adopted from Reference [2] with the permission from Elsevier.

Various studies done on ODS using catalysts that contain transition metals have been reported [34, 35]. One study reported a 97 % removal of the total sulfur in light cycle oil, in ODS using a $MoO_3/SiO_2/Al_2O_3$ catalyst [34]. Azelee et al. [35] obtained 99.5 % and 100 % removal of 4,6-DMDBT and DBT respectively, using a $WO_3/MoO_3/Al_2O_3$ catalyst in their study on ODS using alumina-supported catalysts of Mo, Mn, Fe, Co, Sn and Zn doped with W, Ti and V. The results showed that, the type of catalyst used has little influence on the overall reaction. However, the ODS rate was predominately influenced by the other oxidizable compounds in the diesel, particularly the alkyl-aromatics, which contain sulfur heterocycles, alkyl-aromatics and nitrogen heterocycles [36]. Another study used polymer supported oxidovanadium(IV) catalysts and molecularly-imprinted polymers to remove sulfones in the ODS of model diesel containing thiophene, benzothiophene, DBT and 4,6-DMDBT [3]. Ma et al. [37] used diesel fuel with a similar composition of thiophene, benzothiophene, DBT and 4,6-DMDBT, and achieved a 99 % total sulfur removal within a 30 minutes reaction period, at ambient temperature and pressure, and using ozone in conjunction with an alumina-supported cobalt oxide catalyst followed by extraction using commercial ILs.

The ODS of organic sulfur compounds using the polyoxometalate catalysts of Mo, W and V has also been investigated [38, 39]. The total concentration of sulfur in diesel decreased from 0.86 % to 0.2 % when ODS of diesel containing, thiols, and sulphides was conducted using a bi-phase system with H_2O_2 as an oxidant and vanadium oxodiperoxocomplexes as catalysts, where the sulfur content of the diesel remained relatively constant at 0.22 % after four oxidation-recycling cycles [38]. Trakarnpruk and colleagues investigated, the ODS of gas oils using Mo and W polyoxometalate as a catalyst, and achieved sulfur removal of up to 90 % and 98 % [39, 40]. Another study achieved 75.3 % within 45 minutes at 70 ºC and atmospheric pressure in ODS when using a molybdenum peroxocomplex/acetone catalyst [41]. Sulfur removal was achieved when using an amphiphilic peroxovanadium polyoxometalate catalyst and O_2 at ambient pressure in the ODS of DBT in decalin [42].

ODS using less conventional approaches have also been reported. Filippis and Scarsella [43], examined ODS of BT, DBT and diphenyl sulfide using an unconventional peroxycarboxylic acid functionalized-hexagonal mesoporous silica solid oxidant. They obtained a 99.9 % conversion of DBT and DPS within 30 minutes, and sulfur conversion of > 90 % within 2 hours [43]. Another

study investigated the ODS mechanism using solid oxidants ($K_2Cr_2O_7$ and $KMnO_4$) in a Lewis–Brönsted complex acid (BF_3-CH_3COOH) system (see **Figure 2.5)**. The authors deduced that Lewis acidity caused an increase in the Brönsted acidity of the system, which promoted the dissolution of the solid oxidants, while acting as a catalyst that significantly enhanced the oxidation of organosulfur compounds in the model diesel [44].

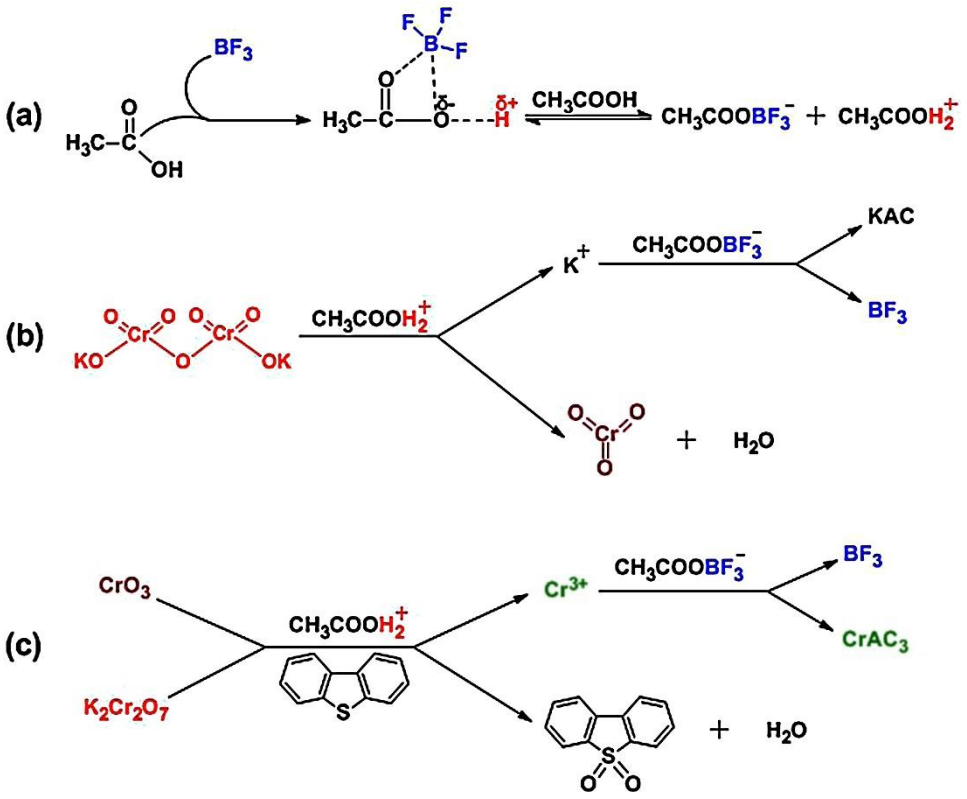

Figure 2.5: Catalysis process of BF_3-CH_3COOH during sulfur oxidation using $K_2Cr_2O_7$. Adopted from Reference [44] with the permission from Elsevier.

However, when ODS is done at an industrial scale, it is an expensive and complex process, because it requires the use of liquid oxidant reagents that are immiscible in petroleum fuels that contain sulfur compounds. This results in a biphasic system with traits that deviates from the ideal ODS system proposed in the literature. Moreover, ODS processes that use gaseous oxidants have a lower desulfurization efficiency and often require the incorporation of a catalyst and co-oxidants, which increases the extent of fuel loss during fuel product separation, and increases the operational cost of the process [31, 32]. Additionally, the ODS process is extremely hazardous, as it involves the utilization and the transportation of flammable oxidants [45].

2.4 Development in biological desulfurization of diesel

Biological desulfurization (BDS) of diesel using micro-organisms were conducted at ambient pressure and low temperatures [46]. During BDS, the microbial up-take of sulfur facilitates both growth and activity, and the process pathway can either be anaerobic or aerobic [47].This is illustrated in **Figure 2.6**. The advantages of using BDS is that the process utilizes microbes that are able to consume the sulfur present in diesel while retaining the structural integrity of the organic compound, without any undesirable side reactions and low emission of H_2S. Moreover, unlike other desulfurization technologies, the BDS process did not reduce the calorific value of diesel [48].

Various studies have reported on BDS using desulfurizing bacterium. For example, Wang et al. [49] investigated enhancing the DBT desulfurization capacity of the desulfurization-negative *Rhodococcus qingshengii* strain CW25, by transferring the enzyme promoters' dszAS1BC and dszABC into the CW25 strain. The results showed that in both the dszAS1BC and dszABC strains, DBT metabolic removal was highest in the early stages of BDS and then decreased to four times less than the average removal obtained using the initial cells. The maximum desulfurization activity obtained using the CW25-dszAS1BC strain was higher than with the CW25-dszABC strain: growth rates showed a stable increase of 13-fold and 7-fold for the CW25-dszAS1BC and CW25-dszABC strains, respectively. Moreover, gene manipulation did not lead to mutation of any microorganisms or promoters during BDS [49].

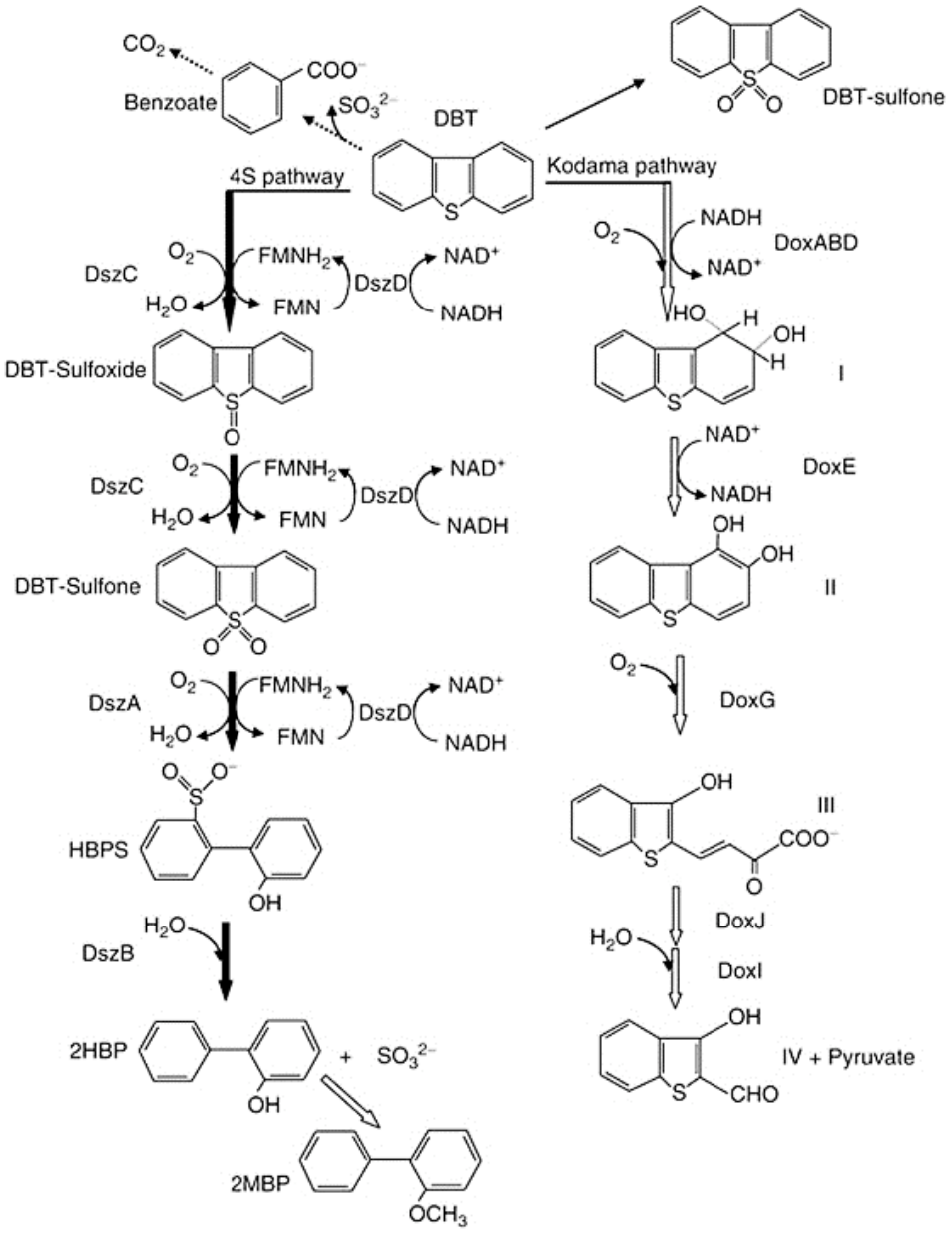

Figure 2.6: Schematics of the aerobic pathways of DBT biodesulfurization. Adopted from Reference [48] with the permission from Elsevier.

Similarly, Yu et al. [50] used *a Rhodococcus erythropolis* strain in the BDS of benzonaphthothiophene, and the metabolised post-desulfurization product was identified as α-hydroxy-β-phenyl-naphthalene. The results obtained showed sulfur removal of 94.5 % in model diesel, and 62.3 % in commercial diesel when using the resting cell biocatalyst at 30 °C for 24 and 72 hours, respectively [50]. Mukhopadhyaya and colleagues achieved 99 % sulfur conversion in

previously hydrodesulfurized commercial diesel using a *Rhodococcus sp*. strain loaded in a trickle-bed reactor [51]. Another study used desulfurizing bacterium *Desulfobacterium aniliniin* to remove thiophenic compounds in commercial diesel at atmospheric conditions [47]. The results of the study showed 82 % sulfur removal within the first 72 hours of BDS [47]. The feasibility of desulfurization through the integration of physical-biological procedures was also investigated [46]. Firstly, DBT was adsorbed in model diesel using π-complex adsorbents containing Ni^{2+}, Cu^{+} ,Ce^{3+}, Co^{2+} metal ions with subsequent regeneration of the adsorbents using a *Pseudomonas delafieldii* strain. The study results showed that the adsorbent containing Cu^{+} had the highest adsorption capacity and could be successfully bio-regenerated, where 85 % of the adsorbent's adsorption capacity retained after regeneration [46].

Although much research has focused on the implementation of BDS as a stand-alone process, it has been deemed economically unviable on an industrial scale, due to its various limitations. One example is the water/volume ratio, which leads to increased operational costs associated with the separation of the two mediums and the water handling and disposal. Another disadvantage of the BDS process is the slow transportation rate of sulfur compounds moving from the diesel phase into the cellular membrane of the micro-organism. Moreover, biocatalyst recovery and regeneration in the bioreactor is a complex process that needs to be researched further. More importantly, currently available biocatalysts have a low desulfurization activity rate, and the desulfurization rate would need to increase at least 500-fold, in order for it to be commercially viable. Furthermore, new developments need to focus on increasing the temperature tolerance of the micro-organisms, improving activity over extended periods, and increasing the stability in a biphasic desulfurization system that often contains toxic solvents [1, 48].

2.5 Developments in adsorptive desulfurization (ADS)

The process of adsorption is often used in the removal of unwanted contaminants in a fluid stream by passing the fluid through the adsorbents in a solid bed. The mechanisms of adsorption using solids are generally classified into two categories: physical (physisorption) and reactive (chemisorption). In physisorption, the adsorbate molecules adhere to the solid adsorbent via weak Van der Waal or electrostatic forces. The process is multi-layered, and not limited by the availability of adsorbent surface area. Physisorption is usually exothermic and reversible either by decreasing the process pressure or by increasing the temperature of the adsorbed fluid. In

contrast chemisorption, is governed by chemical reactions that occur between an adsorbate and a solid adsorbent [52]. The process is slower than physisorption and is limited by the formation of a single monomolecular adsorbate layer. Chemisorption usually involves the breaking of the covalent and ionic bonds, and requires activation energy. Therefore, process reversal require high energy input [1].

In terms of process economics, a high-efficacy desulfurization adsorbent should enable the removal of sulfur to concentrations below 100 ppmv in liquid fuels, while maintaining its desulfurization properties after extended sulfidation-regeneration cycles. The required adsorbent properties can be summarized as follows [52]:

- It should have high sulfur removal selectivity, without any undesirable side reactions.
- Its sulfur loading capacity should be high, to reduce the size of the reactor and minimize operational cost.
- It should retain its structural integrity, mechanical stability and chemical properties even with multiple use.
- Regenerating the adsorbent should be simple and cost effective.

2.5.1 Applications using AC and metal/metal oxide/AC composites

AC is a carbonaceous material with structural and physiochemical properties similar to that of graphite, although its structure is not as ideally symmetrical. The typical structure of AC is shown in **Figure 2.7**. It contains predominantly micro-pores. The meso-pores and micro-pores present in the AC structure are a result of selective oxidation of the crystallites graphite layers. This leads to the formation of crevices and V-shaped pores [53]. AC has been used extensively as an adsorbent, a catalyst and a catalyst support. Oxygen functional groups are bonded onto the surface of AC. These groups can be either acidic (e.g. carboxyls, phenols and lactones) or basic (e.g. carbonyls and pyrones). These oxygen groups act as anchors for precursors and the resulting nanoparticles, which allow the functionalization of AC using a wide range of nanoparticles. Moreover, the functional groups found on the AC surface have an anchoring ability which prevents leaching of the active sites during the adsorption process [54]. In addition to the simple modification of its structural and surface chemistry properties, AC also has unique properties, such as: inertness;

easier reduction of precursors; resistance to acid and base degrading; low production costs [53, 55].

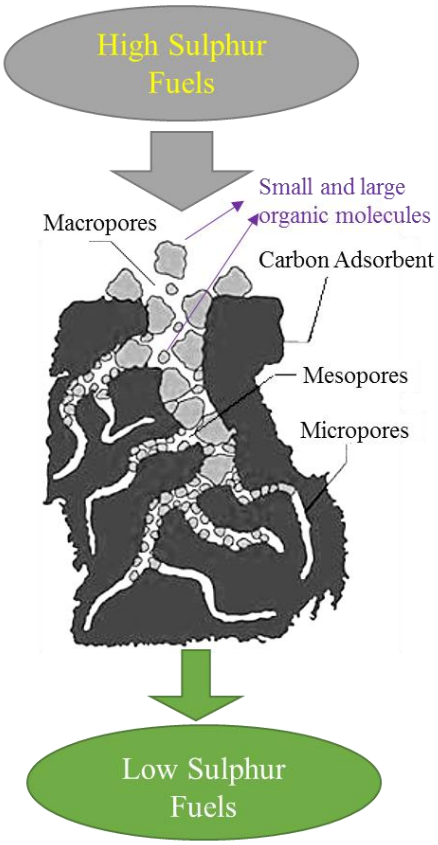

Figure 2.7: The adsorption process using AC (the structure of AC was from [17]).

Numerous studies have been carried out using AC in the desulfurization of commercial and model petroleum fuels [56]. Previous research suggests that, in desulfurization using pure AC the predominant sulfur removal mechanism is physical adsorption. Velu et al. [57] proposed that "sense and grab" and "sense and shoot" mechanisms occurred during ADS of model diesel containing 4,6-DMDBT. They deduced that the "sense and grab" mechanisms governs ADS when using AC supported adsorbents, and that the adsorbents physically grabbed the 4,6-DMDBT, but no chemical reaction occurs. In contrast, when Muzic et al. [58] compared the ADS capabilities of 13X-zeolite and AC in commercial diesel, they found that chemical interactions limit the rate of adsorption, where adsorption kinetics best correlated to the pseudo-second order model.

In their work on fixed bed adsorption of model diesel, Kim et al. [59] found that AC had a higher adsorption capacity and selectivity for both sulfur and nitrogen heterocycles, particularly for the

larger 4,6-DMDBT compound, which contains a methyl moiety. However, in a study on ADS of model diesel containing 4,6 –DMDBT and DBT using AC derived from dates' stones loaded with $ZnCl_2$, Bamufleh [13] observed that steric hindrances lead to the lower adsorption capacity of 4,6-DMDBT. In another study, 90 % sulfur removal was obtained using a lab-scale fixed-bed process in the ADS of commercial diesel using commercial AC [60]. However, upscaling by a factor of 15 had an adverse effect on the breakthrough fuel amount [60]. Moreover, there was a noticeable decrease in the di- and polyaromatic compound concentration in the treated diesel, as well as gradual adsorbent degradation after each sulfidation cycle, due to pore blockage by residual hydrocarbon derivatives in the diesel [60]. Commercial ACs loaded with $PdCl_2$ were used in the model diesel containing benzothiophene and dibenzothiophene. The results showed that incorporating $PdCl_2$ onto the surface of ACs significantly enhanced their desulfurization capacity. It was deduced that the two factors that govern the adsorption capacity are: the direct interactions occurring between the sulfur -Pd^{2+}, π-Pd^{2+}; π-complex interactions occurring between the surface of AC and thiophenic aromatic rings [61].

Another study on ADS of model diesel using polymer-derived activated carbon loaded with Fe and varying amounts of Cu reported that although the addition of Fe and Cu oxides enhances the selective removal of both 4,6-DMDBT and DBT, the volume of adsorbent micropores was the main factor that governs the desulfurization capacity of the adsorbents [62]. Saleh et al. [63] conducted ADS of synthetic diesel using MnO loaded onto granular activated carbon produced from waste tyres. Based on the study results, they deduced that the oxygen functional groups and meso-pores present in the adsorbents induced the rapid uptake of the sulfur compounds during the initial adsorption stage. However, predominant adsorption mechanisms occurred via Lewis acid-base interactions of S-Mn, and π-complexation (see **Figure 2.8**).

Based on the reported results mentioned above, it can be concluded that AC has exceptional properties that make it an ideal adsorbent for the removal of organosulfur compounds in petroleum fuels. In a bid to enhance sulfur selectivity, researchers have focused on incorporating transition metal ions into AC, in order to increase both adsorption selectivity and capacity. However, the research work done using metal/metal oxide/AC composites has been based on ADS of model diesel fuel, but the desulfurization performance of these adsorbents in commercial diesels and the proposed mechanisms have not been explained.

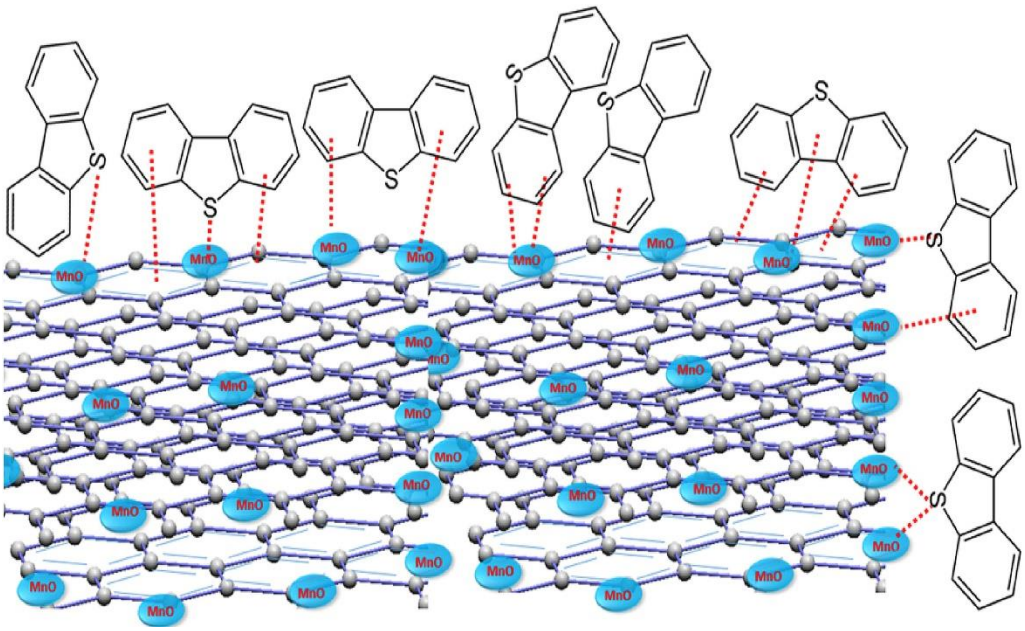

Figure 2.8: Adsorption mechanisms of DBT on MnO/AC adsorbent. Adopted from Reference [63] with the permission from Elsevier.

2.5.2 The π-complexation adsorbents

Some studies have focused on developing adsorbents that selectively adsorb organic sulfur molecules from petroleum fuels via π-complexation bonding interactions [64]. In general, a π-complex forms when a π–electron cloud bonds with a metal atom where the compound rich in π-electrons and metal species act as both electron acceptors and donors (see **Figure 2.9**). During π-complex formation in ADS, a simultaneous σ-bond occurs through overlapping of the π-orbitals of the aromatics sulfur compound and the empty outer s-orbitals of the adsorbent metal atom. The metal atom simultaneously donates electrons from its d-orbitals to the empty anti-bonding π-orbitals of the aromatics sulfur compounds, and makes up the π-component of the bond [64].

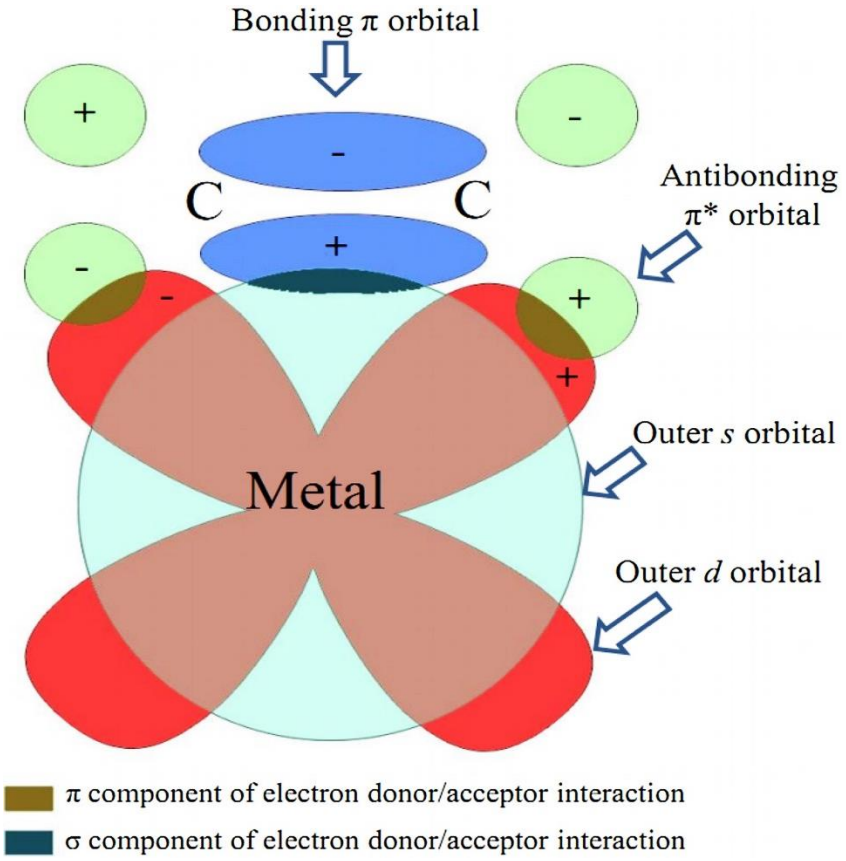

Figure 2.9: A π-complex formed between metal and π-electron cloud. Adopted from Reference [64] with the permission from Elsevier.

Khan et al. [65] used CuCl supported on AC (prepared via the mild reduction of $CuCl_2$) as an adsorbent in the ADS of model diesel containing benzothiophene. The study results showed that Cu supported AC had a faster adsorption rate and adsorbed around 30% more benzothiophene compared to unmodified AC [65]. This was attributed to π-complexation interactions between the benzothiophene and Cu^+ ions [65]. Similarly, Wang et al. [66] found that adsorbents with a π-complexation affinity had a higher adsorption capacity for thiophene, BT and DBT when using AC or π-complexation adsorbents Cu(I)–Y and $AgNO_3$/MCM-41. Another study looked at fixed-bed ADS of JP-5 fuel at ambient conditions using the π-complexation adsorbents CuCl and $PdCl_2$ supported on SBA-15 and MCM-41 [67]. The highest adsorption capacity was obtained with the $PdCl_2$/SBA-15 adsorbent, which had a noticeable breakthrough of approximately 50 ml treated fuel /g of adsorbent [67]. Similarly, Herna'nderz-Maldonado et al. [68] used a CuCl/γ-Al_2O_3 π-complex adsorbent in the fixed-bed ADS of commercial jet fuel and diesel. They found that although the Cu(I)Y-zeolite had a higher sulfur adsorption capacity than CuCl/γ-Al_2O_3, it easily

lost its π-complexation ability and stability through oxidation by moisture and fuel additives which converted it into Cu(II)Y.

Although notable progress has been made in developing π-complexation adsorbents for ADS of model fuels, several shortcomings remain when using these adsorbents in commercial fuels. The presence of aromatics such as toluene have adverse effects on ADS activity [66]. Strong π-complexation reactions occur between the adsorbents and the nitrogen heterocycles present in diesel in high concentrations, which greatly diminishes sulfur compound selectivity. Moreover, π-complex adsorbents such as Cu(I)Y sorbent lose their selectivity for sulfur compounds once they are oxidized, and high moisture levels and additives (e.g. oxygenates) found in fuels quickly deactivate the adsorbents [68].

2.5.3 ADS of diesel using metal species and MOF

It has been reported that the CNT support plays a significant role in increasing the amount of active sites and maintaining the activity of the titania, while inhibiting agglomeration in the ADS of model fuel oil, when using titania-doped CNT in a batch system [69]. Batch ADS of commercial kerosene and diesel was conducted using montmorollonite clay impregnated with metal species Ni, Cr, Fe, Ag, Pb, Mn and Zn. The results showed that loading Zn significantly increased the pore size, while also enhancing the surface area of the montmorollonite clay, which led to a higher adsorbent desulfurization capacity [70]. Other researchers have focused on using metal organic frameworks (MOF) in the selective removal of sulfur in petroleum fuels [71-73]. When using MOF, predominate ADS interactions occur through π-complexation; however, metal - S bond coordination with unsaturated coordination sites of transition metals (e.g. Zn^{2+}, Co^{2+}, Cu^{2+}, Ni^{2+}, and Cu^{+}) has also been reported [71]. Peralta et al. [72] screened various MOF in batch ADS of model diesel. They found that CPO-27-Ni and HKUST-1 MOF with unsaturated coordination sites had the highest desulfurization performance. However, the presence of the nitrogen-containing compound (pyridine) had an adverse effect on sulfur adsorption. Van de Voorde and his co-workers investigated the ADS of model diesel using CPO-27 MOF containing either Ni, Co, Mg, Cu, or Zn [73] (see **Figure 2.10**). The study results indicated that the sort of metal ion used had a direct influence on the adsorbent's selectivity and adsorption capacity, where the outstanding ADS performance of CPO-27-Ni adsorbent was attributed to strong sulfur–Ni interaction [73].

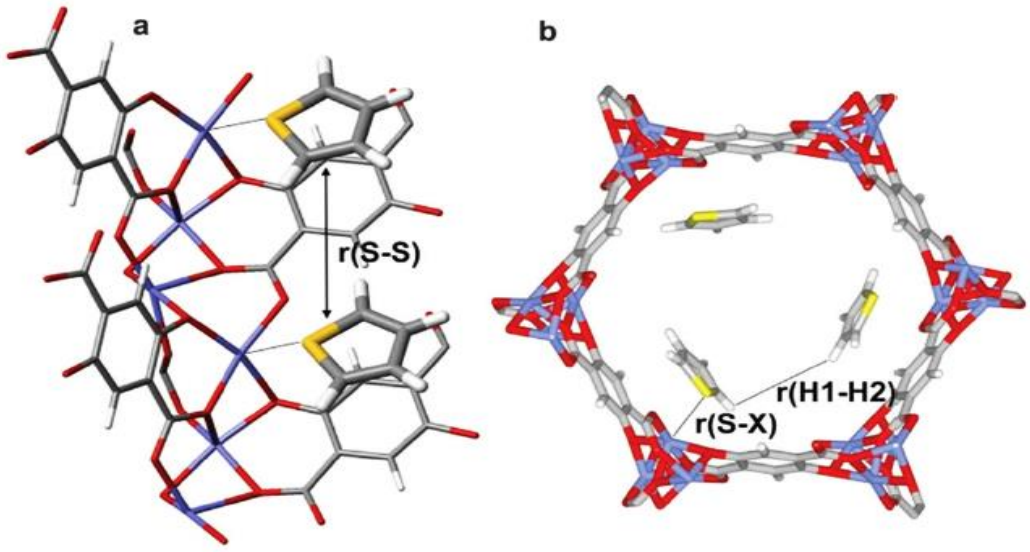

Figure 2.10: Thiophene molecules adsorbed via COP-27 MOF at a) cus-sites, and b) in the hexagonal unit channel of one unit. Adopted from Reference [73] with the permission from Royal Society of Chemistry.

Another study investigated the use of BDC MOF (containing metallic species of Cr, Al, and V, separately) loaded with $CuCl_2$ in the ADS of BT in toluene [74]. Only the V-BDC was oxidized by $CuCl_2$ under ambient conditions, which led to the formation of Cu^+ cations involved in π-complexation interaction and the subsequent higher desulfurization performance of the $CuCl_2$/V-BDC adsorbent [74]. Zhang and co-workers [75] studied the ADS of model diesel using BTC and BDC MOFs loaded with Cr and Cu at low temperatures. They deduced that the adsorption mechanism in MOF occurred through a combination of factors including exposed Lewis acid site coordination with the sulfur compound, pore size, pore shape and framework structure [75]. Han et al. [76] found that when compared with CPO-27-Ni MOF and HKUST-1 MOF, QUST-82 MOF had a relatively high adsorption capacity for DBT, and was an ideal adsorbent for removing both nitrogen and sulfur species in isooctane.

Based on the reported work above, it can be suggested that the use of metal species in ADS leads to an increase in sulfur removal activity, and promotes the selectivity of these sulfur compounds in diesel that contains aromatic compounds. However synthesis of MOF requires a bulk volume of solvents, a high reaction temperature, and an extended reaction time, along with a low yield in the final MOF product [77]. Therefore, the feasibility of using MOF in large-scale industrial desulfurization applications is yet to be established.

2.5.4 The effects of adsorbent acidity

It has been generally accepted that intermediate-soft sulfur compounds could form acid-base complexes with intermediate-soft Lewis acid sites (e.g. Co^{2+}, Ni^{2+}, Cu^{2+} and Zn^{2+}), in accordance with Pearson's hard-soft acid-base (HSAB) theory [76]. Lison [17] used polymer-derived AC's individually loaded with Fe, Cu, Ni, Co and Ag, and investigated their performance on ADS of 4,6-DMDBT and DBT in model diesel. Adsorbents with high Lewis acidic strength showed a higher selectivity for 4,6-DMDBT than that for DBT, due to the higher basicity strength of 4,6-DMDBT. Similarly, AC and Y-zeolite loaded with Ag^{+}, Ni^{2+}, Zn^{2+}, Cu^{2+}, and Fe^{3+} was used in the ADS of model diesel containing the soft Lewis bases, BT and DBT [16]. It was deduced that: the higher adsorption capacity of the Ag/AC adsorbents could be attributed to the Lewis acidity softness of the Ag^{+} ions; and the low adsorption capacity Y-zeolite adsorbents was due to the Na^{+} cation which is a hard Lewis acid [16].

In contrast, Liao and co-workers did a study on ADS model diesel using acid treated HY zeolite [78]. They deduced that the adsorption of thiophene on Lewis acid sites was hindered by competitive interactions with benzene which also has a high affinity for adsorption on Lewis acid sites [78, 79]. However, stronger bond interactions occur between thiophene selectively adsorbed on the BrÖnsted acid site via H-S bonds, but this leads to thiophene oligomerization as BrÖnsted acidity strength increases (see **Figure 2.11**). Therefore: adsorbents with soft to intermediate Lewis acidity should be used in fuel containing low aromatic concentrations; adsorbents with low strength BrÖnsted acid sites should be used in fuel containing high concentrations of aromatics [78].

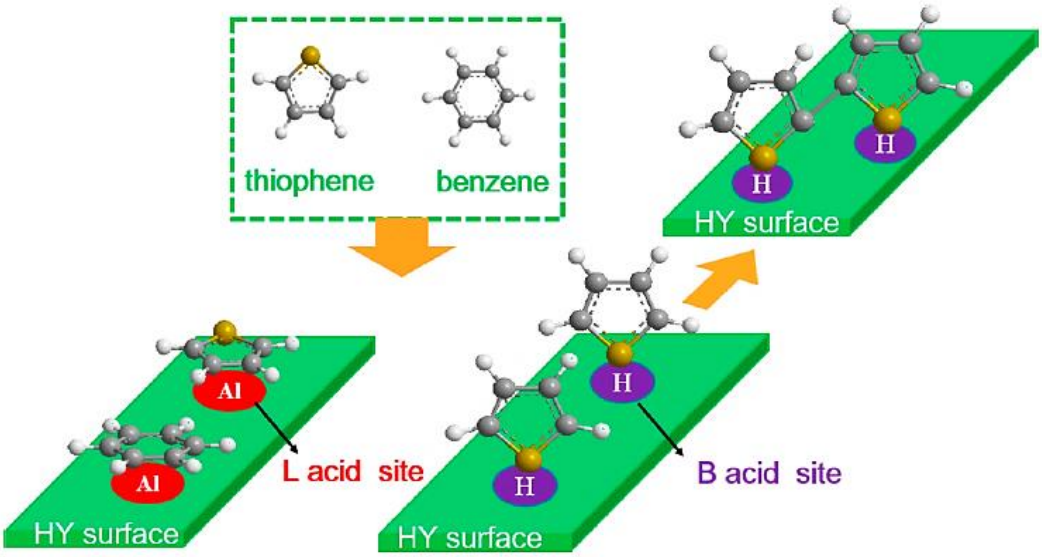

Figure 2.11: Illustration on the adsorption of thiophene and benzene on Lewis and BrÖnsted acidic sites in HY zeolite. Adopted from Reference [78] with the permission from American Chemical Society.

Pearson's HSAB theory is also applicable in the acid treatment of AC as a means of increasing the functional group concentration in AC, and subsequently increasing desulfurization performance. A study done on the desulfurization of model diesel using AC treated with either HNO_3 or NaOH showed that the uptake of DBT, benzothiophene and thiophene using AC treated with HNO_3 was approximately 2.2, 3.4 and 3.8 times higher, respectively, than that of unmodified AC at 90 °C [80]. Shah and colleagues obtain 99.5 % removal of DBT in model fuel and 74.29 % sulfur removal in commercial diesel using AC treated with acetic acid at 60°C in stirred-tank batch mode [81]. The amount of acidic functional groups presents in AC (namely carboxyl groups) played a significant role in the batch-mode ADS of model diesel containing 4,6-DMDBT. However, the addition of polycyclic aromatic compounds led to a noticeable decrease in the adsorption of 4,6-DMDBT due to competitive adsorption interactions [82].

Although the effects of adsorbent acidity on desulfurization performance and the selectivity of sulfur compounds have been reported, the findings are contradictory, particularly in terms of adsorbents containing metallic species. Some researchers argue that adsorbent Lewis acidity is responsible for ADS [83], while others deduced that adsorption occurs on the BrÖnsted acid sites [84, 85]. Pearson's HSAB theory is widely accepted as the basis of ADS occurring through Lewis

acid-base interactions when using adsorbents containing transition metal species, with numerous studies having looked at ADS using period four intermediate-soft Lewis acids. However no definitive trend has been identified that correlates the Lewis acid strength of metal ions to their desulfurization performance.

2.6 Conclusion

In this chapter the different techniques used in the desulfurization of both model and commercial diesel fuel have been reviewed. The focus was on ADS and the limitations of each technology were highlighted. The use of various adsorbents in ADS of diesel were reviewed, i.e. adsorbents containing AC and metal/metal oxide/AC composites, π-complexation and acidic adsorbents. The development of cost-effective adsorbents with high sulfur compound selectivity is still a major challenge in ADS. An in-depth investigation is required into the competitive adsorption interactions occurring between sulfur compounds and other heterocycles in diesel. AC, and particularly composites of AC containing transition metal species have demonstrated superior desulfurization capabilities and selectivity for organic sulfur compounds in diesel and other petroleum fuels. The superior ADS performance of these adsorbents has been largely attributed to their acidic properties. However, in order to compliment Pearson's HSAB theory, an extensive study is required on how the Lewis acid strength of transition metal ions relates to their desulfurization performance. In addition, the effects of adsorbent Lewis acidity on adsorption kinetics and mechanisms needs to be fully elucidated.

Chapter 3

Experimental Procedure

3.1 Introduction

In this study, ADS of both commercial diesel and model diesel fuel was carried out using commercial AC impregnated with period four transition metal oxides (Zn-oxide, Cr-oxide, Mn-oxide, Co-oxide, Fe-oxide, Cu-oxide, Ni-oxide). The sulfur removal capability of the synthesized adsorbents was studied using both batch and fixed-bed modes. The experimental conditions were varied, i.e. model diesel composition, temperature, metal loading, and adsorbent dosage. In this chapter, we provide a detailed account of the materials, characterization, analysis techniques and experimental procedures used.

3.2 Materials

3.2.1 Diesel fuel

The sulfur compounds selected for model diesel synthesis, 4,6-DMDBT (97 %), 4-MDBT (97%) and DBT (> 99%), were an adequate representative of the sulfur compounds commonly found in commercial diesels. Hexadecane, or a combination of hexadecane (99 %) 85 vol % and toluene (99.9 %) 15 vol %, was used as an organic solvent. All chemical reagents were used as received without any further modification at commercial grades supplied by Sigma-Aldrich (South Africa). The compositions of the model diesel samples used throughout the study are listed in **Table.3.1**. The commercial diesel utilized in this study was sourced from a local gas station in Johannesburg, Gauteng. GC-PFPD analysis (see **Figure 3.1**) showed that the diesel contained 520.33 ppmw sulfur consisting of 20 compounds namely, 4-MDBT, 4-EDBT, 4,6-DMDBT, 2,6 / 3,6-DMDBT, 1,4 / 1,6-DMDBT, 4-E,6-DMDBT, 2,4,6-TMDBT, 1,4,6-TMDBT, 3,4,6-TMDBT as well as C4DBT/C5DBT (heavier DBTs with more than 4 total carbons in its alkyl groups.

Table 3.1: The composition of various model diesel used in this study.

Model Diesel	Organic solvent (vol %)		Sulfur content (ppmw S)		
	n-Hexadecane	Toluene	4,6-DMDBT	4-MDBT	DBT
M1	85	15	300	100	100
M2	100	-	300	100	100
M3	100	-	-	-	100
M4	100	-	-	100	-
M5	100	-	300	-	-

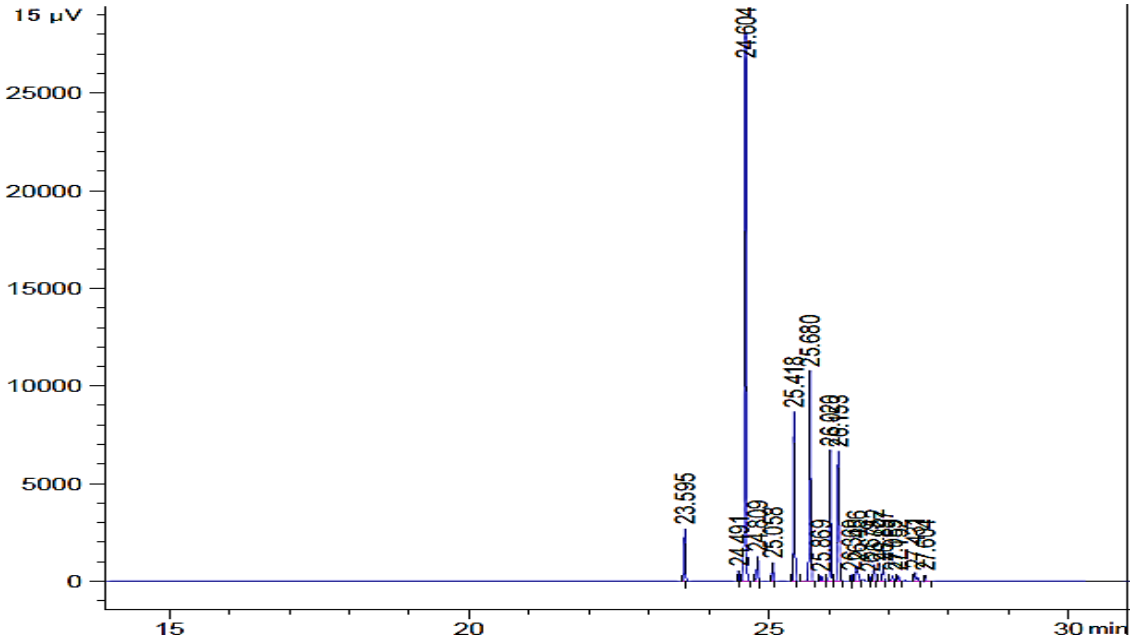

Figure 3.1: GC-PFPD chromatogram of the sulfur content in a commercial diesel used in this study.

3.2.2 Adsorbent preparation

The adsorbents used for desulfurization were prepared by using the incipient impregnation procedure given by [86], where predetermined stoichiometric amounts of metal species (2.5, 5, 10, 15 weight % metal) were loaded onto commercial AC (Merck). The as-synthesized adsorbents were prepared using metal acetate precursors, $Zn(CH_3CO_2)_2{\cdot}2H_2O$ (99.99 %), $Mn(CH_3CO_2)_2{\cdot}4H_2O$ (99.99 %), $Co(CH_3CO_2)_2{\cdot}4H_2O$ (≥ 98 %), $Cr_3(CH_3CO_2)_7{\cdot}(OH)_2$ (99.99 %), $Cu(CH_3CO_2)_2{\cdot}H_2O$ (≥ 98 %), $Ni(CH_3CO_2)_2{\cdot}4H_2O$ (98 %) and $Fe(CH_3CO_2)_2$ (95 %), which were dissolved at ambient conditions in the deionized water. The quantity of the deionized water used

was depend on the precursor's water solubility. The salt solutions were slowly stirred into AC. All metal acetate precursors were used as received at commercial grades supplied by Sigma-Aldrich (South Africa). An illustration of the calculation used to obtain the percentage metal loading is shown in **Appendix A.1**.

To obtain uniform distribution of the precursor onto the AC surface, the metal acetate/AC mixtures were ultrasonicated for 1 hour. The adsorbent was dried by an oven for 12 hours at 70 °C to remove any adsorbed atmospheric moisture. The adsorbents were then placed in a furnace and flushed overnight with nitrogen gas with a flow rate of 10 ml/min to remove oxygen gas in the furnace chamber, followed by calcination. Calcination was then carried out in the same N_2 atmosphere at a heating rate of 5 °C/min from 25 °C to 400 °C, were the temperature was kept constant for 30 minutes at 150 °C, 300 °C and 400 °C, respectively. Once the adsorbents had cooled, they were stored in a desiccator containing Drierite (10-20 mesh) to prevent the adsorption of atmospheric moisture. A visual of the metal oxide/AC adsorbents used in this work is shown in **Figure 3.2**.

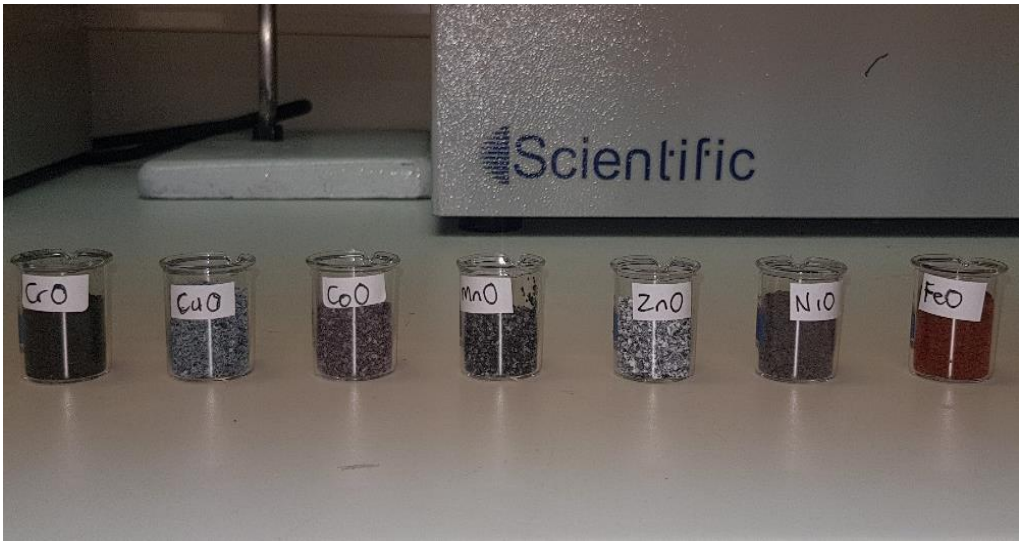

Figure 3.2: The synthesized metal oxide/AC adsorbents utilized in this study.

3.3 Adsorbent characterization

3.3.1 SEM/EDS analysis

Scanning electron microscopy (SEM, JEOL STM - IT300) equipped with Energy dispersive X-ray spectroscopy was used in investigating the morphology and elemental composition of each adsorbent. The instrument features include resolution HV mode of 3-15 nm (30 - 1 kV) and a magnification of × 5 to × 300 000. Before the SEM analysis, each adsorbent was mounted onto carbon tape fitted on a metal plate and coated with carbon film. Prior to the analysis, the SEM/EDS system was purged with N_2 gas to remove residual air and atmospheric moisture adsorbed on the sample. The analysis of each sample took approximately 45 minutes, where five images were taken of each sample.

3.3.2 HR-TEM analysis

High resolution transmission electron microscopy (HR-TEM, JEOL JEM-2010) coupled with Selected Area Electron Diffraction (SAED), was used to identify the crystal structures and arrangements, crystallite sizes, and examine crystal defects present in the metal oxide/AC adsorbents. The instruments features include an accelerating voltage of 200 kV, a point-to-point resolution of 0.19 nm and a maximum tilt angle of 25° goniometer.

3.3.3. PXRD analysis

Powder X-ray Diffraction (PXRD) was used to characterize and identify the crystal phases, atomic structure, and crystallite sizes present on the adsorbents. An X-Ray diffractometer (Rigaku SmartLab) instrument with a CuKα1 (1.5406 Å) x-ray source at 30 mA and 40 kV was used in continuous scanning mode ranging from $2\theta = 5°$ to 90° at an integral of 0.01° and a scan speed of 1 °/min. The crystal phases, atomic structure, and crystallite sizes were confirmed using Smartlab Studio II software with an ICDD database. The results of the crystallite size of the metal oxides were determined using the Williamson-Hall method. The weight percentages of the metal oxide species present in each adsorbent were quantified using the Reference Intensity Ratio method.

3.3.4 FTIR analysis

Fourier Transformer Infrared spectroscopy (FTIR) is one of the most common techniques utilized in identifying surface functional groups present in a given analyte. In this work, a Perkin-Elmer

Spectrum 65 instrument was utilized in identifying the surface functional groups of unmodified AC, the functional groups of metal acetate precursors impregnated AC before calcination, and the formation of metal oxides after calcination. In addition, the infrared spectrum of the sulfur compounds adsorbed after the desulfurization experiments were carried out. All the adsorbents were analyzed in powder form, with a sample loading of 0.5 g at ambient conditions using a 1 cm^{-1} step size for a spectra range of 400 cm^{-1} to 5000 cm^{-1}.

3.3.5 BET analysis

A Brunauer, Emmett and Teller (BET) instrument (Micromeritics Tristar II 3020) with an absolute pressure range of 0 to 950 mmHg and accuracy within 0.5 %, was used to determine the adsorbents pore volume, size distribution and surface area. Each adsorbent sample (≥ 0.2 g) was degassed at 120 ^oC overnight before the analysis. Thereafter, the adsorbents pore volume, the size distribution, surface area and the adsorption-desorption isotherms of N_2 at 77.2 K were measured. Silica alumina was used as a reference material, where analysis of each adsorbent sample lasted for approximately 7 hours.

3.3.6 TGA/DTG analysis

The adsorbents thermal degradation was determined using Thermogravimetric / Derivative thermogravimetry (TGA/DTG) analysis (TA Instruments TGA 5500). The instrument is equipped with a dual input gas-delivery manifold, temperature precision of ±0.1 °C and TRIOS software. Samples were loaded as synthesized at 0.5 g. Analysis was carried on both the adsorbents utilized in the study and metal acetate precursors, at a heating rate of 10 ^oC/min under a constant N_2 atmosphere and temperature ranging from 50 °C to 900 ^oC.

3.3.7 Py-IR

The adsorbents acidic characteristics were analyzed using pyridine-FTIR method. Where, the adsorbents were firstly heated at 110 °C for 6 hours to remove any residual atmospheric moisture. The adsorbents were then saturated with pyridine; where physically adsorbed pyridine was removed through a constant flow of helium at 30 ml/min and 150 °C for 1 hour in a tube furnace [87, 88]. The Lewis and Brönsted acid sites in each adsorbent were then identified using FT-IR (Perkin-Elmer, Spectrum 65). All the adsorbents were analyzed in powder form, with a sample

loading of 0.5 g at ambient conditions using a 1 cm^{-1} step size for a spectra range of 400 cm^{-1} to 5000 cm^{-1}.

3.4 Experimental Procedure

The ADS experiments carried out were set up in two groups. In the first set of experiments (Group 1), the batch mode ADS of model diesel M1 and a commercial diesel was carried out at high (60 °C) and low (30 °C) temperatures, using a stirring speed of 1200 rpm for 3 hours, using unmodified AC and AC loaded with metal oxides (Ni-oxide, Cu-oxide, Fe-oxide, Zn-oxide, Co-oxide, Mn-oxide, Cr-oxide). The effects of adsorbent Lewis acidity, contact time and adsorption kinetics and adsorbent selectivity were investigated. Finally, fixed bed desulfurization experiment of diesel were carried out using unmodified AC and metal oxide/AC. This was done in order to compare how incorporating these metal oxides affected the breakthrough and saturation points of steric sulfur compounds in the commercial diesel.

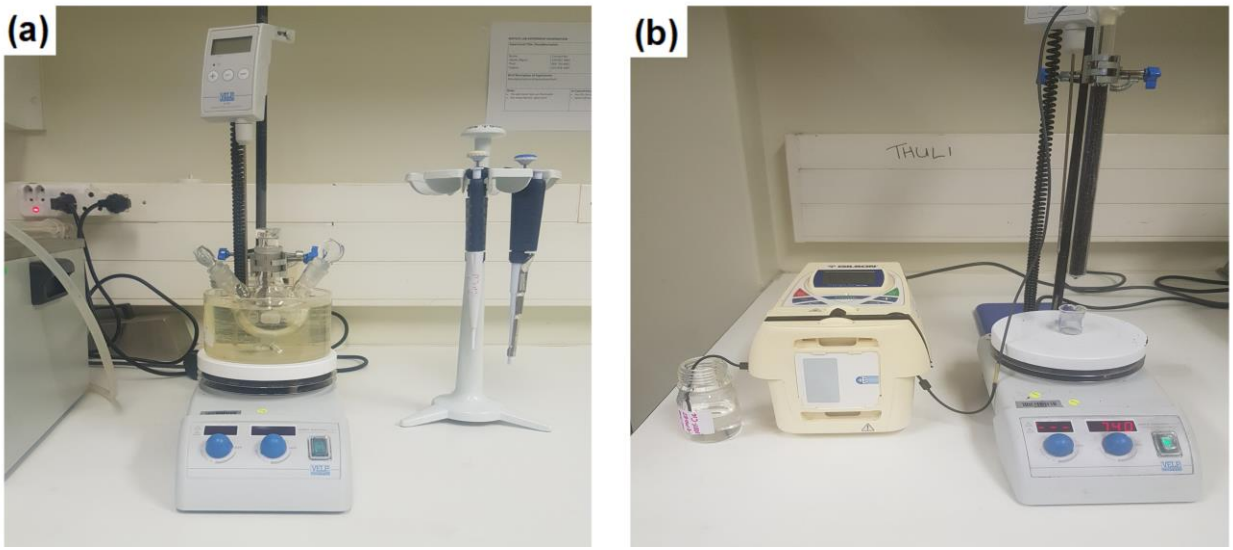

Figure 3.3: experimental set-up used in this study: a) batch mode; b) fixed-bed mode.

The second set of the ADS experiments (Group 2) was carried out using the metal oxide/AC adsorbent that showed the highest desulfurization performance in the previous Group 1 experiments. The adsorption procedures were conducted in batch mode using the model diesel samples (M1, M2, M3, M4 and M5 in Table 3.1), at process temperatures ranging between 30 °C

to 75 °C, and a stirring speed of 1200 rpm. The experiments were grouped into the sections of: (1) investigating the adsorption multicomponent mechanisms, kinetics and thermodynamics; (2) studying the effects of the metal loading, the adsorbent dosage, and the operating temperature. The experimental set-up used for batch and fixed-bed modes is shown in **Figure 3.3**. The detailed layout of Group 1 and Group 2 experiments is provided in **Appendix A.2** and **Appendix A.3**, respectively. All experiments were repeated twice to confirm reproducibility. To ensure the data accuracy, the GC analysis for each of the treated samples was repeated 3 times, and the average peak areas of each sample was used for the calculation of the adsorption capacity.

3.5 Treated diesel sulfur analysis

The quantity and type of sulfur species present in the diesel was identified using gas chromatography (GC, Agilent A7890B), equipped with a Pulsed Flame Photometric Detector (PFPD) which can be used to identify and quantify the sulfur compounds. The instrument calibration using an internal standard was conducted routinely before each set of experiments. The temperature condition used in the GC were as follows: the temperatures of the injection port and PFPD detector were kept at 250 °C; the initial oven temperature was kept at 50 °C for 5 min, followed by a temperature ramp of 10 °C/min to 250 °C, and a final hold for 5 min. Treated diesel samples were collected at the predetermined time intervals, and centrifuged for two minute to remove any residual adsorbent. The sample was then manually injected into the GC-PFPD three times to confirm reproducibility. The reported sulfur concentration values were based on the average sulfur concentration of each sample. The amount of sulfur removed from the treated diesel at time t, was calculated using **Equation 3.1**:

$$Sulfur\ removed = \frac{(C_o - C_t)}{C_o} \times 100\% \qquad (3.1)$$

Where, C_o (mg.kg^{-1}) is the concentration of the sulfur initially found in the diesel, and C_t (mg.kg^{-1}) represented the concentration of the sulfur at time t (min). The adsorption capacities at equilibrium and at time t were represented as q_e and q_t (mg.g^{-1}), and were determined using **Equation 3.2** and **Equation 3.3**, respectively:

$$q_e = \frac{(C_o - C_e)m_d}{W} \qquad (3.2)$$

$$q_t = \frac{(C_o - C_t)m_d}{W} \quad (3.3)$$

Where m_d (kg) is the mass of diesel; W (g) is the mass of adsorbent that was used and C_e (mg.kg^{-1}) is the concentration of sulfur compounds initially found in the diesel.

The experimental methods that were used in this study were outlined in this chapter. All absorbents used were prepared using the same batch of AC to promote uniformity in the adsorbents physiochemical properties. **Chapter 4** focuses on the ADS of both commercial and model diesel fuels over AC adsorbents loaded with period four transition metals oxide. **Chapter 5** looks at investigating the effects of competitive adsorption interactions in a multi-component diesel system.

Chapter 4:

Adsorptive desulfurization using period four transition metals oxide: A study of adsorbent Lewis acid strength derived from the metal oxide ionic-covalent parameter

Part of this work was presented at the following conferences:

- *International Workshop on Porous Materials and their Applications, Council for Scientific and Industrial Research, Pretoria, South Africa, 2018*
- *CATSA, Limpopo province, South Africa, November 2018*

4.1 Introduction

Adsorptive desulfurization (ADS) techniques have gained increasing global attention as means of obtaining ultra-clean diesel fuel due to process simplicity, low cost and the ability to remove all organic sulfur compounds to a significantly low concentration [89]. It has been reported that the addition of metal/metal oxides on ADS adsorbents profoundly affect their adsorption activity [89, 90, 91]. Extensive studies have investigated metal oxides as ADS adsorbents, where the type of metal oxide used ultimately determined sulfur compound selectivity and the extent of their removal during desulfurization [92, 93, 94, 95].

Activated carbon is one of the most widely used commercial adsorbents for various applications; due to its attributes such as high porosity and significant surface area. Recent studies showed the effectiveness of AC in the adsorption of sulfur in diesel [86, 96]. Some authors looked at ADS adsorbents containing AC that was synthesized using various organic materials, including brewer's spent grains [97], walnut char [98], and sewage sludge [99]. Studies have shown that synergistic effects arise when merging the desulfurization properties of activated carbon and metal species, leading to enhanced sulfur adsorption and selectivity towards refractory sulfur compounds [86]. However, predominate work using metal/metal oxide/activated carbon composites has been studied based on ADS of model diesel fuels, where the ADS performance of these adsorbents in commercial diesels and proposed mechanisms has not been reported.

The effects of adsorbent acidity on desulfurization performance have also been investigated, where studies have shown that acid functional groups, as well as Lewis and Brönsted acid sites in adsorbents increased the adsorption and selectivity of sulfur compounds during desulfurization [63]. Some researchers have suggested that sulfur compounds are preferably adsorbed on the Brönsted acid site via H-S bonds. This adsorption was more substantial than that of the Lewis acid site interactions [84, 85]. Moreover, the adsorption of sulfur compounds on Lewis acid sites was hindered by competitive interactions with other aromatics present in the fuel, which also had a high affinity for adsorption on Lewis acid sites [78, 79]. However, the presence of the Brönsted acid site led to alkylation and oligomerization of organic sulfur species as well as aromatics and olefins present in the fuels [78, 100].

Nonetheless, predominate studies on ADS using metal oxide adsorbents have been based on Pearson's HSAB principle which states that acid–base reactions occur preferably between soft Lewis acids and bases; similarly, hard Lewis acids react with hard Lewis bases [97, 101]. Therefore, acid–base interaction occurred preferably between a metal oxide and a metal cation with intermediate Lewis acidity and the sulfur compounds in diesel that are intermediate Lewis bases [89, 93, 100]. However, the Pearson's HSAB classification was derived on the basis of cation electronegativity (covalent forces) and did not take into consideration the way in which the polarizing ability (ionic forces) of a cation influenced its Lewis acidic strength [102, 103].

Portier et al. [104] derived a novel parameter known as the ionic-covalent parameter (ICP) based on both Pearson's qualitative HSAB principles and Zhang's quantitative scale of cation acidic strength, which took into consideration both the covalent (electronegativity) and the ionic (polarizing power) forces of cations. Moreover, they established a relationship where the ICP value of a cation increased in proportion to its Lewis acid strength, and deduced that hard acids had higher ICP values [105]. In contract, soft acids had low ICP values [105]. Various studies used the ICP and optical basicity to derive a Lewis-related acid/basicity scale for transition metal cations and their salts, oxides and mixed oxides [106, 107]. Lenglet and Hochu [108] determined a linear correlation between the iconicity and the ICP of I-II spinel metal oxides, including period four transition metal oxides.

This Chapter reports on the desulfurization activity of period four transition metal oxides (Zn, Cr, Mn, Co, Fe, Cu, Ni) loaded onto AC; and determines how the activity correlates to the ICP and the Lewis acid strength of metal oxide cations. The adsorption kinetics and adsorbent selectivity in the desulfurization of both model and commercial diesel in both batch and fixed-bed modes were also investigated. To the best of our knowledge, using the ICP as a means of determining the Lewis acidity strength of transition metal oxides and their subsequent desulfurization capabilities has not been reported yet. Therefore, this study opens a new research direction in the field of ADS of diesel fuels using transition metals and metal oxides.

4.2 Materials and methods

The methods used in preparing the diesel and adsorbents used in this chapter are outlined in **Chapter 3, section 3.2**. The adsorbents characterization techniques and treated diesel analysis methods are outlined in **Chapter 3, section 3.3** and **section 3.5**, respectively.

4.2.1 Adsorption procedure

All the adsorbents used in this study were dried in a muffle furnace at 110 °C prior to each desulfurization experiment in order to evaporate any physically adsorbed atmospheric moisture. The adsorption experiments were grouped into two sections based on the type of diesel used (model or commercial). In the batch experiments, the adsorbents were first weighed and then added into a three-necked round-bottom flask containing 30 g model diesel. The mixture of fuel and adsorbent was stirred using a heated magnetic stirrer equipped with a temperature-controlling thermocouple at a speed of 1200 rpm in all the experiments. All batch-mode experiments were performed for a duration of 3 hours. During fixed-bed adsorption experiments, each adsorbent was loaded into a glass column with a dimension of 400 mm in length and 1.5 mm in internal diameter, where the adsorbent bed length was fixed at 110 mm. The adsorbent bed was initially treated with n-hexadecane, then commercial diesel fuel was pumped through the adsorbent bed at a liquid hourly space velocity (LHSV) of 0.61 h^{-1}. The treated diesel samples were collected for analysis at time intervals of 0, 15, 30, 45, 60, 90, 120, 150, 180, 240, 300, 360 and 420 minutes. Each sample was centrifuged to remove any residual adsorbent suspended in the diesel and placed in a labelled sample vial. A detailed description of the experimental procedures is provided in **Appendix A.2**.

4.2.2 Adsorption studies

4.2.2.1 Adsorbent selectivity study

The adsorbent's selectivity for the most steric sulfur compounds found in the higher concentration in commercial diesel were also investigated. Adsorbent equilibrium and breakthrough selectivity were determined using **Equations 4.1 – 4.2.** 2,6/3,6 –DMDBT is as a reference compound.

$$K_{d,e} = \frac{q_e}{C_e} \quad (4.1)$$

$$K_{d,b} = \frac{q_b}{C_b} \quad (4.2)$$

Where, $K_{d,e}$ and $K_{d,b}$ are the distribution coefficients of the sulfur species at equilibrium and at breakthrough, respectively. The equilibrium and breakthrough capacities are represented as q_e and q_b ($mg.g^{-1}$), respectively. Whereas, the concentration of sulfur remaining in the diesel at equilibrium and breakthrough was represented as C_e and C_b ($mg.kg^{-1}$), respectively.

$$\alpha = \frac{K_{d(i)}}{K_{d\ (2,6\ /\ 3,6\ -DMDBT)}} \quad (4.3)$$

Where, α is the adsorption selectivity factor of sulfur compound *i* in respect of reference compound 2,6/3,6 –DMDBT, $K_{d(i)}$ and $K_{d(2,6\ /\ 3,6\ –DMDBT)}$ are the distribution coefficients of sulfur compound *i* and the reference compound 2,6/3,6 –DMDBT, respectively.

4.2.2.2 Adsorption kinetics study

The kinetic mechanism of desulfurization involves the transportation of sulfur compounds from the diesel fluid into the pores of an adsorbent. In addition to adsorption itself, various mass transfer phenomena occur. These include film, surface, pore and intra-particle diffusion. To elucidate further on the controlling mechanisms of the adsorption of sulfur compounds found in commercial diesel, the experimental data was fitted to the Pseudo first and second order models, Elovich equation, in addition to the Weber and Morris intra-particle diffusion model. The initial stage of adsorption was described using the Lagergren's pseudo-first-order model [86]. The linearized model is expressed as follows:

$$ln(q_e - q_t) = lnq_e - k_1 t \quad (4.4)$$

Where q_e, and q_t ($mg.g^{-1}$) are the amount of sulfur adsorbed per gram of adsorbent at equilibrium and time *t* (min), respectively; and k_1 (min^{-1}) is the pseudo-first-order equilibrium rate constant. The pseudo-second-order model describes the entire adsorption process, and is based on the assumption that the rate of adsorption is limited by chemical interaction [63]. The linearized form of the pseudo-second-order model, is shown in **Equation 4.5**:

$$\frac{t}{q_t} = \frac{1}{k_2 q_e^2} + \frac{1}{q_e} t \qquad (4.5)$$

Where k_2 ($g.mg^{-1}.min^{-1}$) is the pseudo-second-order equilibrium rate constant. Similarly, the Elovich equation was best used to describe activated adsorption. The model assumption is that active sites on the adsorbent surface facilitate chemisorption [109]. The linearized equation is expressed as follows:

$$q_t = \frac{1}{\beta}[In(\alpha\beta)] + \frac{1}{\beta} Int \qquad (4.6)$$

Where the adsorption capacity at time t (min) is represented as q_t ($mg.g^{-1}$), α is the initial adsorption rate constant ($mg.g^{-1}.min^{-1}$), and 1/β (mg/g) relates to the amount of available adsorption sites. Weber and Morris [110] developed the generally accepted intra-particle diffusion model based on the assumption that the rate at which an adsorbate diffuses into an adsorbent governs the adsorption process [111]. The model is expressed as follows:

$$q_t = k_i t^{1/2} + C \qquad (4.7)$$

Where the adsorption capacity at time t (min) is represented as q_t ($mg.g^{-1}$), C ($mg.g^{-1}$) is a constant that relates to the boundary layer thickness, and the diffusion model rate constant is represented as k_i ($mg.g^{-1}.min^{-0.5}$).

4.2.2.3 Evaluation of Pearson hardness parameter and Ionic-covalent parameter of transition metal oxides used in the adsorbents

According to Parr and Pearson [112], the strength of Lewis acid (cation) can be defined using the following equation:

$$\eta_i = \frac{1}{2}(I_i - A_i) \qquad (4.8)$$

Where η_i is the Pearson hardness parameter of Lewis acid cation i, I_i is the ionization potential and A_i is the electron affinity [103]. The hardness parameters of mixed metal oxide and metal oxide with varying oxygen coordination states (Mn-oxide, Fe-oxide, Co-oxide and Cu-oxide) were calculated as follows:

$$\eta_{th} = \sum \eta_i * f_i \quad (4.9)$$

Where η_{th} is the overall hardness parameter of cations in mixed metal oxide, η_i is the hardness parameter of the individual cations i in the mixed metal oxide, and f_i is the mole fraction of cation i, which contributed to the sum of moles in the mixed metal oxide [113].

Portier et al. [104] suggested a less complex relationship between the oxidation states, electronegativity and ionic radii of cations. They developed an empirical equation to determine the electronegativity of a cation in its various crystallographic arrangements and electronic conditions, such as oxidation state, co-ordination number, ionic radius and spin state.

$$\chi = 0.274z - 0.15zr_i - 0.01r_i + 1 + \alpha \quad (4.10)$$

Where χ is the electronegativity of cation i, z represents the cation oxidation number z, r_i (Å) represents the Shannon ionic radius [114] and α is a corrective constant that is related to the atomic number [104]. They then introduced a novel parameter known as the ionic-covalent parameter (ICP) [104]. This parameter was derived from both Pearson's qualitative HSAB principles and Zhang's quantitative scale of cation acidic strength. The ICP takes into consideration of both the covalent (electronegativity) and ionic (polarizing power) forces of a cation:

$$ICP_i = \log\left(\frac{z}{r_i^2}\right) - 1.38\chi + 2.07 \quad (4.11)$$

Where z/r_i^2 is the polarizing power of the cation determined from its oxidation sate and Shannon ionic radius, and χ is the electronegativity determined by using **Equation 4.10**. A subsequent correlation was established between cation ICP and its Lewis acid strength, where the ICP value of cations increased in proportion to Lewis acid strength, and hard acids have higher ICP values, while soft acids have low ICP values [105]. The ionic covalent parameters of mixed metal oxide and metal oxide with varying oxygen coordination states (Mn-oxide, Fe-oxide, Co-oxide, and Cu-oxide) were determined using **Equation 4.12**:

$$ICP_{th} = \sum ICP_i * f_i \quad (4.12)$$

Where ICP_{th} is the overall ionic-covalent parameter of the mixed metal oxide, ICP_i is the ionic-covalent parameter of the individual cations i in the mixed metal oxide, and f_i is the mole fraction of cation i which contributed to the sum of moles in the mixed metal oxide [113].

4.2.2.4 Evaluation of adsorption breakthrough curves

Various fixed-bed adsorption models were utilized in determining the maximum adsorption capacity and kinetics of adsorbents in fixed-bed applications. The linearized Thomas model was employed and is expressed as follows:

$$ln\left(\frac{C_o}{C_t} - 1\right) = \frac{k_{Th}q_{Th}M}{Q} - k_{Th}C_o t \quad (4.13)$$

Where Co and Ct ($mg.kg^{-1}$) represents the concentration sulfur compounds in the diesel initially and at time *t*, respectively. The diesel flow rate is represented as Q ($ml.min^{-1}$), M is the mass of adsorbent bed (g). The kinetic rate constant and calculated maximum adsorption capacity of the sulfur compound are represented as k_{Th} ($mL.min^{-1}.mg^{-1}$) and q_{Th} ($mg.g^{-1}$), respectively. The Yoon-Nelson model was derived on the basis that the adsorbate uptake and adsorption breakthrough were directly proportional to the decreasing rate of adsorption. It does not take into consideration the type of adsorbent used, the adsorbent properties or the physical features of the adsorbent bed [115]. The linearized Yoon-Nelson model is expressed as follows:

$$ln\frac{C_t}{C_o - C_t} = k_{YN}t - k_{YN}\tau_{YN} \quad (4.14)$$

Where, k_{YN} (min^{-1}) and τ_{YN} (min) are the kinetic rate constant and the time required to reach 50 % linear breakthrough of sulfur compound, respectively. The filtration advection–dispersion equation, is based on largely irreversible solute–adsorbent interactions (strong van der Waals, steric, Lewis acid–base), where solutes do not swap on and off the adsorbent surface and results in a steady-state breakthrough of $C_t/C_o < 1$ [116]. The linear filtration advection–dispersion equation is expressed as follows:

$$ln\frac{C_t}{C_o} = -\frac{k_f}{v}L \quad (4.15)$$

Where the length of the adsorbent bed (transportation length), the advective diesel velocity, and the rate constant are represented as L (m), v (m.min^{-1}) and k_f (min^{-1}), respectively.

4.3 Results and discussion

4.3.1 Adsorbent characterization

4.3.1.1 BET analysis

Listed in **Table 4.1** are the BET analysis results obtained for unmodified AC and the metal oxide incorporated AC adsorbents. There was a noticeable decrease in the pore volume and surface area of the adsorbents, which was attributed to the blockage of the pore vacancies in the AC matrix upon loading with the metal oxides.

Table 4.1: BET parameters obtained from N_2 physisorption.

Parameter		BET surface area (m2/g)	Total pore volume (cm3/g)	Average pore diameter (nm)
Adsorbent	**AC**	997.8	0.523	2.081
	Co-oxide/AC	729.5	0.407	2.236
	Cr-oxide/AC	716.1	0.379	2.126
	Cu-oxide/AC	808.2	0.422	2.097
	Fe-oxide/AC	835.9	0.459	2.195
	Mn-oxide/AC	798.8	0.506	2.514
	Ni-oxide/AC	843.7	0.436	2.066
	Zn-oxide/AC	765.6	0.401	2.099

The adsorption–desorption isotherms of N_2 in unmodified AC and metal oxide/AC adsorbents were also determined. According to the curves shown in **Figure 4.1**, the metal oxide/AC adsorbents demonstrated characteristics of the type I isotherm with an H4 hysteresis loop. The result indicated that both mesopores and micropores were present in the AC , where loading the metal oxides onto the AC surface did not alter the initial narrow slit-like pore structure of the carbon [117].

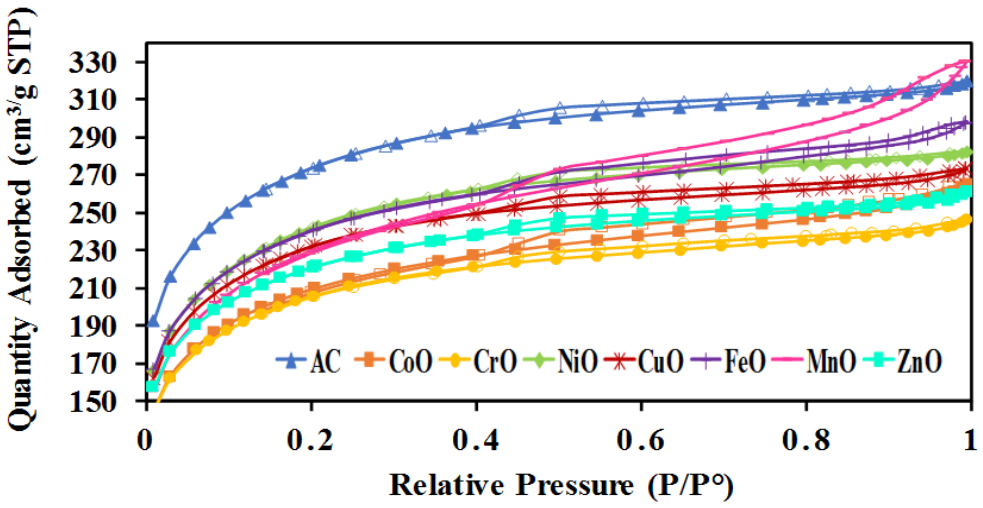

Figure 4.1: The N_2 adsorption–desorption isotherms and resulting isotherm hysteresis loops obtained for AC loaded with metal (10 wt. %) oxides and unmodified AC.

4.3.1.2 PXRD analysis

The crystalline structures of unmodified AC and metal oxide/AC adsorbents were identified using PXRD, as shown in **Figure 4.2**. Unmodified AC diffraction peaks (**Figure 4.2a**) showed the characteristics of crystalline hexagonal graphite (ICDD Card No. 00-056-0160). The presence of buckminsterfullerene carbon arrangements was also observed within the AC matrix, with a characteristic peak at 20.89 ° (ICDD Card No. 00-047-0787). The formation of mixed cobalt oxides was visible (**Figure 4.2b**) with characteristic peaks appearing at 2θ = 36.76 °, 42.45 °, 44.75 ° and 65.07 ° corresponding to (311), (400), (440) planes of Co_3O_4 (ICDD Card No. 03-065-3103) and (110), (111) planes of CoO (ICDD Card No. 01-072-1474). The formation of mixed cobalt oxides was expected at calcination temperatures below 1000 °C, whereas increasing the temperature above 1000 °C should have reduced the oxide nanoparticles to CoO [118]. The obtained space group and lattice parameters (**Table B.1**) indicated the formation of face-centred cubic Co_3O_4 and monoclinic CoO. The diffraction peaks of the chromium oxide/AC adsorbent (**Figure 4.2c**) corresponded with the formation of rhombohedral Eskolaite – Cr_2O_3 (ICDD Card No. 00-002-1362). The PXRD pattern of the copper oxide/AC adsorbent (**Figure 4.2d**) had diffraction peaks for both monoclinic CuO (ICDD Card No.00-041-0254) and cubic Cu_2O (ICDD Card No. 00-078-2076). The iron oxide/AC adsorbent (**Figure 4.2e**) contained cubic maghemite/γ-Fe_2O_3 crystals (ICDD Card No. 01-083-0112). The PXRD pattern of the manganese oxide/AC

adsorbent (**Figure 4.2f**) had diffraction peaks consistent with the formation of both Mn_3O_4 (ICDD Card No. 01-080-0382) and α-MnO_2 (ICDD Card No. 01-072-1982). Qualitative PXRD analysis (**Table B.1**) showed the formation of ditetragonal dipyramidal body-centred hausmannite (Mn_3O_4) and tetragonal dipyramidal α-MnO_2. The nickel oxide/AC adsorbent (**Figure 4.2g**) had diffraction peaks that identified the formation of face-centred cubic NiO (ICDD Card No. 01-073-1523). The diffraction peaks of the zinc oxide/AC adsorbent (**Figure 4.2h**) corresponded to the formation dihexagonal pyramidal zincite – ZnO (ICDD Card No. 01-074-9940). The crystallite sizes of the metal oxides present in each adsorbent were determined using the Williamson-Hall method. The values are listed in **Table B.2** (shown in Appendices). Predominate crystallite diameters ranged between 4 nm and 16 nm. However, larger crystals were obtained in the Cr_2O_3 and ZnO adsorbents at 30.75 nm and 49.2 nm, respectively. The weight percentages of the metal oxide species present in each adsorbent are shown in **Table B.2**, and were quantified using the Reference Intensity Ratio method. PXRD results in summary show that period four transition metals oxide were successfully synthesized, and loaded onto the support of AC.

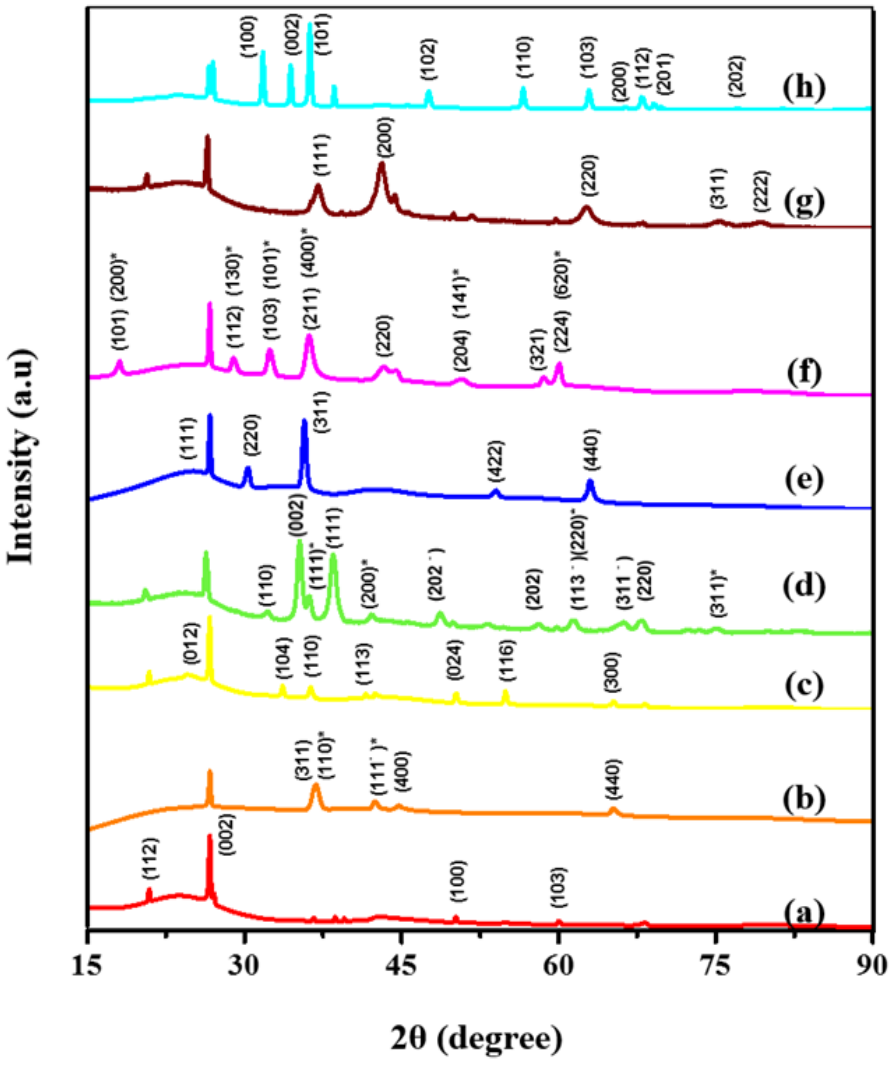

Figure 4.2: PXRD patterns obtained for (a) AC, (b) Co-oxide/AC, (c) Cr-oxide/AC, (d) Cu-oxide/AC, (e) Fe-oxide/AC, (f) Mn-oxide/AC, (g) Ni-oxide/AC and (h) Zn-oxide/AC.

4.3.1.3 HR-TEM analysis

The crystallinity, the approximate size of the individual crystals and the agglomerated clusters of the synthesized metal oxides/AC adsorbents were further characterized using HRTEM analysis (**Figure 4.3**), with lattice fringe patterns shown in the appendices **Figure B.1**. The Co_3O_4 and CoO nanoparticles obtained (**Figure 4.3b**) agglomerated to form clusters ranging between ≈ 100 nm and 300 nm. The lattice fringe pattern (**Figure B.1b**) indicated a d-spacing of 0.2845 nm in accordance with the (200) crystal plane of Co_3O_4. The bright spots in the resulting SAED pattern showed the crystalline nature of the Co_3O_4/CoO nanoparticles, where the smearing of the spots was attributed to a slight loss in crystallinity due to the adsorbent synthesis method. The obtained

TEM image in **Figure 4.3c** showed that the Cr_2O_3 nanoparticles are cubic, similar to those reported by other researchers [119], with a crystallite size ranging between ≈ 30 nm and 100 nm. These nanoparticles were agglomerated to form clusters with a length of ≈ 300–400 nm (see **Figure 4.3c**). The lattice fringe pattern of the metal oxide was clearly visible (**Figure B.1c**) with a d-spacing of 0.3598 nm, and contained no dislocation due to defects. The d-spacing correlated with the inter-planar distance of the (012) plane in rhombohedral Cr_2O_3, which further supports the PXRD results. The subsequent SAED pattern showed that the Cr_2O_3 occurred as single crystals, where the (012), (113) and (104) planes were observed, corresponding to rhombohedral Cr_2O_3 (**Figure 4.3c**). The CuO and Cu_2O nanoparticles deposited on the surface of the AC (**Figure 4.3d**) had a spherical morphology and agglomerated to form clusters ranging between ≈ 100 nm and 250 nm. A d-spacing of 0.2701 nm was obtained from the lattice fringe pattern (**Figure B.1d**) in the selected section, which correlated with the 0.273 nm of the $(\bar{1}10)$ plane of monoclinic CuO. The bright spots observed in the SAED pattern showed the crystalline nature of the agglomerated CuO/Cu_2O nanoparticles. The γ-Fe_2O_3 nanoparticles were predominately agglomerated into clusters, where hexagonal-crystals were also observed (**Figure 4.3e**). The d-spacing of 0.296 nm obtained in a lattice fringe pattern (**Figure B.1e**) related to the (311) plane of γ-Fe_2O_3.

The crystalline form of the metal oxide was further verified by the bright spots observed in the SAED pattern, and these corroborated the crystalline characteristics of the Mn_3O_4 and α-MnO_2 nanoparticles (**Figure 4.3f**), which agglomerated to form clusters ranging in size between 100 nm and 500 nm. The intensity lattice fringe pattern (**Figure B.1f**) at a d-spacing of 0.4903 nm showed that the growth was dominant either in the (101) plane for Mn_2O_3 or the (200) plane for α-MnO_2. As shown in **Figure 4.3g**, the NiO nanoparticles were cubic and agglomerated to form circular clusters on the surface of the AC, where the clusters had diameters ranging between ≈ 50 nm and 120 nm. The resultant lattice fringe pattern (**Figure B.1g**) has a d-spacing value of 0.239 nm, which was in accordance with the inter-planar distance of the (111) plane in cubic NiO. Concentric rings were observed in the SAED pattern, which shows the polycrystalline nature of the NiO nanoparticles. The TEM image in **Figure 4.3h** shows substantially large hexagonal prism zincite (ZnO) crystals with tapered edges, where the crystallite size ranged between ≈ 200 nm and 500 nm. The lattice fringe pattern of the ZnO was in accordance with the (101) crystal plane (**Figure B.1h**) which has a d-spacing of 0.2558 nm. The subsequent SAED image showed that the ZnO was single crystalline, where the bright spots of the (101), (002) planes were observed.

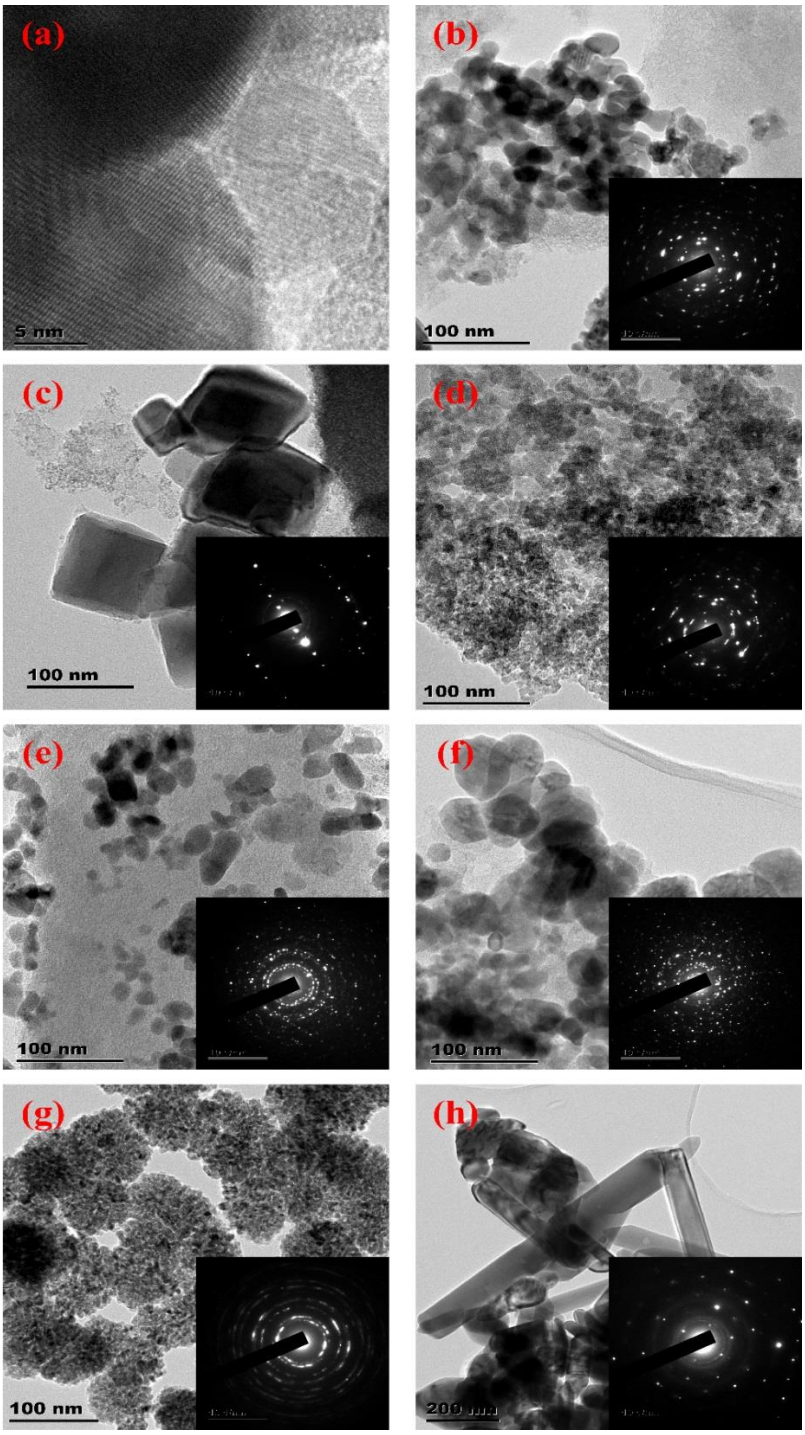

Figure 4.3: TEM images and SAED patterns obtained for (a) AC, (b) Co-oxide or AC, (c) Cr-oxide or AC, (d) Cu-oxide or AC, (e) Fe-oxide or AC, (f) Mn-oxide or AC, (g) Ni-oxide or AC and (h) Zn-oxide or AC.

4.3.1.4 SEM/EDS analysis

The SEM analysis results as shown in **Figure 4.4** indicated that the surface of the adsorbents was uneven, with irregular-shaped AC particles of random size and orientation. The elemental mapping SEM images of the unmodified AC and metal oxide/AC adsorbents (**Figure 4.4 a–h)** proved the presence of each transition metal and oxygen on the surface of the AC. However, the visibility of the elemental carbon in all the images suggested that the metal oxides were unevenly distributed on the AC surface. This supported the results of the TEM analysis, which showed metal oxide agglomeration occurred in all the adsorbents. The elemental composition of the unmodified AC and metal oxide/AC absorbents are shown in **Figure B.2 a–h**. The unmodified AC contained elemental traces of silicone and aluminum, whereas the metal oxide/AC adsorbents contained additional traces of calcium, sodium, molybdenum and sulfur. The weight percentage of metal in each adsorbent varied between ≈ 9.3 % and 11.5 %, and was almost equal to the stoichiometric amount of 10%, along with sufficient weight percentages of required oxygen. These results demonstrated the successful incorporation metal oxide species on the AC surface.

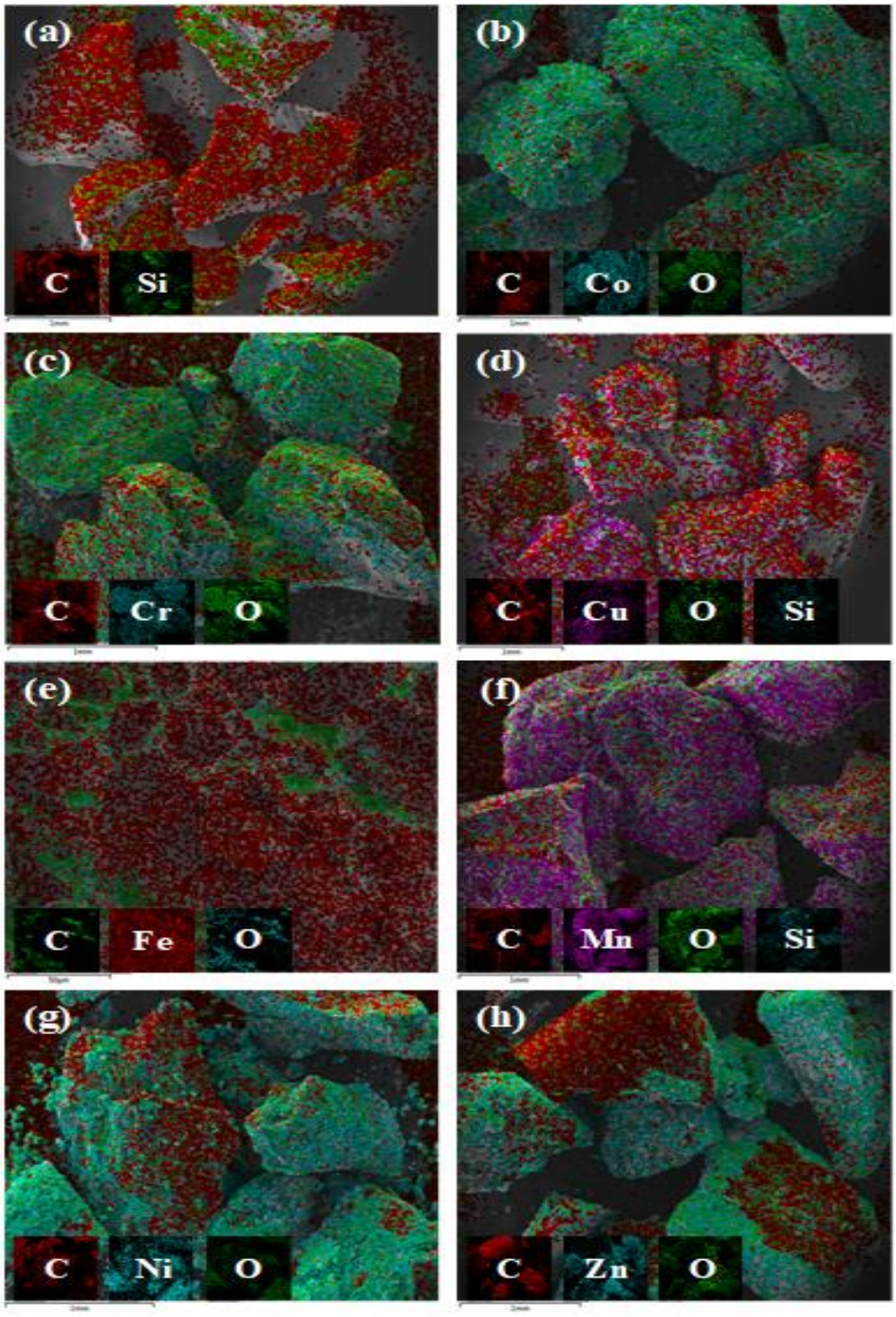

Figure 4.4: SEM images and elemental mapping for (a) AC, (b) Co-oxide/AC, (c) Cr-oxide/AC, (d) Cu-oxide/AC, (e) Fe-oxide/AC, (f) Mn-oxide/AC, (g) Ni-oxide/AC and (h) Zn-oxide/AC.

4.3.1.5 TGA/DTG analysis

Thermogravimetric / Derivative thermogravimetry was used to determine the ideal calcination temperature that would led to the formation of each metal oxide, in addition to identifying the

fundamental stages involved in the thermal decomposition of the metal acetate precursor once it was loaded onto the AC. The thermal decomposition of the unmodified AC occurred between 601 °C and 898 °C, which resulted in a total weight loss of about 82 % (**Figure 4.5a**). The thermal decomposition of the metal acetate/AC adsorbents occurred in either three or four stages. Where the first stage was attributed to the dehydration of the metal acetate, stages 2 and 3 were attributed to the reduction of the acetate group and formation of the metal oxide; and stages 3 and 4 were attributed to the reduction of the metal oxide and/or the thermal degradation of the AC. The thermal decomposition of $Co(C_2O_2H_3)_2 \cdot 4H_2O$/AC led to the formation of the oxides at temperatures between 156.89 °C to 379.79 °C with a mass loss of 17.18 % almost equal to the theoretical value of 18.77 % **(Figure 4.5b)**. The decomposition of the AC occurred between 379.79 °C and 693.64 °C, resulting in a mass loss of about 19 %. The thermal decomposition of $Cr_3(C_2O_2H_3)_7 \cdot (OH)_2$ resulted in a 16.9 % weight loss, which was lower than the theoretical 22.85% required to form Cr_2O_3 (**Figure 4.5c**). The thermal decomposition of $Cu(C_2O_2H_3)_2 \cdot H_2O$/AC resulted in a weight loss of 23.9 % almost equal to the 22.82 % theoretical value, which led to the formation of metallic copper (**Figure 4.5d**). Moreover, the presence of AC mitigated the evaporation of the metallic copper and increased the decomposition temperature required to form CuO from 365 °C to approximately 450 °C, and decreased the decomposition rate of the of the metal acetate. The thermal decomposition of $Fe(C_2O_2H_3)_2$/AC and the formation of the ferric oxide occurred between 133.27 °C and 324.83 °C (**Figure 4.5e**), where a significant weight loss of about 63.97 % occurred between 324.83 °C and 796.25 °C. This weight loss was attributed to the thermal degradation of AC. The formation of the oxides in the $Mn(C_2O_2H_3)_2 \cdot 4H_2O$/AC adsorbent occurred between 222.74 °C to 898.404 °C (**Figure 4.5f**), with a total mass loss of 31.96 % that is almost equal to the theoretical value of 33.504 %. The decomposition of AC did not occur. The thermal decomposition of $Ni(C_2O_2H_3)_2 \cdot 4H_2O$/AC resulted in a total mass loss of 39.01 % almost equal to the theoretical value of 36.03 % (**Figure 4.5g**), indicating that the decomposition of the activated carbon occurred, most likely at a temperature above 553 °C. Decomposition of the acetate ligands occurred in two stages between 233.36 °C and 453.73 °C. The presence of AC also increased the decomposition temperature required to form NiO from 365 °C to 553 °C, and decreased the decomposition rate of the nickel acetate. In the thermal decomposition of $Zn(C_2O_2H_3)_2 \cdot 2H_2O$/AC dehydration occurred up to 168.13 °C, with a mass loss of 9.378 % (Figure 4.5h). However, further heating above 250 °C led to adsorbent vaporization resulting in a 99 % adsorbent weight loss.

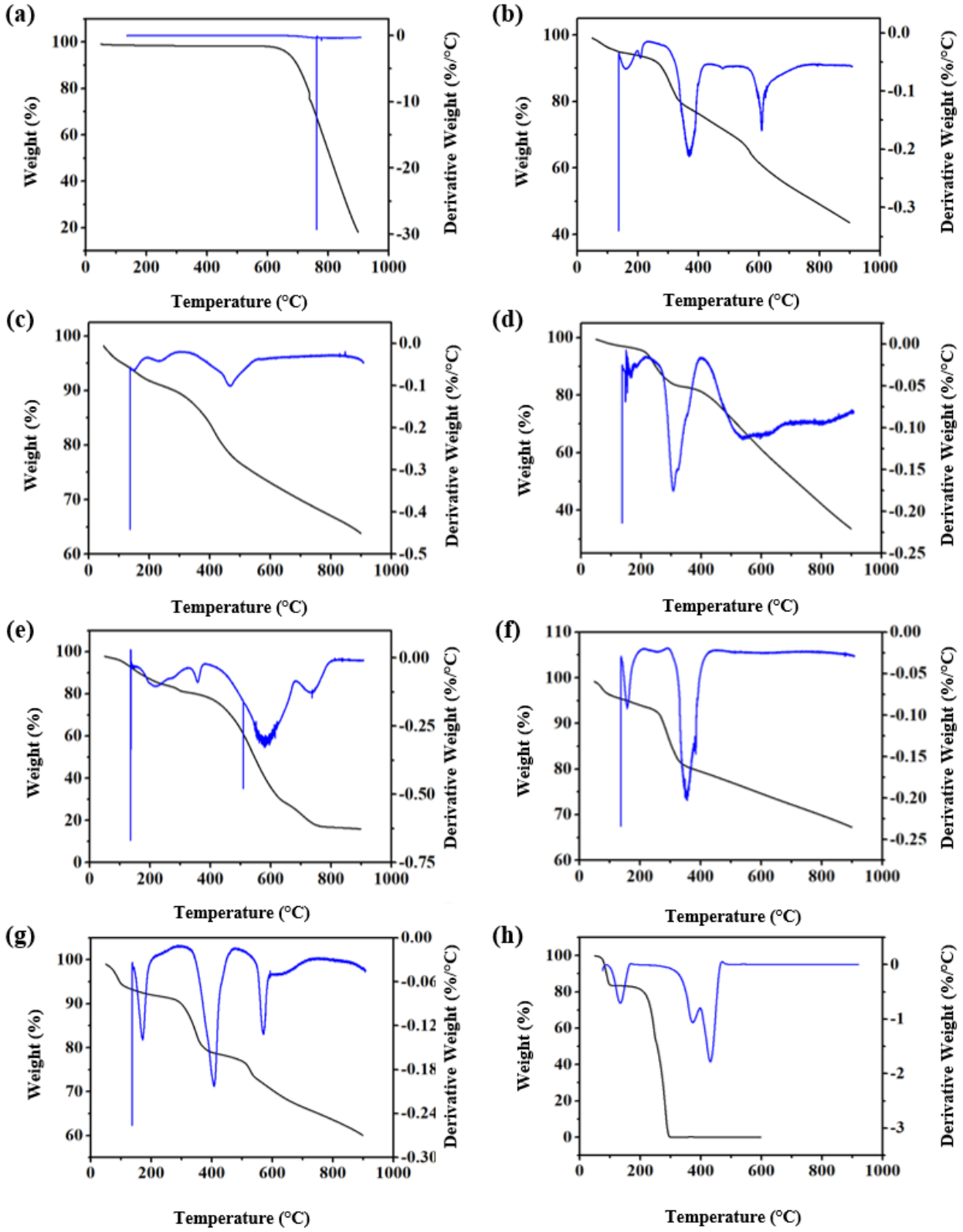

Figure 4.5: The TGA/DTG plots observed for (a) AC, (b) Co-oxide/AC, (c) Cr-oxide/AC, (d) Cu-oxide/AC, (e) Fe-oxide/AC, (f) Mn-oxide/AC, (g) Ni-oxide/AC and (h) Zn-oxide/AC.

4.3.1.6 FT-IR analysis

The FT-IR spectra obtained for metal oxide/AC adsorbents after calcination are shown in **Figure 4.6**. The C–H stretching vibrations were visible at bands appearing at 2989 cm^{-1} and 2901 cm^{-1} [120], which suggested that either the acetate was not completely decomposed, or the adsorption of atmospheric moisture onto the AC. The weak band occurring around 2200 cm^{-1} was assigned to atmospheric CO_2 that adsorbs onto the metal cations of the metal oxides [121]. The in-plane bending vibrations of C-O-H appeared at 1430 cm^{-1}, while the band at 1544 cm^{-1} was assigned to asymmetric stretching vibrations of COO- [96]. The formation of metal oxide stretching bands occurred between 450 cm^{-1} and 550 cm^{-1}. Moreover, the metal hydroxide Me-OH and/or the metal oxide bonded to hydrogen MeO-H bending vibration was also visible at around 1059 cm^{-1} [10].

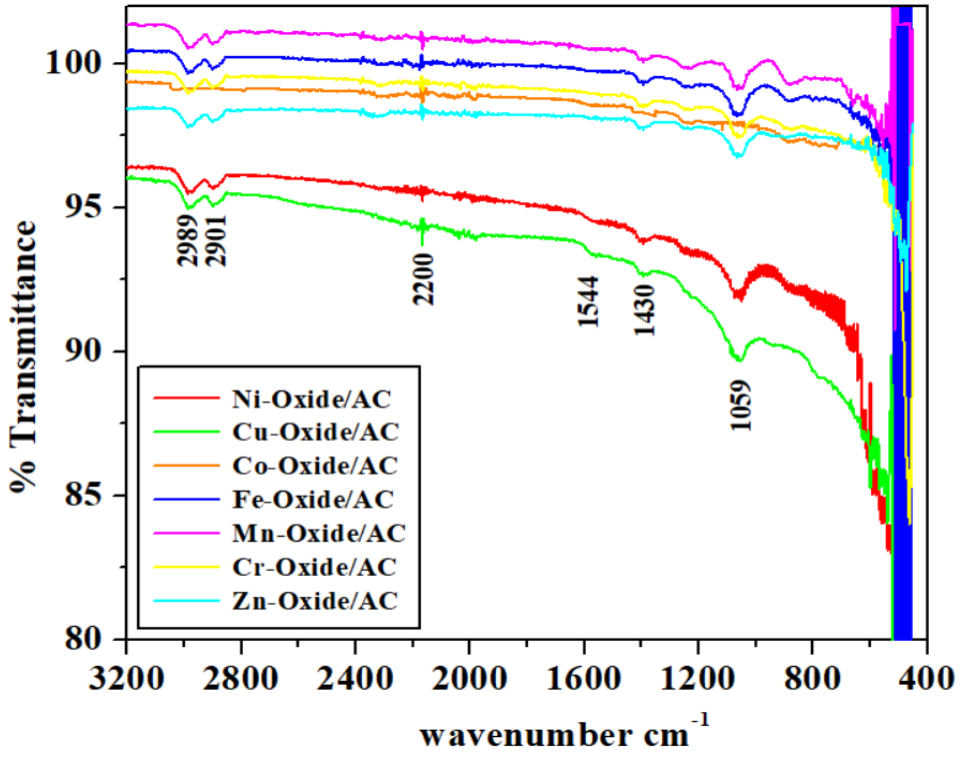

Figure 4.6: The FTIR spectrum obtained for the metal oxide/AC adsorbents loaded with 10 wt. % metal.

4.3.1.7 Py-IR analysis

FTIR-pyridine analysis was used in identifying the Brönsted and Lewis acid sites of the adsorbents (**Figure 4.7**), where pyridine acted as a probe molecule to differentiate between Lewis and Brönsted acid sites. In general, non-bonded pyridine stretching vibrations are assigned to bands 1439 cm^{-1} and 1583 cm^{-1} [122]. Once the pyridine bonds to the acid sites, the aforementioned

bands shift to the 1540–1548 cm^{-1} region for co-ordinately bonded Brönsted acid sites, where the pyridine ion bonded with the proton of the Brönsted acid site [123]. However, the band shifts to the 1440–1460 cm^{-1} region for co-ordinately bonded Lewis acid sites, where the pyridine ion donated electrons to the Lewis acid site [123]. The intensity of the bands are directly proportional to the concentration of surface Lewis and Brönsted acid sites [122]. The FT-IR spectra seen in **Figure 4.7** indicate that all the adsorbents, including unmodified AC, contained both Lewis and Brönsted acid sites [124], ascribed by the bands appearing between 1454–1457 cm^{-1} and 1544–1546 cm^{-1}, respectively. The unmodified AC adsorbent had an intense broad band at 1544 cm^{-1}, which indicated that the adsorbent had a higher concentration of Brönsted acid sites. This was expected, since the addition of metal oxides is expected to introduce additional Lewis acid sites. The Lewis acid site concentration of the adsorbents followed an order of Ni-oxide/AC > Cu-oxide/AC > Co-oxide/AC > Fe-oxide/AC > Mn-oxide/AC > Cr-oxide/AC > Zn-oxide/AC > AC.

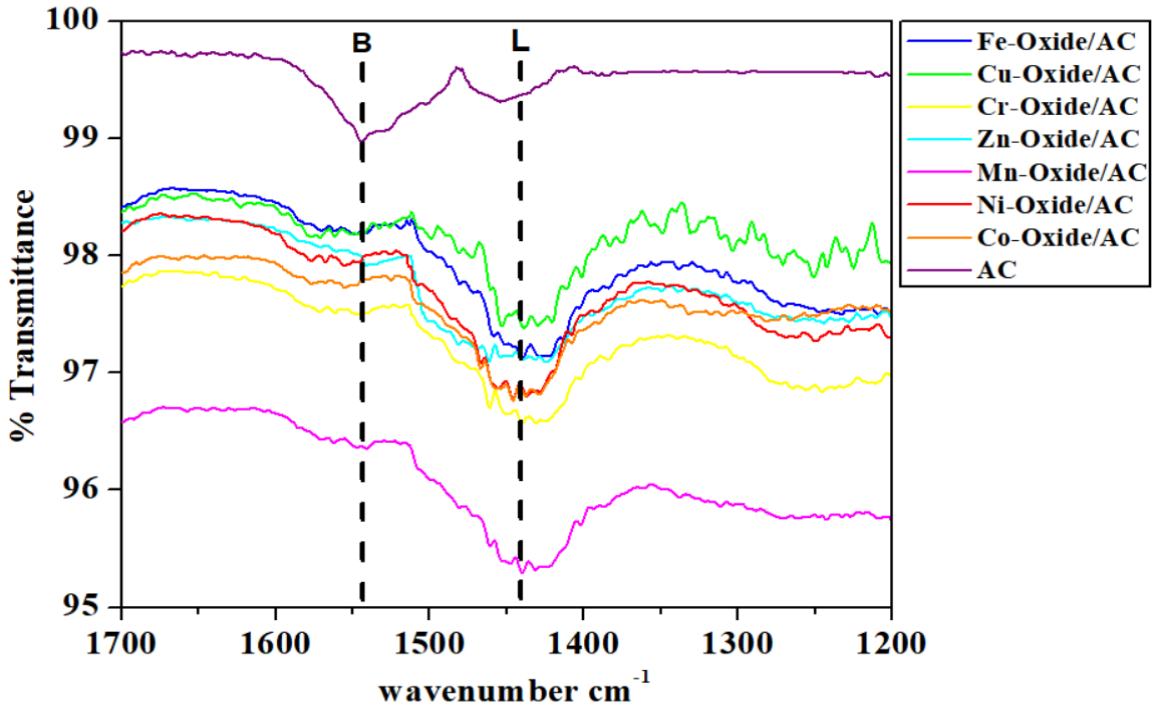

Figure 4.7: The FT-IR spectrum obtained the metal oxide/AC adsorbents loaded after adsorption of pyridine in He, at 150 °C.

4.3.2 Adsorption evaluation of model diesel

4.3.2.1 Effects of adsorption time on overall desulfurization activity

The effect of contact time on the adsorption of model diesel containing 4,6-DMDBT, 4-MDBT and DBT over the period four metal oxide/AC adsorbents and unmodified AC is shown in **Figure 4.8**. The adsorption capacity trend of the adsorbents followed the order: Ni-oxide/AC > Cu-oxide/AC > Co-oxide/AC > Fe-oxide/AC > Mn-oxide/AC > Cr-oxide/AC > Zn-oxide/AC > AC metal oxide/AC. This suggested that loading metal oxide onto the surface of the AC enhanced its desulfurization performance. Adsorbent selectivity for all adsorbents was observed to follow the order of: 4,6-DMDBT > 4-MDBT > DBT. The adsorption rate was highest within the first 90 minutes of the process, irrespective of metal oxide incorporation, which was most likely caused by higher availability of vacant active adsorption sites in the initial process stage. A similar observation was made in [63, 80].

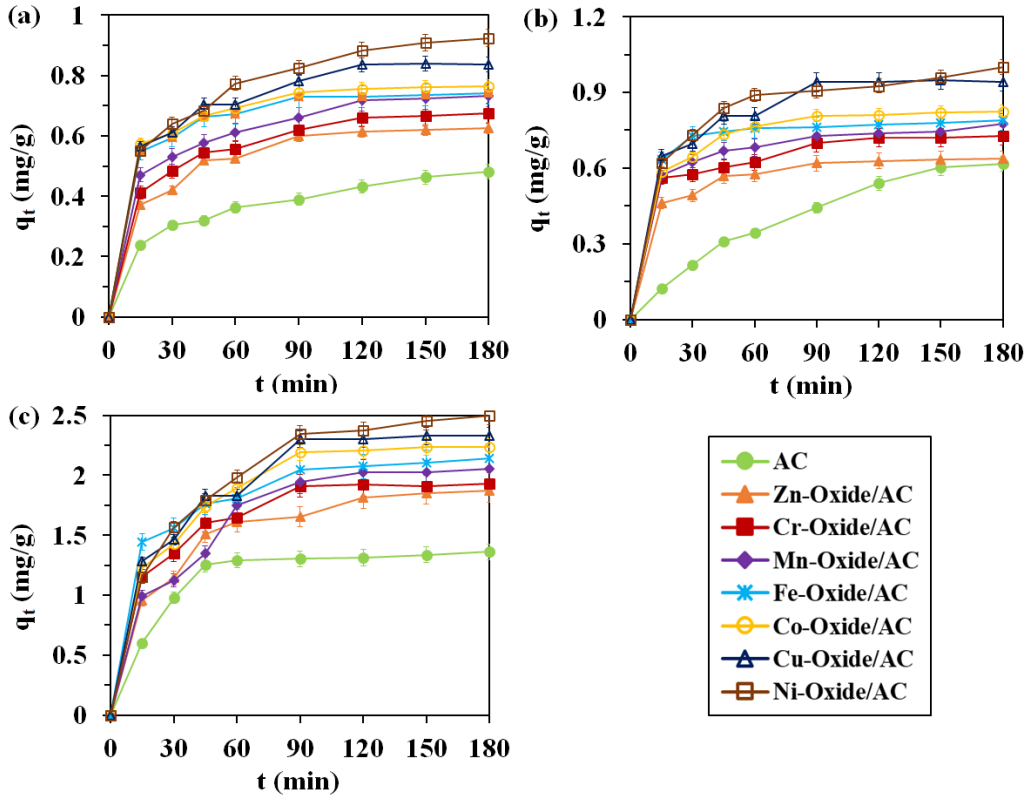

Figure 4.8: Experimental results showing how contact time affected the sulfur adsorption capacity of (a) DBT, (b) 4-MDBT and (c) 4,6-DMDBT, when using the various metal oxide/AC and unmodified AC adsorbents (10 wt. % metal loading, 30 g model diesel, 3 g adsorbent, at 30 °C for 3 hrs).

4.3.2.2 Effects of temperature on adsorptive desulfurization

The effects of temperature on the percentage sulfur removal of 4,6DMDBT, 4-MDBT and DBT in model diesel at 30 °C and 60 °C are shown in **Figure 4.9**. For all the adsorbents used, an increase in temperature led to an increase in the percentage of sulfur removed at equilibrium, in all three sulfur compounds. This was an expected outcome that was attributed to enhanced kinetic and thermodynamic mechanisms, where adsorption became more favourable with increasing the process temperature. A percentage sulfur removal trend of 4-MDBT > DBT > 4,6-MDBT was obtained at both high and low temperatures. The adsorption trend was the result of an increase in the electron density due to the methyl group of the 4-MDBT and stearic hindrance due to methyl groups in the 4 and 6 positions of the 4,6-MDBT [93, 125]. Although AC had a larger BET surface area and pore volume (**Table 4.1**) than the metal oxide/AC adsorbents, the metal oxide/AC adsorbents exhibited higher adsorption capacities (**Figure 4.8**) and percentage removal (**Figure 4.9**) for all three sulfur compounds. These results were comparable to those obtained by Swat et al. [86] in their study on the ADS of model diesel containing thiophene, benzothiophene and DBT, using AC adsorbents loaded with ZnO and NiO.

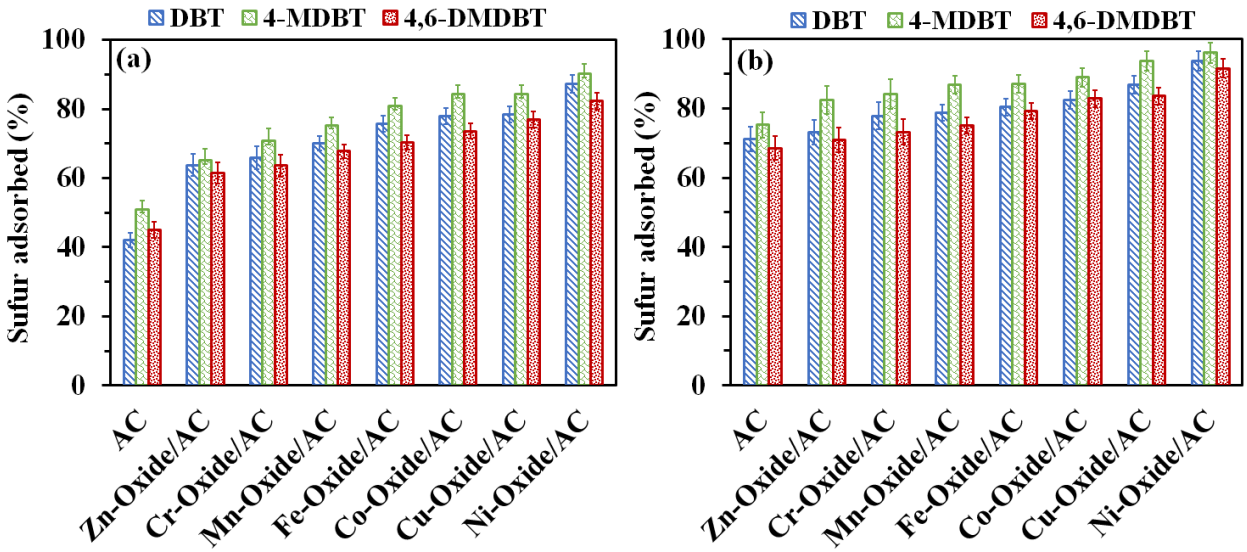

Figure 4.9: A comparison of the effect of temperature on total percentage sulfur removal at (a) 30 °C and (b) 60 °C desulfurization temperatures (10 wt. % metal loading, 30 g model diesel, 3 g adsorbent, for 3 hrs).

4.3.2.3 Effects of adsorbent acidity on adsorptive desulfurization

A comparison of the effects of adsorbent Lewis acidity on the percentage of sulfur adsorbed at high and low temperatures is shown in **Figure 4.10**. The Ni-oxide/AC adsorbent had the highest adsorption performance, where desulfurization activity was in the order of: Ni-oxide/AC > Cu-oxide/AC > Co-oxide/AC > Fe-oxide/AC > Mn-oxide/AC > Cr-oxide/AC > Zn-oxide/AC > AC. A desulfurization trend was observed in the metal oxide used, where activity increased in proportion to the concentration of Lewis acid sites identified using pyridine FT-IR analysis. The intermediate Lewis acid sites of the metal oxide cations act as electrophiles, whereas the sulfur compounds in model diesel are intermediate Lewis bases and act as nucleophiles [102]. These results indicated that increasing adsorbent Lewis acidity resulted in the subsequent increase in acid–base interactions and the uptake of sulfur compounds during desulfurization.

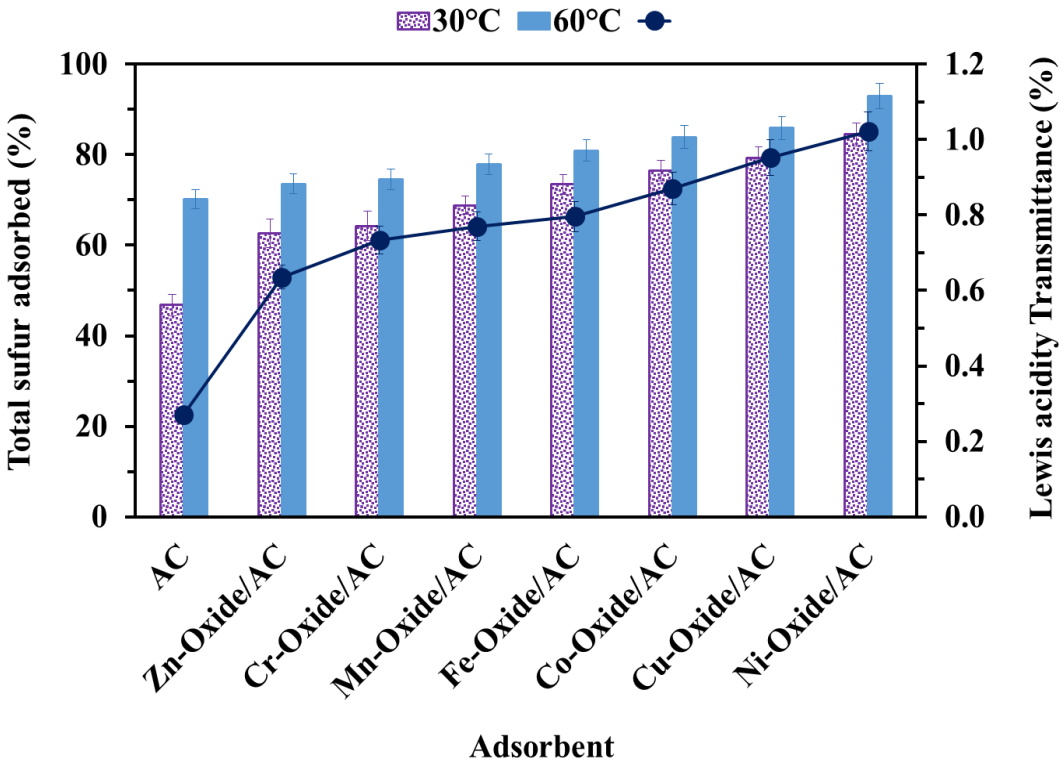

Figure 4.10: Effects of adsorbent Lewis acidity on sulfur removal performance in model diesel treated at high and low temperatures (10 wt. % metal loading, 30 g model diesel, 3 g adsorbent, for 3 hrs).

The overall Pearson harness parameters and ionic covalent parameters of the metal oxide adsorbents used in this study were obtained using **Equation 4.8 – 4.12**, and are listed in **Table 4.2**. The weight percentages (wt. %) of each metal oxide in the adsorbent is based on the values

obtained in the PXRD analysis. The co-ordination number, spin state, ionic radius and atomic number corrective constant of the adsorbents are listed in **Table B.3** in the Appendices. According to Pearson's HSAB theory, acid–base reactions occur preferably between soft Lewis acids and bases; similarly, hard Lewis acids react with hard Lewis bases. Period four transitions metal cations are generally classified as intermediate-soft Lewis acids that react preferably with sulfur compounds present in diesel which are intermediate-soft Lewis bases [125]. Based on Pearson's absolute hardness theory [103], the Lewis acidity hardness of the metal oxides should followed the order of Fe-oxide > Zn-oxide > Cr-oxide > Mn-oxide > Co-oxide > Ni-oxide > Cu-oxide (**Table 4.2**). In contrast, the ICP values of the adsorbent (based on metal oxide cation covalent and ionic forces, coordination number and spin state) and subsequent Lewis acidity hardness followed the order of Zn-oxide > Cr-oxide > Mn-oxide > Co-oxide ≥ Fe-oxide > Cu-oxide > Ni-oxide.

Table 4.2: The composition, oxidation state, electronegativity, Pearson hardness parameter and ICP of adsorbents used in this study.

Adsorbent	MeO	Wt. %	z	χ	η_i [a]	η_{th}	ICP_i [b]	ICP_{th}
Zn-oxide/AC	ZnO	100	2+	1.521	10.88	10.88	0.72	0.72
Cr-oxide/AC	Cr_2O_3	100	3+	1.658	9.1	9.1	0.68	0.68
Mn-oxide/AC	Mn_3O_4	91.37	2+	1.493	9.02	9.01	0.67	0.631
			3+	1.674	8.80		0.62	
	α-MnO_2	8.63	4+	1.921	10.6		0.57	
Fe-oxide/AC	γ-Fe_2O_3	100	3+	1.776	12.08	12.08	0.72	0.63
			3+	1.704			0.58	
Co-oxide/AC	Co_3O_4	72	2+	1.587	8.22	8.54	0.65	0.63
			3+	1.791	8.9		0.60	
	CoO	28	2+	1.587	8.22		0.65	
Cu-oxide/AC	CuO	83.5	2+	1.671	8.27	7.91	0.55	0.58
	Cu_2O	16.5	1+	1.501	6.28		0.67	
Ni-oxide/AC	NiO	100	2+	1.573	8.5	8.5	0.52	0.52

[a] Data obtained from Pearson [103], with the permission from American Chemical Society.

[b] Values obtained in this study and can be referenced to those obtained in Lebouteiller and Courtine [107].

The percentage sulfur removal obtained using the various metal oxide adsorbents at low and high temperatures was plotted against the Pearson Lewis acidty hardness (η_{th}) and ionic covalent parameters (ICP_{th}) values of the adsorbent (**Figure 4.11**). No correlation was established between Pearson Lewis acid hardness of the metal oxides and percentage sulfur removal at high and low process temperature; where resultant linear correlations ranged between r = -0.465 and -0.477, while squared regression coefficients were observed at R^2 = 0.216 and 0.227. However, a strong linear relationship was observed between metal oxide cation ionic covalent parameter (ICP). In correlation with Portier's ICP theory, the adsorption of intermediate Lewis acid sulfur compounds became more favourable as the ICP and subsequent Lewis acidity hardness of the adsorbents decreased. This was validated by the strong negative correlation values $r \leq -0.955$ and $R^2 \geq 0.912$ values obtained from the plots. An ICP value of 0.621 was obtained for Co_3O_4, where the overall adsorbent ICP_{th} increased to 0.63 due to the presence of CoO. An ICP value of 0.636 was obtained for Mn_3O_4, where the presence of α-MnO_2 decreased the overall adsorbent ICP_{th} to 0.631. The similar ICP obtained for the Fe-oxide/AC, Mn-oxide/AC and Co-oxide/AC adsorbents might be attributed to the formation of mixed metal oxides. These findings suggested that the ICP was a more accurate scale to measure the Lewis acidic strength of metal oxides with different crystal structures and metal geometries and subsequent desulfurization performance adsorbents. In contrast to Lewis acidity derived from Pearson's Absolute hardness theory, the Lewis acidity derived from Portier's ICP theory took into consideration the changes in Lewis acid strength of metal oxides due to both the covalent (electronegativity) and ionic (polarizing power) forces caused by the metal cation crystallographic arrangements and electronic conditions, such as oxidation state, co-ordination number, ionic radius and spin state. For example, according to Pearson's theory ZnO with an oxidation state of Zn^{2+} has a Lewis acidity hardness of 10.88, irrespective of its crystallographic arrangements. However, ZnO with a wurzite structure has an ICP of 0.72 and rock salt ZnO with a face centred cubic arrangement has an ICP value of 0.60 [107], where the Lewis acidity hardness of the metal oxide increases with the ICP value of the metal oxide.

Moreover, the dehydroxylation of metal oxide surfaces leads to coordinately unsaturated (cus) Lewis acid site formation, in the form of metal cations [126]. Acid–base interaction can occur through the donation of the sulfur atom lone pair electrons to the metal oxide cation, or through π-complex formation between the delocalised π-electrons of the sulfur compounds aromatic rings and the metal oxide cation [63]. However, hard Lewis cations are more stable and surrounded by closed packed oxygen anions which sterically shield off the metal cations. This steric phenomenon prevents or weakens the binding of Lewis bases to the cations during acid–base interactions. Also, owing to their high stability, the metal oxides do not readily reduce to form coordinately unsaturated (cus) Lewis acid sites [127].

The Zn-oxide/AC adsorbent contained ZnO (wurzite structure), with Zn^{2+} cations in tetrahedral coordination with oxygen [128]. The Mn-oxide/AC contained Mn_3O_4 and α-MnO_2 with Mn^{2+} coordinated to oxygen in tetrahedral geometric arrangement and Mn^{3+} Mn^{4+} cations coordinated to oxygen in octahedral geometric arrangements [129, 130]. The Fe-oxide/AC adsorbent contained γ-Fe_2O_3 (space group 212 : P4332) with a formula of $Fe_8(Fe_{13\ 1/3}\square_{2\ 2/3})O_{32}$, where the 8 Fe^{3+} and 13 1/3 Fe^{3+} are in trihedral and octahedral coordination with oxygen, respectively; and $\square_{2\ 2/3}$ represents vacant Fe^{3+} octahedral sites [131]. The Co-oxide-AC adsorbent contained Co_3O_4 and CoO with Co^{2+} coordinated to oxygen in tetrahedral geometric arrangement and Co^{3+} cations at low-spin state coordinated to oxygen in octahedral geometric arrangements [132]. Therefore, the lower Lewis acidity transmittance identified through pyridine ion adsorption and decreased adsorption of sulfur compounds in these adsorbents was also attributed to oxygen anion steric hindrances and the limited formation of coordinately unsaturated acid sites, in addition to cation Lewis acidity hardness [101]. In contrast, the Ni-oxide/AC and Cu-oxide/AC adsorbents which contained cubic NiO with face-centred Ni^{2+} and monoclinic CuO with base-centred Cu^{2+} were less susceptible to oxygen steric shielding [133, 134].

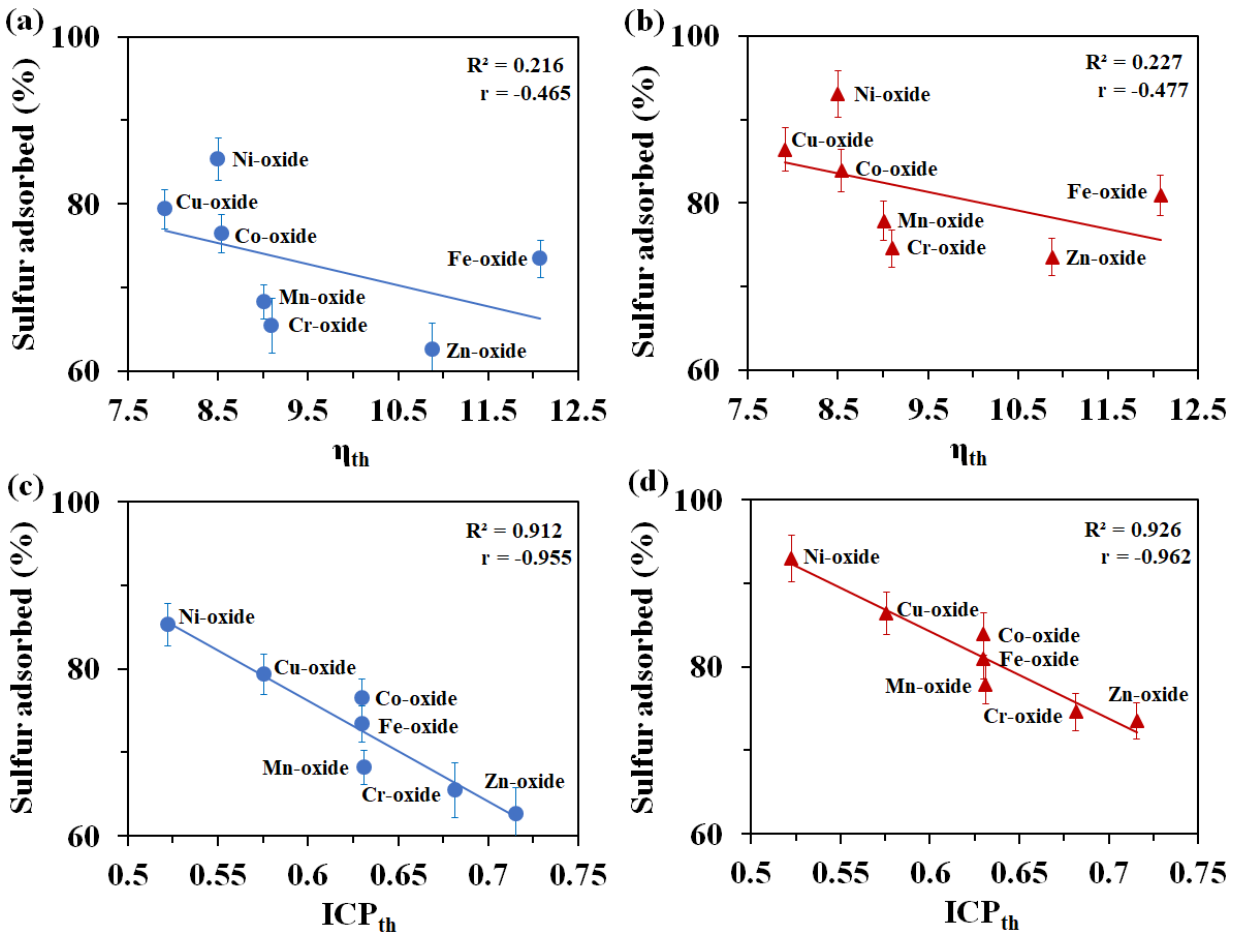

Figure 4.11: Linear relationship between percentage sulfur removal at (a) 30 °C and (b) 60 °C versus overall Pearson hardness ($\boldsymbol{\eta}$), and (c) 30 °C and (d) 60 °C versus overall ionic-covalent parameter (ICP) of metal oxide cation (10 wt. % metal loading, 30 g model diesel, 3 g adsorbent, for 3 hrs).

4.3.3 Adsorption evaluation of commercial diesel

4.3.3.1 Effects of contact time on adsorptive desulfurization

The ADS of commercial diesel was conducted in batch mode at a temperature of 30 °C using unmodified AC and the metal oxide/AC adsorbents. The amount of total sulfur adsorbed was highest for the Ni-oxide/AC adsorbent with 95.17 % removal, where adsorbent desulfurization activity followed the order Ni-oxide/AC > Cu-oxide/AC > Co-oxide/AC > Fe-oxide/AC Mn-oxide/AC > Cr-oxide/AC > Zn-oxide/AC > AC. The addition of metal oxides onto AC led to an increase in the removal of the most steric sulfur compounds, where more than 80 % of these compounds was adsorbed after only 1 hour (see **Figure 4.12**), in contrast to unmodified AC, which had only 70 % sulfur removal within the first hour. The selectivity of sulfur compounds (see **Table 4.3**) when Ni-oxide/AC, Cu-oxide/AC, Co-oxide/AC, and Fe-oxide/AC adsorbents were used decreased in the order of 4-MDBT ≥ 1,4,6-TMDBT > 3,4,6-TMDBT > 4-E,6-MDBT > 2,4,6-TMDBT > 4,6-DMDBT. For Mn-oxide/AC, Cr-oxide/AC, and Zn-oxide/AC adsorbents, selectivity decreased in the order of 4-MDBT > 1,4,6-TMDBT > 3,4,6-TMDBT > 4-E,6-MDBT > 2,4,6-TMDBT > 4,6-DMDBT. Noticeably, the Ni-oxide/AC, Cu-oxide/AC, Co-oxide/AC and Fe-oxide/AC adsorbents had a higher selectivity for 1,4,6-TMDBT, where the compound was completely removed within the initial 60 minutes of adsorption. The lower adsorbent selectivity for 4,6-DMDBT was a results of increased steric hindrance in the 4,6 position and lower electron density relative to other sulfur compounds with similar hindrance but extra methyl groups. In contrast, the unmodified AC adsorbent selectivity decreased in the order of 4-MDBT >> 1,4,6-TMDBT > 3,4,6-TMDBT >4,6-DMDBT ~ 2,4,6-TMDBT ~ 4-E,6–MDBT, where the higher selectivity for 4 MDBT was attributed to smaller molecular size, which facilitated its intra-particle diffusion into the pores of the AC. The diesel used contained 4-E,6-MDBT with the bulkier ethyl group; and although it contributed to only 12.3 % of the untreated fuel's total sulfur concentration, it was the most difficult to adsorb using unmodified AC at 73.57 % removal. However, there was a substantial increase in adsorbent selectivity upon the incorporation of metal oxides, where 4-E,6-MDBT removal ranged between 77.56 % and 93.97 %. It has been suggested that DBT derivatives with alkyl groups in both 4- and 6- positions such 4,6-DMDBT, 4-E,6-MDBT, 2,4,6-TMDBT, 1,4,6-TMDBT, and 3,4,6-TMDBT, are more susceptible to steric hindrance, due to the size of the alkyl group and steric shielding of the sulfur atom by the substituent [135, 136]. Nonetheless,

taking into account that these 4,6- substituent DBT molecules were equivalent to 73 % of the total sulfur content in the diesel, the uptake of these compounds was still high and ranged between 73.57 % and 80.96 % using AC and between 75.19 % and 100 % using the metal oxide/AC adsorbent. When metal oxides were incorporated onto the AC, all of the 2,6/3,6-DMDBT, 1,4/1,6-DMDBT, and C4DBT/C5DBT (heavier DBTs with more than four total carbons in their alkyl groups) compounds were removed in the first 10 minutes of desulfurization. There was a noticeable trend in adsorbent selectivity (**Table 4.3**), where the selectivity of individual sulfur compounds increased with as the adsorbent ICP_{th} decreased (overall ionic-covalent parameter of the mixed metal oxide).

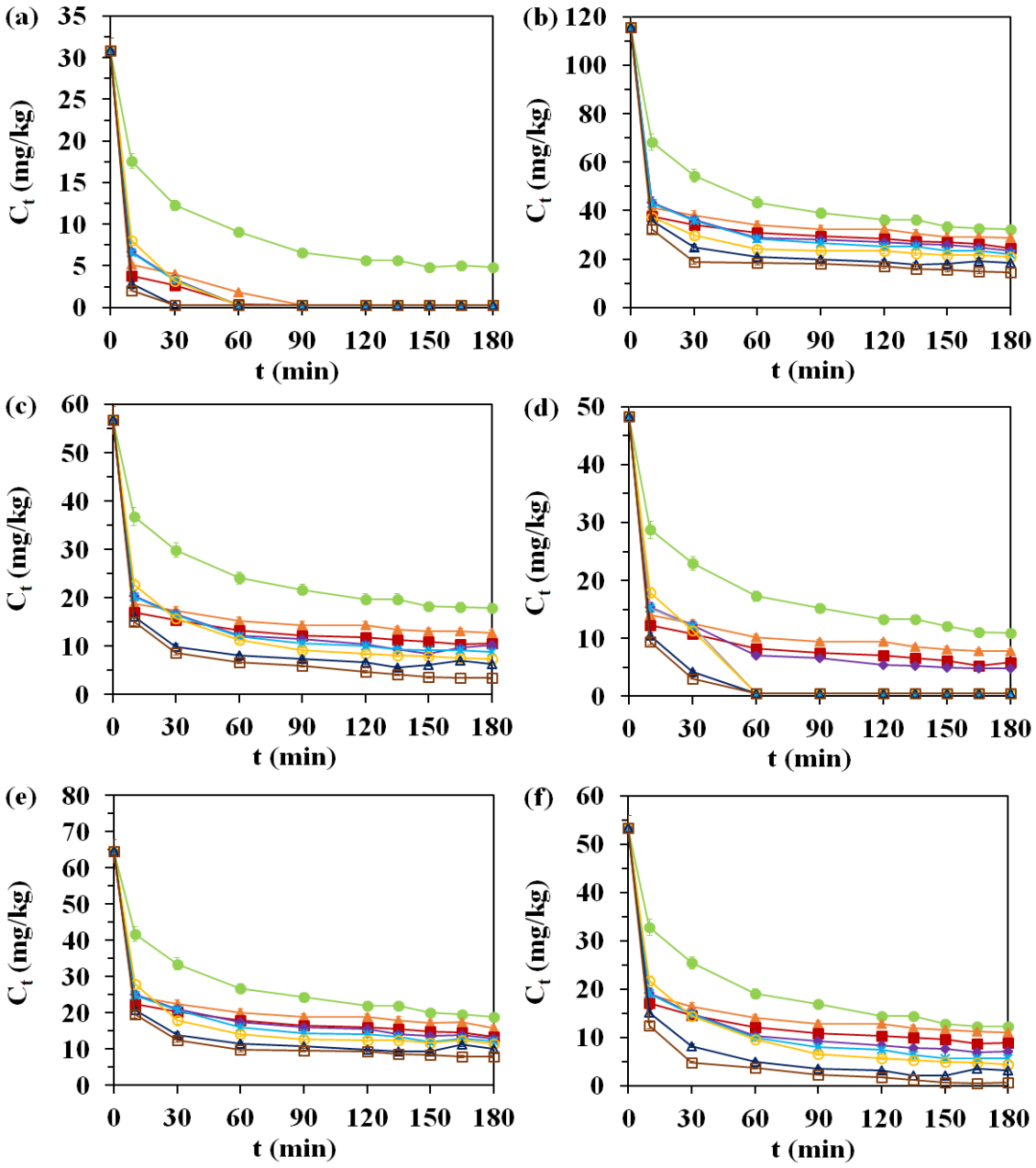

Figure 4.12: A comparison of the reduction in concentrations of steric sulfur compounds (a) 4-MDBT, (b) 4,6-DMDBT, (c) 4-E,6-MDBT, (d) 1,4,6-TMDBT, (e) 2,4,6-TMDBT, (f) 3,4,6 –TMDBT (10wt. % metal loading, 30 g commercial diesel, 3 g adsorbent, at 30 °C for 3 hrs).

Table 4.3: Equilibrium adsorbent selectivity of metal-oxide/AC and AC adsorbents in ADS of commercial diesel, with 2,6/3,6-DMDBT as a reference compound.

	Adsorbent							
ICP_{th} Compound	**AC**	**Zn-oxide/AC**	**Cr-oxide/AC**	**Mn-oxide/AC**	**Fe-oxide/AC**	**Co-oxide/AC**	**Cu-oxide/AC**	**Ni-oxide/AC**
		0.72	**0.68**	**0.631**	**0.63**	**0.63**	**0.58**	**0.52**
4,6-DMDBT	0.029	0.03	0.038	0.039	0.043	0.046	0.053	0.07
4-E,6-MDBT	0.028	0.035	0.044	0.045	0.055	0.067	0.081	0.158
2,4,6-TMDBT	0.029	0.031	0.035	0.04	0.043	0.047	0.054	0.077
1,4,6-TMDBT	0.043	0.0522	0.074	0.092	1	1	1	1
3,4,6-TMDBT	0.034	0.039	0.051	0.066	0.085	0.113	0.164	0.842
4-MDBT	0.098	1	1	1	1	1	1	1
2,6/3,6-DMDBT	1	1	1	1	1	1	1	1

4.3.3.2 Adsorption kinetics

A summary of the kinetic parameters determined for the desulfurization of commercial diesel using the metal-oxide/AC and AC adsorbents is given in **Table 4.4**. The parameters were derived from the linear plots of the pseudo first and second order models shown in **Figure 4.13a** and **Figure 4.13b**, respectively. The pseudo-first order model was a satisfactory fit for unmodified AC, with $R^2 = 0.942$. However, the linear plots of the pseudo-first order model resulted in squared regressions ranging between $R^2 = 0.659$ to $R^2 = 0.922$ for the metal-oxide/AC adsorbents; with calculated values of q_e lower than the experimental values. This suggested that, for unmodified AC, adsorbent physical adsorption played a role in controlling the adsorption rate. In contrast, the pseudo-second order model correlated well with the experimental data, where coefficients (R^2) were > 0.99 for all used adsorbents (**Table 4.4**). This implies that the adsorption process occurred through chemisorption reactions. These results are comparable to those reported by Safieh et al. [137], in the selective adsorption of DBT in commercial diesel using AC loaded with MnO_2, where the adsorption kinetics was described by the pseudo second-order model. The experimental data was also fitted to the Elovich equation, where the linear plots of q_t vs In q_t are illustrated in **Figure**

4.13c. The squared regression coefficients obtained for the Elovich model ranged between R^2 = 0.952 to R^2 = 0.994, which further confirms that chemisorption was the controlling mechanism where the metal oxides on the AC surface acting as active adsorption sites. Moreover, the initial adsorption rate α ($mg.g^{-1}min^{-1}$) increased substantially from 5.044 $mg.g^{-1}min^{-1}$ in unmodified AC, to between 1×10^4 and 1.1×10^9 $mg.g^{-1}min^{-1}$, when the metal oxides/AC adsorbents were used. Similarly, in Aribike et al. [99], the Elovich model best described the ADS of commercial diesel using activated sewage sludge at different temperatures levels, where R^2 values ranged between 0.94 - 0.97. The Weber-Morris equation [110] was used to determine the role of intra-particle diffusion in the sulfur adsorption process. The intra-particle diffusion plots (**Figure 4.13d**,) of all the adsorbents were nonlinear, but were related as three different straight lines. This indicates that adsorption occurred in three stages, with each representing a separate adsorption controlling mechanism. The first stage represented the rapid external surface adsorption of the sulfur compounds occurring through readily available active sites on the adsorbent surface, which was complete within the initial 60 minutes for all the adsorbent used. The second stage represented the slower intra-particle diffusion of the sulfur compounds into the adsorbent pores and matrix [138], which occurred between 60 and 120 minutes. The intra-particle diffusion correlation coefficient ranged between R^2 = 0.931 and R^2 = 0.999. However, intra-particle diffusion was not the only rate-controlling mechanism, as the linear plots of the second stage did not meet the origin [86]. The third stage is when intra-particle diffusion lessens and adsorption equilibrium is reached [139]. A rate constant (k_i) of 0.088 $mg.g^{-1}min^{-0.5}$ was obtained using unmodified AC (**Table. 4.4**) which is higher than those of the metal oxide/AC adsorbents, with a noticeable increase seen in the adsorption capacity of the AC during the intra-particle diffusion stage. This suggests that in the AC adsorbent, the adsorption that occurred in the pores of the AC could not be neglected and that it played a significant role in controlling the adsorption rate. This was further validated through a comparison of boundary layer constants C ($mg.g^{-1}$) in **Table 4.4**, which showed that the boundary layer effect related to adsorption occurring via surface diffusion [139]. It was more prominent in the metal oxide/AC adsorbents ($C \geq 3.34$ mg/g), but much lower for the unmodified AC (C = 1.75 mg/g). Similar observations on adsorption kinetics occurring in three stages have been reported on [138, 139].

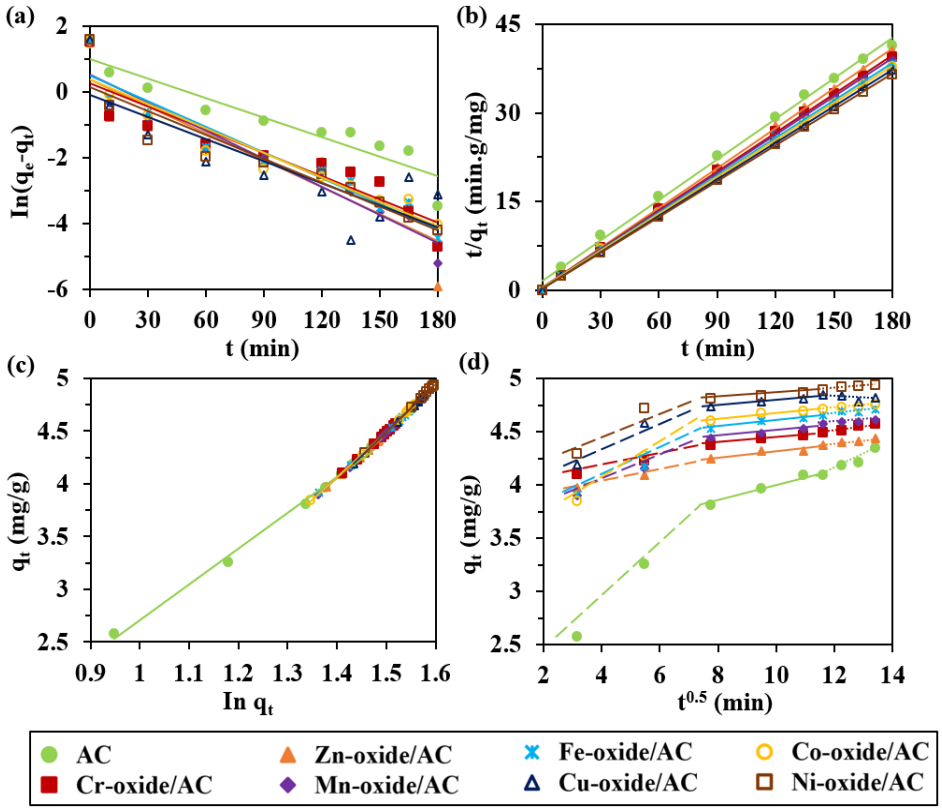

Figure 4.13: Comparison of the best fit straight lines for (a) pseudo-first order, (b) pseudo-second order (c) Elovich model, and (d) Weber–Morris plots obtained using metal oxide/AC adsorbents and unmodified AC (10 wt. % metal loading, 30 g commercial diesel, 3 g adsorbent, at 30 °C for 3 hrs).

Table 4.4: Kinetic parameters obtained for desulfurization of commercial diesel using various adsorbents at 30 °C.

Model	Parameter	Adsorbent							
		AC	Zn-oxide/AC	Cr-oxide/AC	Mn-oxide/AC	Fe-oxide/AC	Co-oxide/AC	Cu-oxide/AC	Ni-oxide/AC
Pseudo-1st order	$q_{e\ exp}$ (mg.g^{-1})	4.35	4.43	4.56	4.62	4.72	4.76	4.82	4.94
	$q_{e\ cal}$ (mg.g^{-1})	2.72	1.32	1.32	1.68	1.87	1.58	0.94	1.18
	k_1 (min^{-1})	0.019	0.026	0.024	0.03	0.030	0.027	0.025	0.02
	R^2	0.942	0.881	0.847	0.922	0.912	0.921	0.659	0.865
Pseudo-2nd order	$q_{e\ exp}$ (mg.g^{-1})	4.35	4.43	4.56	4.62	4.72	4.76	4.82	4.94
	$q_{e\ cal}$ (mg.g^{-1})	4.25	4.45	4.57	4.65	4.74	4.79	4.82	4.96
	k_2 (min^{-1})	0.09	0.128	0.124	0.102	0.099	0.100	0.197	0.153
	R^2	0.996	0.999	0.999	0.999	0.999	0.999	0.999	0.999
Elovich	$1/\beta$ (mg.g^{-1})	0.59	0.16	0.17	0.26	0.29	0.31	0.22	0.21
	α (mg.g^{-1}min^{-1})	5.044	5.7×10^{8}	1.1×10^{9}	1.5×10^{5}	2.8×10^{4}	1×10^{4}	1.9×10^{7}	6.2×10^{7}
	R^2	0.982	0.988	0.987	0.982	0.969	0.952	0.991	0.994
Weber-Morris	C (mg.g^{-1})	1.75	3.78	3.99	3.79	3.46	3.34	3.85	4.31
	k_i (mg.g^{-1}min$^{-0.5}$)	0.088	0.024	0.044	0.066	0.030	0.029	0.022	0.05
	R^2	0.999	0.973	0.979	0.916	0.969	0.931	0.999	0.795

4.3.3.3 Evaluation of breakthrough curves

The breakthrough curves of the sufur compounds which were present commercial diesel in the highest concentration or were the most steric, over AC and Ni-oxide/AC adsorbents at ambient temperature and 0.31 h^{-1} LHSV are illustrated in **Figure 4.14a** and **Figure 4.14b**. A comparative observation of the two figures showed that when NiO was loaded onto the AC, the breakthrough of 4,6-DMDBT, 4-E,6-MDBT and 2,4,6 -TMDBT increased from 1.476 g-diesel/g-adsorbent to 1.968 g-diesel/g-adsorbent. Similarly, the breakthrough of 4-MDBT was 1.968 g-diesel/g-adsorbent in the AC; however, the Ni-oxide/AC breakthrough point was notably higher at 3.936 g-diesel/g-adsorbent. The observed increase in adsorption capacity with Ni-oxide addition was consistent with the results obtained in the batch-mode ADS. Bu et al.[82] obtained a breakthrough of approximately 1.26 g-diesel/g-adsorbent for 4,6 –DMDBT and 1.68 g-diesel/g-adsorbent for total sulfur in commercial diesel with 400 ppmw sulfur content, using AC and a LHSV of 0.5 h^{-1}.

A summary of the breakthrough model parameters and correlation coefficients obtained for the fixed-bed desulfurization of commercial diesel using the Ni-oxide/AC and AC adsorbents is provided in **Table 4.5**. The values were calculated from the linear regression analysis of the breakthrough models. The breakthrough curves obtained using AC (**Figure 4.14c**) were best described by the Yoon-Nelson model and the Thomas model, which suggested that a decrease in the AC adsorption rate was directly proportional to the sulfur compounds adsorption and their breakthrough. However, to a noticeable extent the adsorption also correlated to Langmuir kinetics, where the adsorption rate followed second-order reversible kinetics without axial dispersion [140]. ADS using the Ni-oxide adsorbent (**Figure 4.14d**) was best described by the filtration advection–dispersion equation, where $C_t/C_o < 1$. This suggests that adsorption was kinetic-driven, where largely irreversible interactions (strong van der Waals, steric, Lewis acid–base) occurred between the adsorbent and sulfur compounds, competitive adsorption interactions were mitigated and a continuous increase in the adsorbent bed length would have eventually resulted in $C_t/C_o = 0$. A comparison of adsorbent breakthrough rate constants showed that the AC would have reached saturation at a faster rate than the Ni-oxide/AC adsorbent. Furthermore, a comparison of the τ_{YN} values in **Table 4.5** suggested that the Ni-oxide/AC adsorbent had a higher adsorption capacity than that of unmodified AC, because adsorption capacity is directly proportional to τ_{YN} (min) [141]. These findings showed that the fixed-bed ADS performance of the Ni-oxide/AC adsorbent was superior to that of unmodified AC.

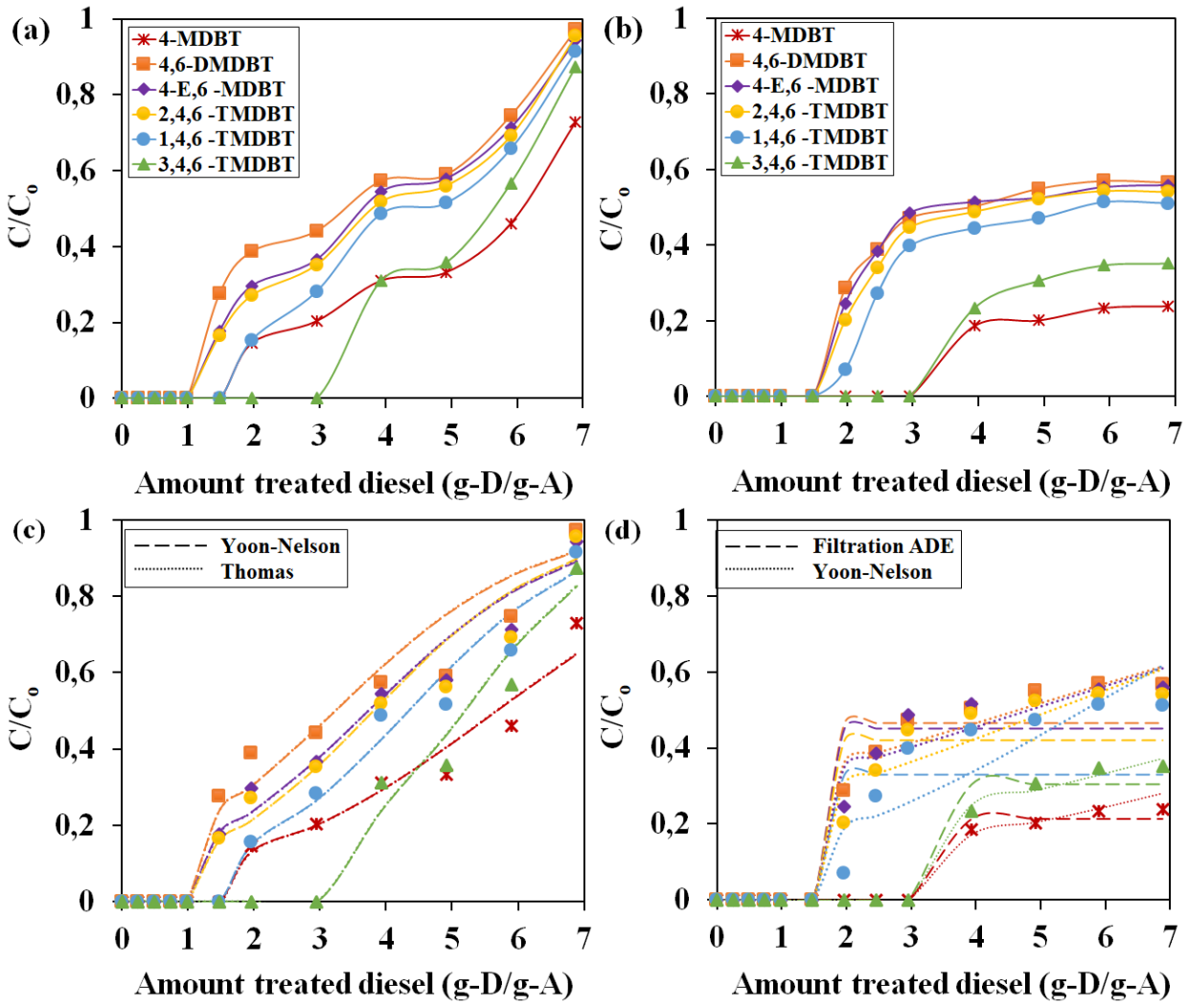

Figure 4.14: Sulfur adsorption breakthrough curve of commercial diesel when using (a) unmodified AC, and (b) Ni-Oxide/AC adsorbents. Fitted model breakthrough curves of sulfur compounds in commercial diesel using (c) AC and (d) Ni-Oxide/AC. (10 wt. % metal loading, fuel LHSV of 0.31 h^{-1}, at ambient temperature for 7 hrs).

Table 4.5: Parameters obtained for the breakthrough models using AC and Ni-oxide/AC adsorbents (10 wt. % metal loading, fuel LHSV of 0.31 h^{-1}, at ambient temperature and pressure for 7 hrs).

Adsorbent	Model	Parameter	Sulfur Compound					
			4-MDBT	4,6-DMDBT	4-E,6 – MDBT	2,4,6 - TMDBT	1,4,6 - TMDBT	3,4,6 - TMDBT
AC	Thomas	q_{Th} (mg/g)	0.175	0.374	0.212	0.247	0.209	0.277
		k_{Th} (ml/min.mg)	0.329	0.114	0.236	0.217	0.303	0.345
		R^2	0.929	0.811	0.907	0.884	0.929	0.886
	Yoon-Nelson	τ_{YN} (min)	345.9	196.9	227.6	232.5	264.7	316.4
		k_{YN} (min^{-1})	0.008	0.011	0.011	0.012	0.012	0.015
		R^2	0.977	0.879	0.914	0.888	0.931	0.896
Ni-oxide/ AC	Filtration	k_f (min^{-1})	0.008	0.004	0.004	0.005	0.006	0.006
	ADE	R^2	0.999	0.933	0.922	0.919	0.813	0.997
	Yoon-Nelson	τ_{YN} (min)	688.4	282.7	293.9	315.9	346.2	585.6
		k_{YN} (min^{-1})	0.004	0.004	0.004	0.004	0.006	0.0032
		R^2	0.998	0.816	0.761	0.844	0.792	0.994

4.4 Conclusion

To elucidate further on the relationship between adsorbent desulfurization performance and Pearson's HSAB theory, the present study looked at investigating the removal of refractory sulfur compounds in both commercial and model diesel using period four transition metal oxides loaded on AC. Adsorbent characterization showed that metal oxides were successfully incorporated onto the surface of AC in various weight percentages and crystallography configurations. The adsorption of sulfur compound occurred via Lewis acid active sites of the metal oxides, where the loading of metal oxides significantly enhanced the sulfur adsorption capacity of AC and increased its selectivity for steric sulfur compounds in commercial diesel. A clear relationship was established between adsorbent Lewis acidity and adsorbent desulfurization performance using a novel concept in ADS, which suggests that the ICP is a more accurate measure of Lewis acidic strength of transition metal oxides with varying crystallography and therefore better predicts their subsequent desulfurization performance. Results showed that no correlation existed between sulfur

removal and the Pearson hardness η_{th} of the intermediate metal oxide cations. However, a strong inverse linear relationship was observed where sulfur removal decreased as the ICP_{th} of the adsorbent metal oxide increased. Therefore, the decrease in the adsorbents' desulfurization performance was attributed to the increase in ICP-derived Lewis acid hardness of adsorbent metal oxides. The selectivity of steric sulfur compounds in the commercial diesel also increased inversely with adsorbent metal oxide ICP_{th}. The adsorption kinetic of commercial diesel in batch-mode ADS occurred via chemisorption in all the adsorbents used. The fixed-bed ADS of commercial diesel using the unmodified AC and Ni-oxide/AC adsorbents was best described by the Yoon-Nelson model, whereas adsorption using the Ni-oxide/AC adsorbent was correlated using the filtration advection–dispersion equation.

Chapter 5

An investigation into competitive adsorption in a multicomponent diesel system using Nickel Oxide /Activated Carbon

Part of this work was presented at the following conferences:

- *International Workshop on Porous Materials and their Applications, Council for Scientific and Industrial Research, Pretoria, South Africa, 2018*
- *CATSA, Limpopo province, South Africa, November 2018*

5.1 Introduction

Selective adsorptive desulfurization (ADS) has received increased attention. In contrast to the HDS process, the main advantage of ADS is that the process can be carried out at ambient conditions, without the use of costly and hazardous hydrogen gas. Furthermore, the process can effectively remove refractory thiophene compounds in fuels leading to treated diesel with sulfur concentration < 1 ppmw [142]. The challenge thus far has been in developing a desulfurization adsorbent with increased selectivity and adsorption capacity for the larger, more steric, sulfur species in diesel, while having a simple and effective regeneration route [9, 12]. Numerous studies have reported on ADS using various transition metals ions including Cu, Mn, Ce and Ag, dispersed onto different inorganic supports, e.g., molecular sieves, zeolite and titania alumina [117, 124, 143, 144]. Although most transition metals can enhance ADS through π-complexation in addition to sulfur-metal interactions, Ni has shown great potential in the ADS of refractory sulfur species due to its ability to react readily with sulfur to produce nickel sulfides [145, 146] and form pi-bonds [147]. The improvement in activity upon addition of Ni has been observed in different systems: Zeolite [148, 149] , MOFs [147], aluminosilicates [150], and Ni/carbon materials [151]. The Ni modified adsorbents have shown a higher selectivity for sulfur removal, which indicated a direct relationship between metal acidity and sulfur adsorption selectivity. Proper understanding and interpretation of adsorption isotherms is crucial for the overall improvement of adsorbents and effective design of adsorption system [152].

The understanding of multicomponent adsorption is of significance in ADS. This is because diesel contains varying concentrations of organic sulfur compounds, which leads to various interactions between the compounds during adsorption. The adsorption of a particular sulfur compound is affected by the presence of other compounds due to the size, structure and the position of the alkyl groups on the sulfur compounds in addition to the number of adsorbent active sites and porosity. Therefore, single component isotherm models are not applicable to a multicomponent ADS systems [58].To date only two studies have been published on binary isothermal modeling of the diesel ADS process. Thaligari et al. [153] looked at binary isothermal modeling in the ADS of DBT and quinolone in model diesel using Zn impregnated AC, and found that adsorption equilibrium was best described by the Redlich–Peterson isotherm. Bamufleh [13] in his use of granular AC adsorbent activated using ZnCl showed that the binary ADS of model diesel containing 4,6-DMDBT and DBT correlates to the ideal adsorption solution theory (IAST) Langmuir isotherm. However, the modelling of competitive adsorptive interactions between only two sulfur compounds in diesel is an inadequate comparison as in diesel contains a variety of sulfur compounds in varying concentrations.

In this Chapter we reported for the first time on using extended multicomponent isotherms in ADS systems, as well as empirical kinetic and thermodynamic models. With the aim of showing how the incorporation of transition metal oxides (NiO) onto AC effected competitive interactions in the ADS of model diesel containing three sulfur compounds DBT, 4-MDBT and the more steric 4,6-DMDBT. The data was fitted into the following isotherm models: extended Langmuir, modified competitive Langmuir, extended Freundlich and Sheindorf-Rebuhn-Sheintuch. The physiochemical properties, structure and morphology of the adsorbents were also investigated, using various characterization techniques.

5.2 Materials and methods

The methods used in preparing the diesel and adsorbents used in this chapter are outlined in **Chapter 3, section 3.2**. The adsorbents characterization techniques and treated diesel analysis methods are outlined in **Chapter 3, section 3.3** and **section 3.5**, respectively.

5.2.1 Adsorption procedure

All prepared adsorbents were dried in a muffle furnace at 110 ℃ in order to evaporate any physically adsorbed atmospheric moisture before being used in the batch experiments. The adsorbents were weighed, and then added to a 3-neck round-bottom flask containing 30 g of the model diesel. The adsorbent/fuel mixture was stirred at 1200 rpm in these experiments using a heated magnetic stirrer, equipped with a temperature controlling thermocouple. All the experiments lasted for a duration of 3 hours. The adsorption experiments were grouped into three sets:

1) Investigating the effect of Ni loading and adsorbent dosage on sulfur removal using model diesel M1 at 30 °C. Ni(x%)O/AC was used to present the NiO supported on AC, where x% refers to the Ni loading in the adsorbent was x% by weight. In this research, x% equaled to 2.5%, 5%, 10%, or 15%.
2) Equilibrium isothermal experiments were performed at 30 °C using model diesel M2, M3, M4 or M5, where, for each type of model diesel four experiments were carried out using varying amounts of adsorbent loading (2.5, 5, 7.5 and 10 wt. % of fuel).
3) Adsorption thermodynamic and kinetic analysis at temperatures ranging from 30 °C to 75 °C using model diesel M1.

A detailed description of the experimental procedures is provided in **Appendix A.3**.

5.2.2 Adsorption studies

5.2.2.1 Multicomponent equilibrium isotherms

As stated earlier, the understanding of multicomponent adsorption is of significance in ADS. Therefore, in this chapter the relationship between the adsorption capacities of a specific sulfur compound in the presence of the other compounds in multicomponent model diesel was investigated. This was archived using four multicomponent isotherm models.

The extended Langmuir isotherms model was derived on the basis that all the adsorbent active site of are the same and equally available to the adsorbates, the adsorbates do not interact and they adsorb on the same active sites [154]. The isotherm model is given by:

$$q_{e,i} = \frac{q_{m,i}K_{L,i}C_{e,i}}{1+\sum_{j=1}^{N}(K_{L,j}C_{e,j})} \quad (5.1)$$

Where, the equilibrium adsorption capacity and concentration of sulfur compound *i* obtained from the ADS of multicomponent diesel M2 are represented as $q_{e,i}$ (mg.g^{-1}) and $C_{e,i}$ (mg.kg^{-1}), respectively. The monolayer adsorption capacity of sulfur compound *i*, is represented as $q_{m,i}$ (mg.g^{-1}), the Langmuir model constant is shown as $K_{L,i}$ (kg.mg^{-1}). The parameters q_m and K_L of each sulfur compound were determined using the non-linear regression analysis of q_e vs C_e.

The modified competitive Langmuir isotherm model was derived on the basis that, in addition to competition occurring between the adsorbate, the adsorption process in also influenced by interactions occurring between the adsorbates. Therefore, an interaction factor (η) is used to describe the adsorption process [155].The model is expressed as:

$$q_{e,i} = \frac{q_{m,i}K_{L,i}\left(\frac{C_{e,i}}{\eta_{L,i}}\right)}{1+\sum_{j=1}^{N}\left(K_{L,j}\left(\frac{C_{e,j}}{\eta_{L,i}}\right)\right)} \quad (5.2)$$

Where, the equilibrium adsorption capacity and concentration of sulfur compound *i* obtained in the ADS of multicomponent diesel M2 are represented as $q_{e,i}$ (mg.g^{-1}) and $C_{e,i}$ (mg.kg^{-1}), respectively. The monolayer adsorption capacity $q_{m,i}$ (mg.g^{-1}) and Langmuir model constant $K_{L,i}$ (kg.mg^{-1}) of sulfur compound *i*, were obtained from the ADS of single component diesel (model diesel M3, M4 and M5). The interaction factor η of each sulfur compound was determined using the non-linear regression analysis of q_e vs C_e.

The extended Freundlich isotherm model based on the assumptions that the adsorption process in heterogeneous and interactions occur between the adsorbates [156].The model is given by:

$$q_{e,i} = \frac{k_{F,i}C_{e,i}^{\left(1/n_i\right)+x_i}}{C_{e,i}^{x_i}+y_iC_{e,j}^{z_i}} \quad (5.3)$$

Where, the equilibrium adsorption capacity and concentration of sulfur compound *i* obtained from the ADS of multicomponent diesel M2 are represented as $q_{e,i}$ (mg.g^{-1}) and $C_{e,i}$ (mg.kg^{-1}), respectively. The adsorption intensity and Freundlich constant of sulfur compound *i* are represented as $n_{,i}$ and $k_{F,i}$ (mg.g^{-1}), respectively. Both parameters were derived from the data of

single-component Freundlich models. The parameters x_i, z_i and y_i were determined using the non-linear regression analysis of q_e vs C_e.

The Sheindorf-Rebuhn-Sheintuch equation is a competitive model derived from Freundlich isotherm model [156]. The assumptions made by the Sheindorf-Rebuhn-Sheintuch equation (corresponding to **Equation 5.4**) is that there is an exponential distribution of adsorption energies for each adsorbate, where the distribution is proportional to the distribution in the single-component adsorption process. Therefore, a competition factor (α_{ij}) was used to determine the extent of competitive adsorption occurring in sulfur compound *i* in the presence of sulfur compound *j* [157].

$$q_{e,i} = k_{F,i} C_{e,i} \left(\sum_{j=1\ j\neq i}^{N} \left(C_{e,i} + a_{i,j} C_{e,j} \right) \right)^{\left(1/n_i\right)-1} \quad (5.4)$$

Where, the equilibrium adsorption capacity and concentration of sulfur compound *i* obtained from the ADS of multicomponent diesel M2 are represented as $q_{e,i}$ (mg.g^{-1}) and $C_{e,i}$ (mg.kg^{-1}), respectively. The adsorption intensity and Freundlich constant of sulfur compound *i* are represented as $n_{,i}$ and $k_{F,i}$ (mg.g^{-1}), respectively. Both parameters were derived from the data of single-component Freundlich models. The competition factor (α_{ij}) of sulfur compound was determined using the non-linear regression analysis of q_e vs C_e. The competition factor is always equal to or greater than zero, where a higher value indicated a greater extent of competition [157].

Adsorption interactions which occurred between the sulfur compounds were further evaluated using the ratio of adsorption capacities, which is defined as:

$$R_{qi} = \frac{q_{mi}}{q_{oi}} \quad (5.5)$$

Where, q_{mi} is the adsorption capacity of compound *i* in multicomponent model diesel and q_{oi} is the adsorption capacity of compound *i* in the single-component model diesel, treated under the same operating conditions [152]. The ratio describes the type of interaction which occurred between adsorbates in a multicomponent adsorption system. Synergistic interactions occurred when $R_{qi} > 1$, where the presence of other sulfur compounds in the model diesel enhanced the adsorption of sulfur compound *i*. On the contrary, when $R_{qi} < 1$, antagonistic interactions occurred where the other sulfur compounds in the model diesel inhibited the adsorption of sulfur compound *i*. If no

interactions occurred, $R_{qi} = 1$ and the presence of other compounds in the diesel did not affect the adsorption of sulfur compound *i*.

The sum of squares of the error function (SSE) was used to determine the validity of results obtained for each isotherm, and is given as follows:

$$SSE = \sum_{i=1}^{P} \left(q_{e,cal} - q_{e,exp}\right)_i^2 \quad (5.6)$$

Where, $q_{e,cal}$ (mg/g) is the calculated equilibrium adsorption capacity, and $q_{e,exp}$ (mg/g) is the experimental equilibrium adsorption capacity that was obtained for each sulfur compound.

5.2.2.2 Adsorption kinetics

The transportation of an adsorbate moving from a fluid into the adsorbent pores is a complex phenomenon, and apart from adsorption itself, there are various mass transfer phenomena that occur such as, intra-particle, surface and pore diffusion. To further elucidate on the adsorption kinetics of sulfur compounds in model diesel M1, the experimental data was fitted into the pseudo first and second order models as well as the intra-particle diffusion model.

The initial stage of adsorption is generally described using the Lagergren's pseudo-first-order model, [86]. The linearized model was described in **Chapter 4, Equation 4.4**. The pseudo-second-order model describes the entire adsorption process, and is based on the assumption that the rate of adsorption is limited by chemical interaction [63]. The linearized model was described in **Chapter 4, Equation 4.5**. The kinetics of adsorption of sulfur compounds on the adsorbents can also be described from a mechanical standpoint. Weber and Morris [110] developed the generally accepted intra-particle diffusion model, based on the assumption that the rate at which an adsorbate diffuses towards an adsorbent governs the adsorption process [111]. The linearized model was described in **Chapter 4, Equation 4.7**.

The adsorption activation energy (E_a) was used to determine how temperature affected the adsorption rate of the sulfur compounds [111]. Where E_a is the energy that the sulfur compound must overcome in order to react with the adsorbent molecules or surface functional groups. The Arrhenius equation can be used in showing how the pseudo-second order rate constant (k_2) is dependent on adsorption temperature, and is given by.

$$\ln k_2 = \ln A - \frac{E_a}{RT} \quad (5.7)$$

Where, the pseudo second order rate constant is shown as k_2 [158], E_a is the activation energy (kJ/mol), A is the frequency factor which is a temperature independent constant, R is the universal gas constant ($J.mol^{-1}.K^{-1}$) and T (K) is the adsorption temperature [111]. E_a values were obtained from the slope of plotting ln k_2 vs 1/T. Where, the magnitude of activation energy E_a was used to differentiate between physical or chemical adsorption. In physical adsorption, E_a is usually < 4.2 kJ/mol and the process occurred through weak electrostatic and Van der Waals forces where equilibrium was rapidly achieved [158, 159]. In contrast, strong chemical bonding forces governed the adsorption process if the E_a values ranged between 8.4 to 83.7 kJ/mol in activated chemical adsorption [158, 159].

5.2.2.3 Adsorption thermodynamics

Thermodynamic parameters can be used to determine the adsorption characteristics of most materials. Therefore we used this technique to further elucidate on the nature of the adsorption of sulfur compounds. Gibbs free energy (G) is a fundamental characteristic that indicates whether adsorption is spontaneous at various temperatures. The change in Gibbs free energy (ΔG) was evaluated using **Equation 5.8** [160]:

$$\Delta G = -RTInK_d \quad (5.8)$$

$$K_{d,} = \frac{C_{ad,e}}{C_e} \quad (5.9)$$

Where, the adsorption Gibbs free energy of sulfur compound *I* is represented by ΔG ($kJ.mol^{-1}$). K_d is the adsorption distribution coefficient of compound *i*, defined as the ratio of the concentration of sulfur compound *i* adsorbed onto the solid adsorbent ($C_{ad,e}$), to that of the equilibrium concentration of sulfur compound *i* remaining in the model diesel (C_e) [158]. The temperature of model diesel is represented by T (K) and R (8.314 $J.mol^{-1}.K^{-1}$) is the universal gas constant. The ΔG of the adsorption process was related to the change in enthalpy ΔH and entropy ΔS by:

$$\Delta G = \Delta H - T\Delta S \quad (5.10)$$

The Van't Hoff equation is often used to express the adsorption distribution coefficient (K_d) as a function of temperature [160]:

$$In\ K_d = -\frac{\Delta H}{RT} + \frac{\Delta S}{R} \quad (5.11)$$

Where, the change in enthalpy ΔH of the adsorption process and ΔS is the change in entropy were obtained from the slope and intercept of the Van't Hoff plots [161].

5.3 Results and discussion

5.3.1 Adsorbent characterization

5.3.1.1 BET analysis

The textual parameters of the AC before and after modification with NiO are given in **Table 5.1**. An increase in metal loading resulted in an expected decrease in adsorbent pore volume and surface area. The N_2 adsorption-desorption isotherms of unmodified AC, and NiO/AC adsorbents with varying NiO loadings are shown in **Figure 5.1**. The curves were almost identical and demonstrate characteristics of a type I isotherm with an H4 hysteresis loop occurring in the relative pressure range of 0.4–1.0 [117]. This suggested that the AC contained both micro and mesopores, and the loading of NiO onto its surface did not alter the initial narrow slit-like pore structure of the AC [117].

Table 5.1: BET parameters obtained from N_2 physisorption.

Parameter	Units	Adsorbent				
		AC	**$Ni_{(2.5\%)}O$/AC**	**$Ni_{(5\%)}O$/AC**	**$Ni_{(10\%)}O$/AC**	**$Ni_{(15\%)}O$/AC**
BET Surface Area	m^2/g	997.8	976.2	966.9	843.7	778.8
Total Pore Volume	cm^3/g	0.523	0.505	0.503	0.436	0.403
Average Pore Diameter	nm	2.081	2.089	2.062	2.066	2.061

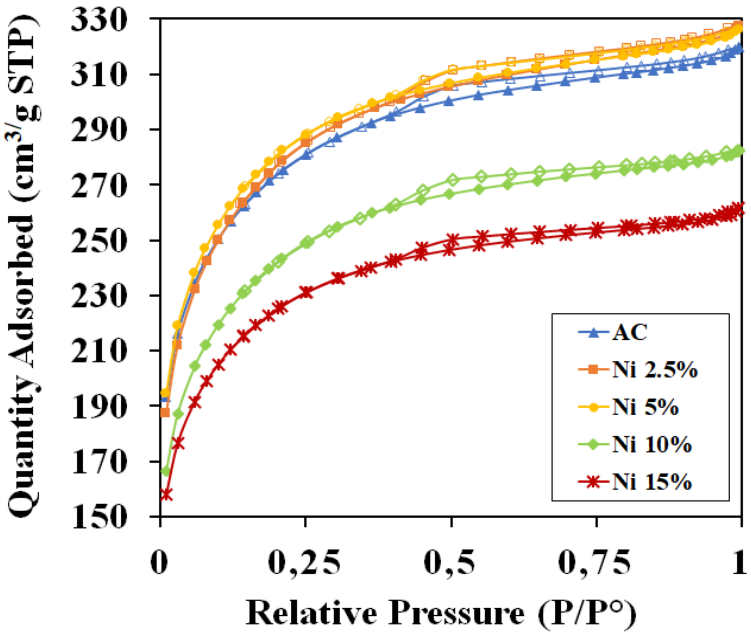

Figure 5.1: The N_2 adsorption-desorption isotherms obtained for unmodified AC and NiO/AC adsorbents with varying percentages of Ni loading.

5.3.1.2 PXRD analysis

The PXRD pattern of the synthesized $Ni_{(10\%)}O$/AC adsorbent is shown in **Figure 5.2**. The x-ray diffraction peaks which appeared at 2θ = 26.68 °, 50.63 °, 59.92 ° were characterized to the (002), (102) and (103) planes of crystalline hexagonal graphite and were indexed to ICDD standards (Card No.00-056-0160) which identified the presence of the granular AC. Buckminsterfullerene carbon arrangement within the AC matrix, were observed at 20.89 ° (ICDD Card No. 00-047-0787).The diffraction peaks which appeared at positions 2θ = 37.07 °, 43.1 °, 62.64 °, 75.36 ° and 79.33 ° were indexed to planes (111), (200), (220), (311) and (222) respectively, which was in accordance with the ICDD standards (ICDD Card No. 01-073-1523) of cubic NiO [162]. The average particle size of NiO was determined as 13.3 nm using the Williamson-Hall method.

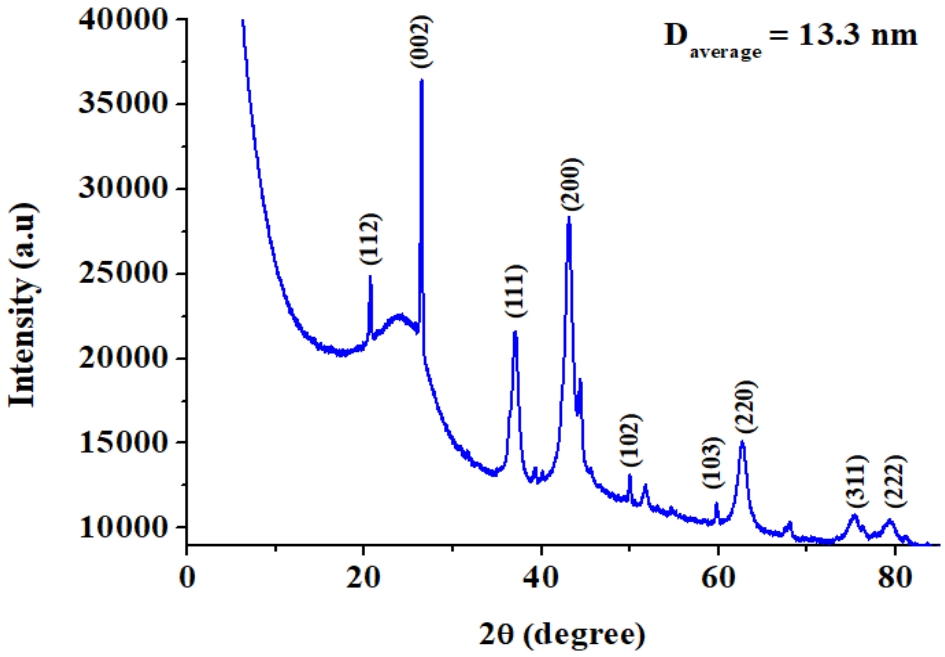

Figure 5.2: The PXRD patterns of the Ni(10%)O/AC adsorbent.

5.3.1.3 HR-TEM and SEM analysis

The morphology of the NiO nanoparticles on the surface of the AC was characterized using HR-TEM analysis. As shown in **Figure 5.3 a and b**, the NiO nanoparticles were cubic and agglomerated to form nanoclusters on the surface of the AC, where agglomeration increased with the amount of metal loaded and/or with the concentration of the $Ni(CH_3CO_2)_2 \cdot 4H_2O$ precursor used. The diameter of a single grain ranged between 8-14 nm, while the clusters had diameters ranging between 20-30 nm. Previous studies suggested that NiO agglomeration was a direct consequence of the precursor salt concentration [163] and thermal reduction temperature [164]. Zhu et al. [165] deduced that agglomeration of NiO nanoparticles occurred due to strong synergistic interactions between the nickel precursor and the carbon support during synthesis, where the synergistic effect directs the orientated growth of nanoparticles. The lattice fringe pattern is shown in **Figure 5.3c**; the value of the d-spacing is 2.39 nm was in accordance with the inter-planar distance of the (111) plane in cubic NiO. The selected area electron diffraction (SAED) pattern obtained for the NiO nanoparticles is shown in **Figure 5.3d**. The observed concentric rings in the SAED pattern showed the polycrystalline nature of the NiO nanoparticles. The outlined ring pattern is assigned to the (111), (200), (220), (311) and (222) planes of cubic NiO, which was consistent with the diffraction pattern of the $Ni_{(10\%)}O$/AC adsorbent.

The SEM images of the $Ni_{(10\%)}O$/AC are shown in **Figure 5.4 a and b**, where the elemental mapping showed NiO dispersed on the AC matrix. The elemental composition of the $Ni_{(10\%)}O$/AC adsorbent was confirmed by EDS analysis (**Figure 5.4c**). The measured weight percent compositions were, 75.77 %, 10.52 % and 13.01 % for carbon (C), nickel (Ni) and oxygen (O), respectively. Moreover, the adsorbent also contained trace amounts (0.7 %) of Si and Al impurities, and were most likely present in the AC source material.

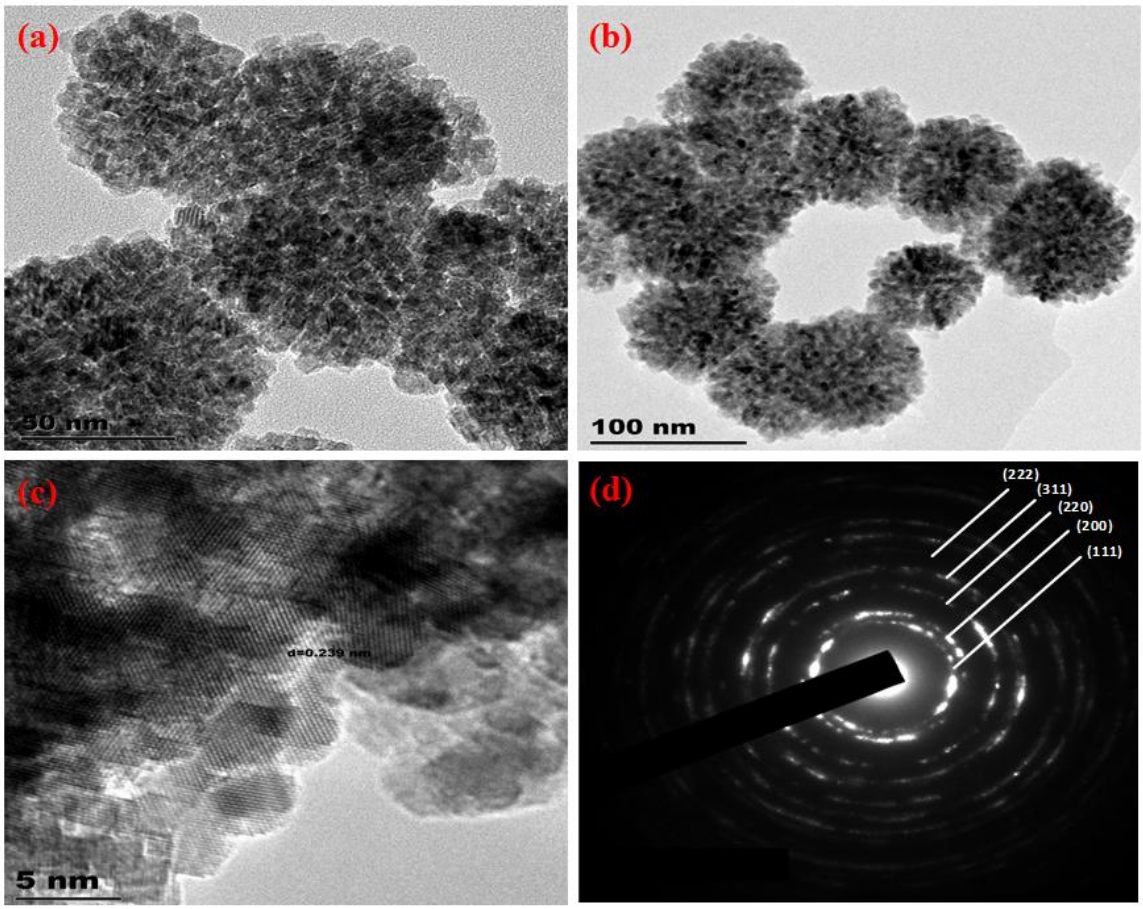

Figure 5.3: TEM images a) 50 nm, b) 100 nm and c) 5 nm and d) SAED pattern of the $Ni_{(10\%)}O$/AC adsorbent.

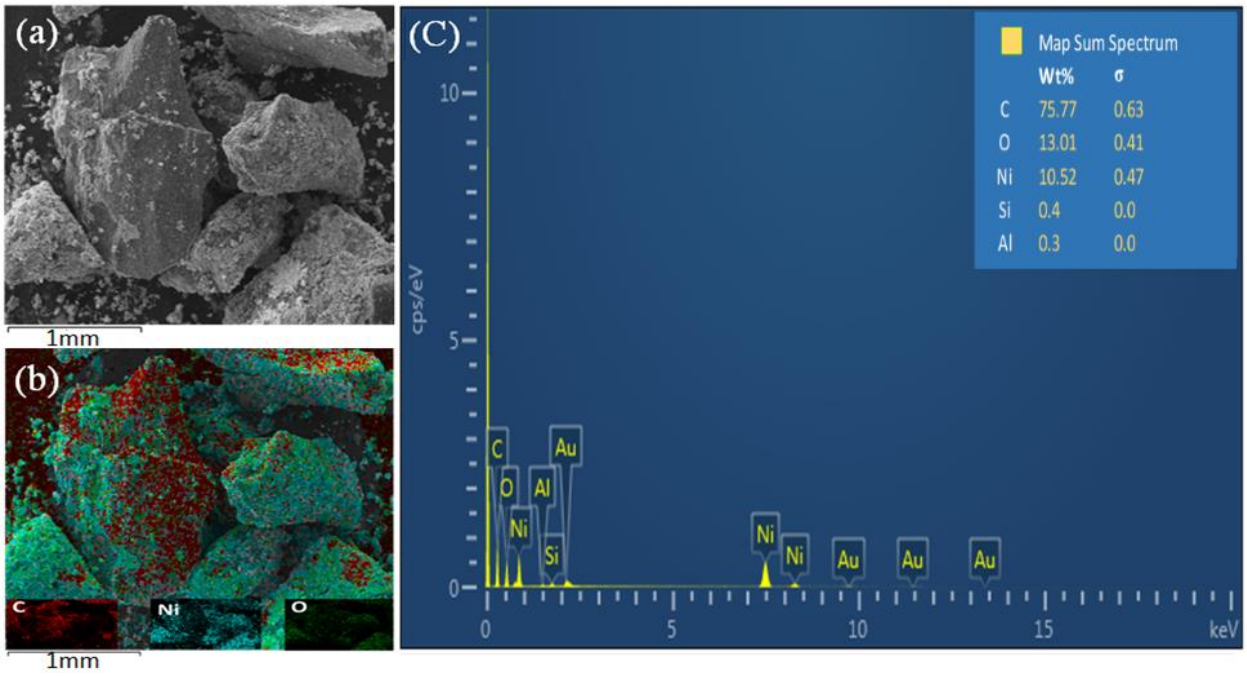

Figure 5.4: The a) SEM image, b) elemental mapping and c) EDS spectrum obtained for the $Ni_{(10\%)}O$/AC adsorbent.

5.3.1.4 FTIR analysis

The surface functional groups present on the adsorbent before and after calcination were investigated using FT-IR. The spectrum in **Figure 5.5**, represent unmodified AC, AC loaded with the $Ni(CH_3CO_2)_2$ precursor and the $Ni_{(10\%)}O$/AC adsorbent. The stretching vibrations of hydroxyl O-H of the carboxylic groups and/or chemisorbed H_2O were assigned to the 3502 cm^{-1} and 3472 cm^{-1} bands. The band at 1760 cm^{-1} was assigned to the stretching vibrations of carbonyl group C=O and the asymmetric stretching vibrations of COO^- were assigned to the band at 1544 cm^{-1}. Moreover, the bands at 1026 cm^{-1} and 943 cm^{-1} are attributed to stretching vibrations of C-OH and out-plane bending vibrations of O-H of the carboxylic and phenol groups. The rocking vibration band of the Ni-C bond was observed around 677 cm^{-1} [166]. With respect to the $Ni_{(10\%)}O$/AC adsorbent, the stretching band at around 467 cm^{-1} shows the formation of NiO on the surface of the AC after calcination, and the metal hydroxide Ni-OH or metal oxide bonded to hydrogen NiO-H was identified through the bending vibration around 1060 [167].

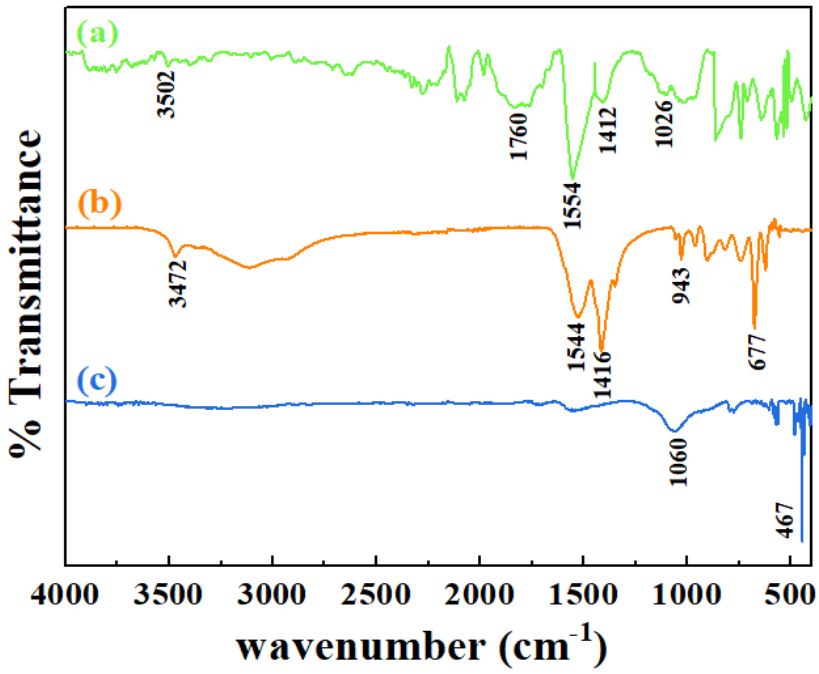

Figure 5.5: The FT-IR spectrum of a) unmodified AC and the $Ni_{(10\%)}O$/AC adsorbent b) before and c) after calcination.

5.3.1.5 Py-IR analysis

FT-IR analysis of the $Ni_{(10\%)}O$/AC and AC adsorbents was carried out using pyridine as a probe molecule in order to identify the adsorbents Brönsted and Lewis acid sites. Generally non-bonded pyridine stretching vibrations are assigned to bands 1439 cm^{-1} and 1583 cm^{-1} [168]. However, the bands shift to the 1540-1548 cm^{-1} and 1440-1460 cm^{-1} regions once they are coordinately bonded to surface Brönsted and Lewis acid sites, respectively [123]. Moreover, the band intensity is directly proportional to the concentration of surface Brönsted and Lewis acid sites [168]. The FT-IR spectrum of the pyridine adsorbed onto $Ni_{(10\%)}O$/AC and AC are shown is **Figure 5.6**. A comparison of the spectra showed that the adsorbents contained both Brönsted and Lewis acid sites, characterized by the bands which were observed at 1544 - 1546 cm^{-1} and 1454 - 1457 cm^{-1} respectively. However, the $Ni_{(10\%)}O$/AC adsorbent has a higher band intensity at 1457 cm^{-1}, suggesting that this adsorbent contained a larger amount of Lewis acid compared to Brönsted acid sites, where the Ni^{2+} ions acted as intermediate Lewis acid sites [102]. In contrast, the intense band at 1544 cm-1 appearing in the unmodified AC suggested that the adsorbent had a higher concentration Brönsted acid sites. The intermediate Lewis acid sites of the Ni^{2+} ions are classified as electrophiles, while the sulfur compounds in model diesel are intermediate Lewis bases and

acted as nucleophiles [125]. Therefore, increase in the Lewis acidity of the adsorbent would lead to increased acid-base interactions during adsorption, thus enhancing sulfur uptake during desulfurization.

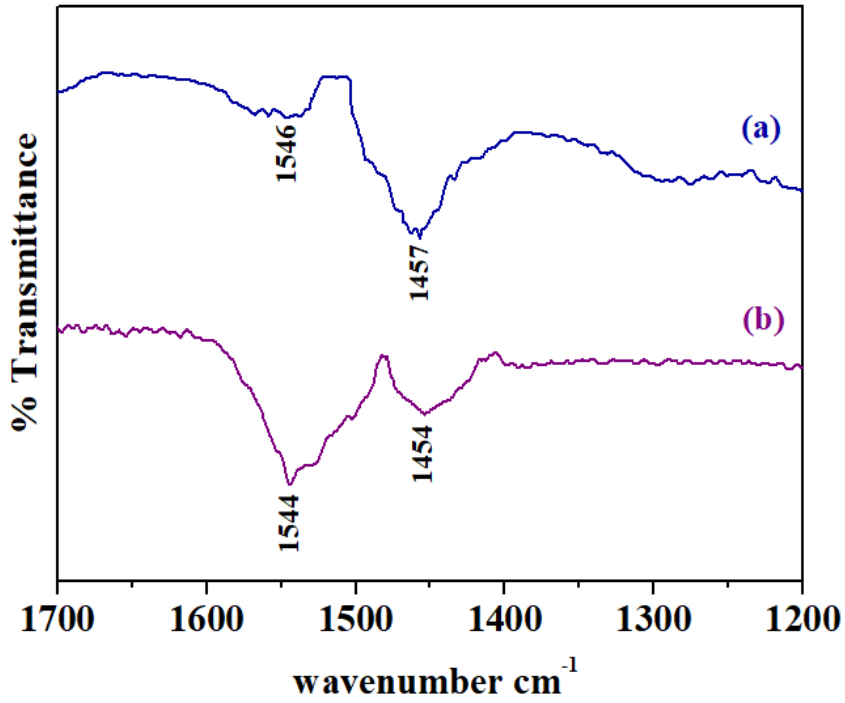

Figure 5.6: FTIR spectrum of pyridine adsorbed on a) $Ni_{(10\%)}O$/AC and b) unmodified AC , in helium at 150 °C.

5.3.1.6 TGA/DTG analysis

Prior to calcination, TGA/DTG analysis of the pure $Ni(CH_3CO_2)_2{\cdot}4H_2O$ and $Ni(CH_3CO_2)_2{\cdot}4H_2O$/AC composite material was carried out in order to understand their thermal stability and to obtain the ideal adsorbent calcination parameters. The thermal decomposition of pure $Ni(CH_3CO_2)_2{\cdot}4H_2O$ is shown in **Figure 5.7a**. Dehydration of the salt occurred at a maximum of 93.47 °C and reached completion at 194.63 °C with a 32.33 % weight-loss, which is higher than the theoretical value of 28.96 %. Decomposition of the two acetates occurred in one stage between 233.36 °C and 365.41 °C. A weight loss of 33.86 % occurred at a rapid rate of 1.63 %/°C, which was a result of NiO formation at 350.60 °C. A weight loss of 10.17 % occurred between 365.41 °C and 453.73 °C with a 76.35 % total weight loss obtained, which implied that the salt was reduced to metallic Ni at temperatures above 365.41 °C, where the theoretical weight loss for the formation of Ni is 76.41 %. The reduction of the $Ni(CH_3CO_2)_2{\cdot}4H_2O$/AC composite material

(**Figure 5.7.b**) occurs in four stages. The incorporation of the AC support led to a decrease in the dehydration temperature from 93.47 °C to 89.85 °C, and decreased the NiO formation temperature from 350.60 °C to 348.91 °C. There was a noticeable increase in reduction temperature required to form metallic Ni which increased from 365.41 °C to 422.86 °C. The presence of AC also led to a decrease in the weight loss rate from an average of 1.19 %/°C to 0.21 %/°C. A total weight loss of 39.01 % was obtained, which is almost equal to the theoretical value of 36.03 %, indicating decomposition of the activated carbon occurred, at a temperature above 553.64 °C.

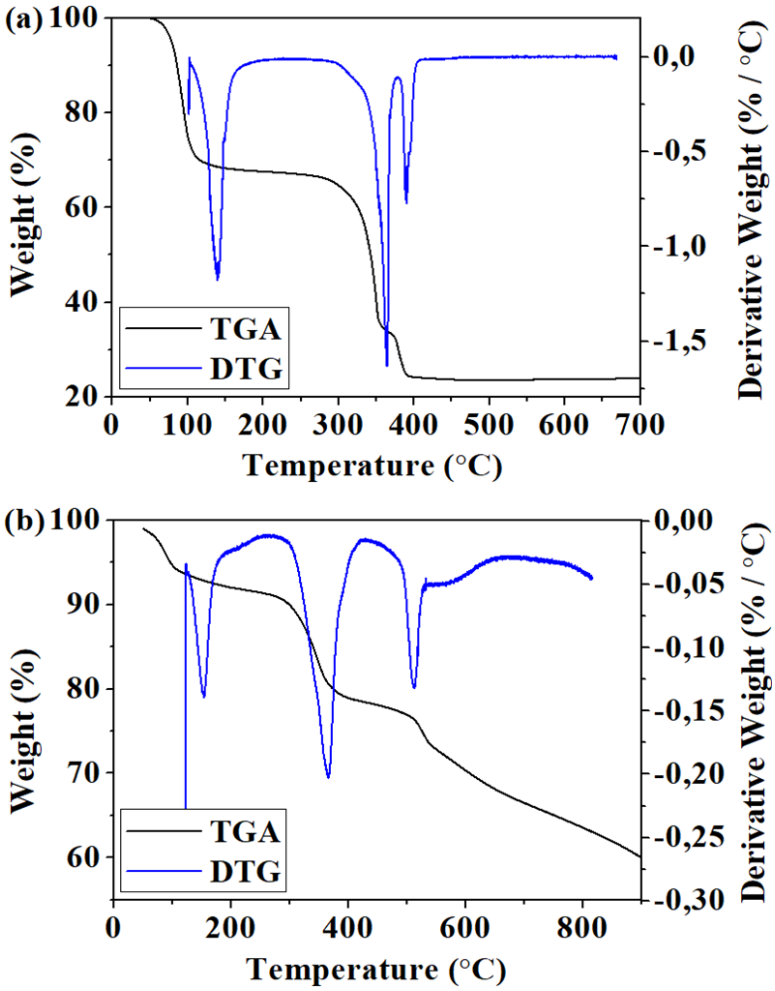

Figure 5.7: The TGA/DTG plots observed for a) unmodified $Ni(CH_3CO_2)_2{\cdot}4H_2O$ and b) $Ni(CH_3CO_2)_2{\cdot}4H_2O$ loaded onto AC.

5.3.2 The effect of adsorbent metal loading

The effect of metal loading on the adsorption of the three thiophenic compounds when using the NiO/AC and unmodified AC are shown in **Figure 5.8**. The adsorption of all three sulfur compounds over the NiO/AC adsorbents was higher than that obtained using unmodified AC. The results showed that both the adsorption capacity and percentage removal of all three sulfur compounds increased with nickel loading up to 10 wt. %. Increasing the metal loading to 15 wt. % led to a slite decrease in percentage sulfur removed and adsorption capacity; this may have been a consequence of the decrease in pore volume. These results are also consistent with the work done by Saleh et al. [63], where ADS efficiency of MnO/AC adsorbents decreased hen metal loading was increased above 10%. A comparision of ADS activity shown in **Figure 5.8** with BET results (**Table 5.1**), indicated that adsorbent surface area and porosity decreased with metal loading, which suggests that desulfurization performance was not predominately governed by surface area and pore volume. Moreover, in all three compound, the $Ni_{(10\%)}O$/AC had a higher adsorption capacity than AC, especially for the more steric 4,6-DMDBT compound. Both adsorbents had an adsorption capacity trend of 4,6-DMDBT > 4-MDBT > DBT, attributed to the increasing electron denstity of the sulfur compounds. Rapid adsorption occurred within the initial 60 minutes of adsorption [169], irrespective of the adsorbent used and Ni loading, which was a results of the high availability of vacant active adsorption sites during the intital stage of the process [63]. Therefore, adsorbents with a Ni loading of 10 wt. % was used for the remainder of the study.

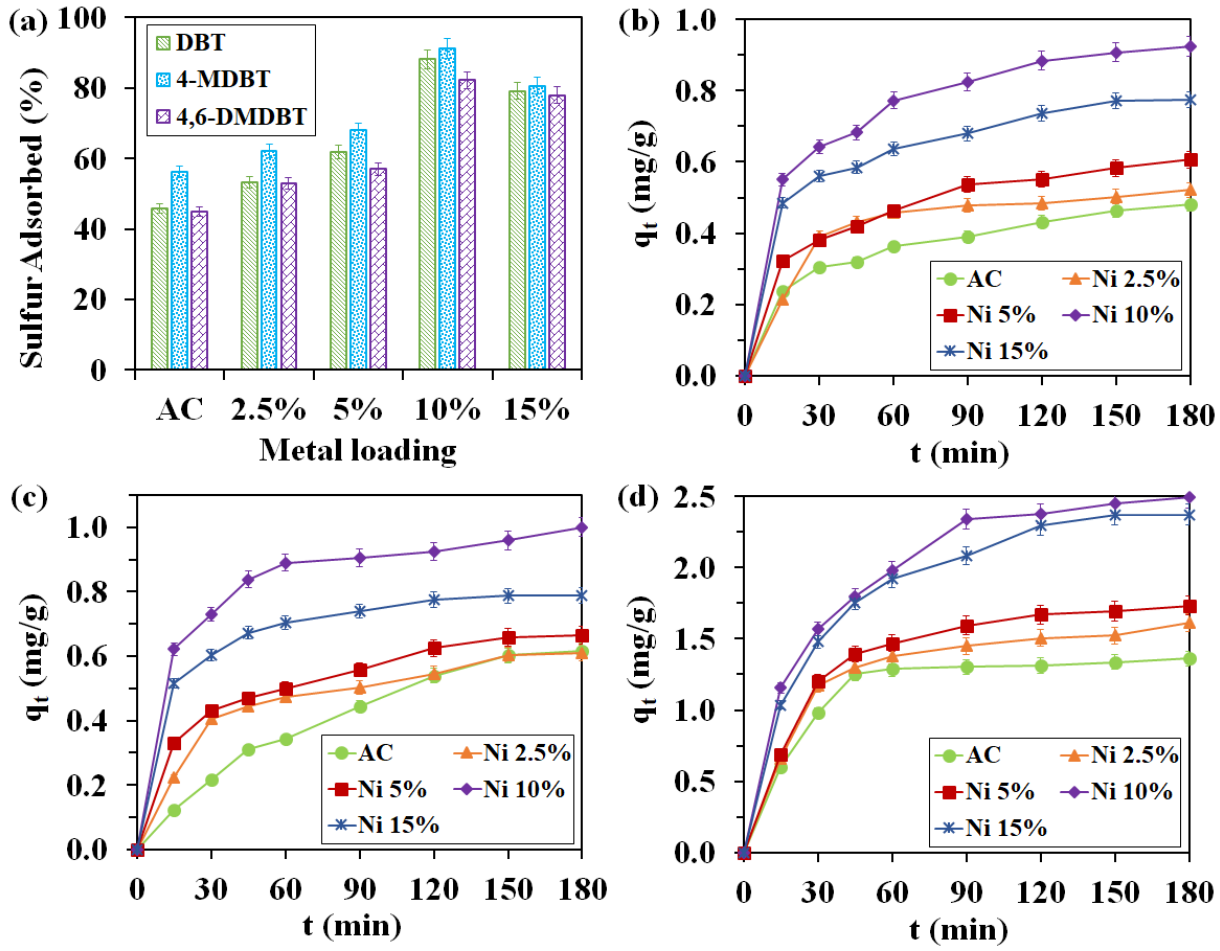

Figure 5.8: The effect of nickel loading on a) percentage sulfur removal and adsorption capacity of b) DBT c) 4-MDBT and d) 4,6-DMDBT (30 g model diesel: M1, 3 g adsorbent, at 30 °C for a 3 hrs duration).

5.3.3 The effect of adsorbent dosage

Determining the optimum adsorbent dosage is crucial when conducting adsorption studies [170]. Further investigations looked into how $Ni_{(10\%)}O$/AC adsorbent dosage influenced the removal of sulfur compounds in model diesel M1 (**Figure 5.9**). The results indicated that the percentage removal of DBT, 4-MDBT and 4,6-DMDBT increased as adsorbent dosage was increased from 0.75 g to 3 g. This was expected as the number of active adsorption sites and surface area increased proportionally with adsorbent dosage [169]. These values are comparable with those reported by other researchers that carried out the ADS of model diesel using AC and AC loaded with transition metal oxides [80, 86]. The adsorption amount q_t (mg/g) not to be mistaken with adsorption capacity, decreased with adsorbent dosage.

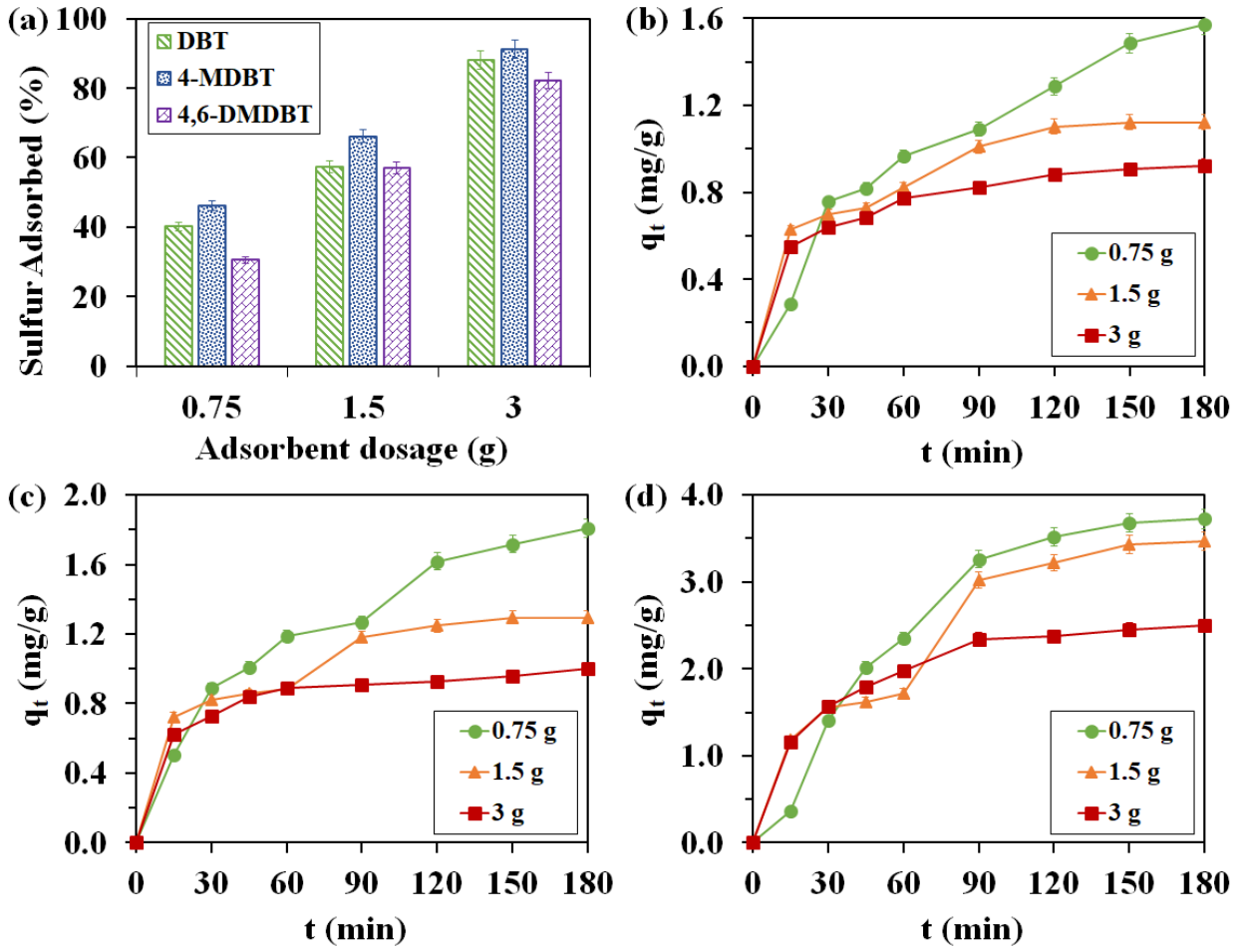

Figure 5.9: The effect of Ni($_{10\%}$)O/AC adsorbent dosage on desulfurization on a) percentage sulfur removal and adsorption amount of b) DBT c) 4-MDBT and d) 4,6-DMDBT (30 g model diesel: M1, at 30 °C for 3hrs).

5.3.4 The effect of adsorption temperature

The effect of adsorption temperature on the adsorption capacities of both NiO$_{(10\%)}$O/AC and AC in model diesel M1 are shown in **Figure 5.10**. A rise in process temperature from 30 °C to 75 °C caused an increase in both the adsorption rates and equilibrium capacities of 4,6-DMDBT, MDBT and DBT. This was the results of increased diffusivity of the sulfur compounds with temperature, which in turn induced an increase in their adsorption rate and diffusion onto the adsorbents. These results were similar to those obtained in the ADS of model diesel using Sn/AC [171] and NiCeY zeolite [111] adsorbents, where sulfur removal increased up to 60 °C and 70 °C, respectively.

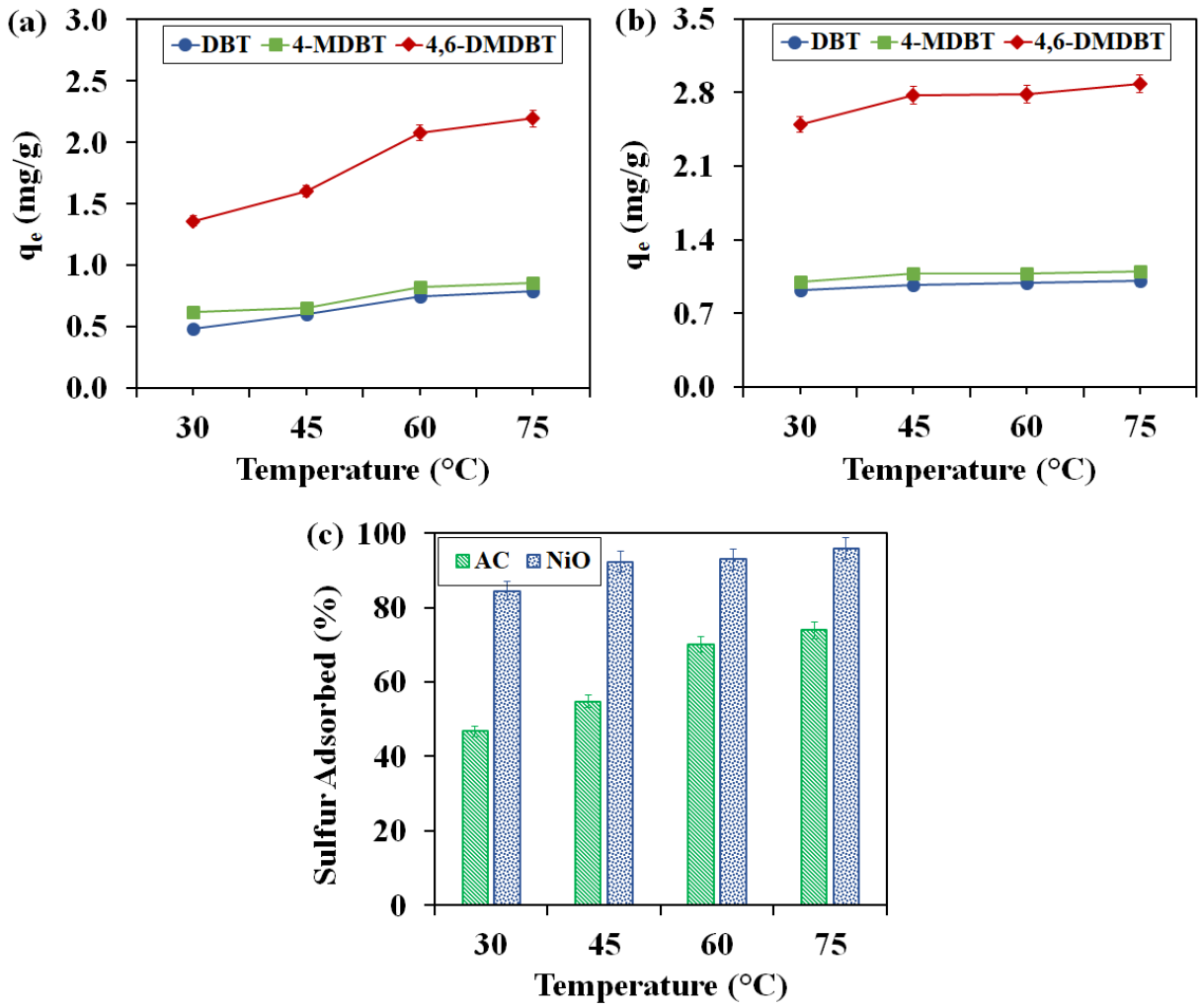

Figure 5.10: A comparison of the effect of temperature on sulfur equilibrium adsorption capacity when a) AC and b) $Ni_{(10\%)}O$/AC adsorbents were used, and c) effect of temperature on total percentage sulfur removal (3 g adsorbent, 30 g model diesel M1).

5.3.5 A comparison of singular and multicomponent diesel ADS

The effects caused by the presence of toluene on the competitive adsorption interactions in the three sulfur compounds when using $Ni_{(10\%)}O$/AC and unmodified AC are shown in **Figure 5.11**. As expected, a higher percentage of sulfur removal was obtained in single compound diesel (M3-M5) irrespective of the adsorbent used. The effect of the presence of toluene is clearly visible in **Figure 5.11,** where the percentage removal of 4,6-DMDBT, 4-MDBT and DBT increased by 7.58 %, 7.77 % and 9.1 %, respectively when using the AC absorbent. However, when the $Ni_{(10\%)}O$/AC adsorbent was used, the effect of toluene on the removal of all three compounds was mitigated,

and the percentage removal of 4,6-DMDBT, 4-MDBT and DBT increased by only 3.21 %, 3.64 % and 3.63 %, respectively. Similar observations of competitive adsorption interactions occurring between toluene and sulfur compounds in model diesel fuels were made in ADS using Cu–Ce bimetal ion-exchanged Y zeolite [124] and K-doped NiY zeolite [148]. These results indicated the $Ni_{(10\%)}O$/AC adsorbent had higher sulfur removal capabilities than unmodified AC for both binary (M1 and M2) and single (M3-M5) compound diesel, which further validated the benefits of loading NiO onto AC as a means of enhancing the performance of ADS.

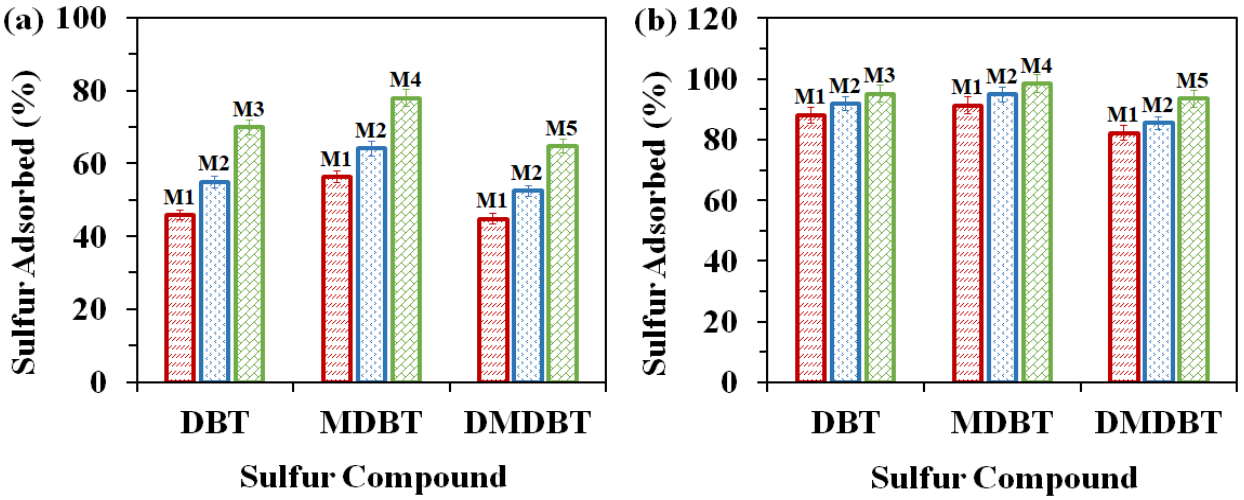

Figure 5.11: A comparison of percentage sulfur removal performance of a) AC and b) $Ni_{(10\%)}O$/AC in the desulfurization of multicomponent (M1 and M2) and singular (M3,M4,M5) sulfur compounds model diesel (3 g adsorbent dosage, 30 g model diesel at 30 °C for 3 hrs).

5.3.6 Multicomponent equilibrium isotherms

The extended Langmuir, modified competitive Langmuir, Sheindorf-Rebuhn-Sheintuch and extended Freundlich isotherm plots obtained for sulfur compounds in multicomponent model diesel (M2), using $Ni_{(10\%)}O$/AC and AC adsorbents are shown in **Figure 5.12**. The SSE values and squared regression R^2 obtained for the plots are listed in **Table 5.2**, and were used to determine how well the isotherm models correlated to the experimental data. The fitted parameters obtained for each model are shown in **Table 5.3**. Results show that for all three sulfur compounds used, the highest coefficients of R^2 and lowest SSE values were obtained from the Sheindorf-Rebuhn-Sheintuch Equation, in both the $Ni_{(10\%)}O$/AC and unmodified AC adsorbents. This indicated that for both adsorbents, the experimental data was best described using the Sheindorf-Rebuhn-Sheintuch model, which suggested that multilayer adsorption occurred as proposed by the

Freundlich isotherm, with an exponential distribution of adsorption energies for each sulfur compound, that was proportional to that obtained for the single-component model diesel [155]. Similar results were obtained by Bamufleh [13], who reported that the binary adsorption of DBT and 4,6-DMDBT on granular AC best correlated to the IAST Freundlich isotherm. The competition coefficients αij obtained for the SRS model are listed in **Table 5.3**.

Results showed that when the $NiO_{(10\%)}O$/AC adsorbent was used, the value of the competition coefficient between 4-MDBT($\alpha_{MDBT:DMDBT} = 0$) and 4,6-DMDBT ($\alpha_{DMDBT:MDBT} = 0$) were both equal to zero, therefore no competitive interaction occurs between the sulfur compounds. However, the competitive interactions between DBT and either 4,6-DMDBT ($\alpha_{DMDBT:DBT} = 0.74$) or 4-MDBT ($\alpha_{MDBT:DBT} = 0.49$) had an adverse effect on the adsorption of DBT. The values of competition coefficients obtained for adsorption of DBT ($\alpha_{DBT:DMDBT} = 0$, $\alpha_{DBT:MDBT} = 0$) were both equal to zero which indicates that adsorption 4,6-DMDBT and 4-MDBT was not affected by the presence of DBT. Which implied that 4-MDBT and 4,6-DMDBT adsorbed onto different sites of the NiO/AC hence no competition occurred, while DBT adsorbed onto the same site as 4-MDBT and 4,6-DMDBT hence it adsorption was affect by both compounds. On the other hand, when unmodified AC adsorbent was used, the values of the competition coefficient shows that competitive interactions occurred between 4,6-DMDBT ($\alpha_{DMDBT:MDBT} = 4.11$) and 4-MDBT ($\alpha_{MDBT:DMDBT} = 0.296$), where 4-MDBT was more affected by the competitive interactions with 4,6-DMDBT (4.11 > 0.296). Moreover, the presence of the two larger steric compounds markedly affected the adsorption of DBT ($\alpha_{DMDBT:DBT} = 1.1$ and $\alpha_{MDBT:DBT} = 1.05$). Similarly to the NiO/AC adsorbent, the values of competition coefficients obtained for sorption of DBT when AC was used ($\alpha_{DBT:DMDBT} = 0$, $\alpha_{DBT:MDBT} = 0$) were equal to zero indicating that the presence of DBT did not affect the adsorption 4,6-DMDBT and 4-MDBT [156].

The results from the SRS coefficients indicated that the addition of NiO onto the surface of the AC mitigated the competitive adsorption phenomena between 4,6-DMDBT and 4-MDBT, which were the two most steric compounds used in the model diesel. This mitigation was attributed to new active adsorption sites created by loading NiO onto AC. The results presented in **Table 5.3** show that when NiO was loaded onto the AC, the interaction ratio (q_m/q_{oi}) of all three compounds increased, where the synergistic properties of the sulfur compounds were enhanced. Furthermore,

through loading the NiO onto the AC, synergistic interactions occurred between 4.6-DMDBT and the other compounds, where R_{qi} >1.

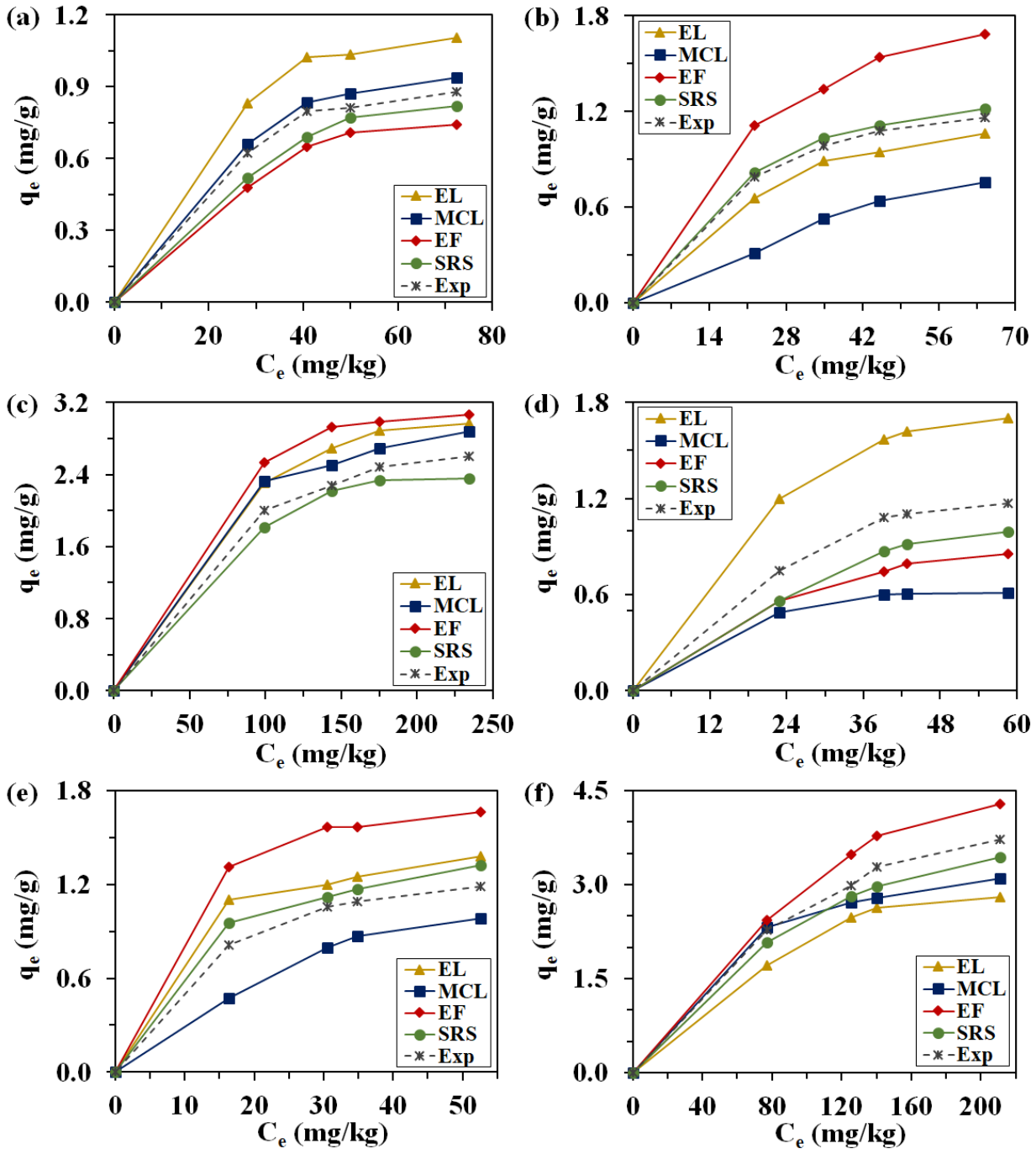

Figure 5.12: A comparison between the equilibrium isothermal results obtained through model prediction and experimental data for a) DBT, b) 4-MDBT, c) 4,6-DMDBT using unmodified AC adsorbent, and d) DBT, e) 4-MDBT f) 4,6-DMDBT using the $Ni_{(10\%)}O$/AC adsorbent.

Table 5.2: Results of R^2 and error values obtained from the non-linear regression analysis of multiple component isotherm models when $Ni_{(10\%)}O$/AC and unmodified AC were used (model diesel M2 at 30°C).

Adsorbent			**AC**			**$Ni_{(10\%)}O$/AC**		
Compound			DBT	4-MDBT	4,6-DMDBT	DBT	4-MDBT	4,6-DMDBT
Extended Isotherm Models	EL	R^2	0.909	0.991	0.991	0.879	0.981	0.949
		SSE	2.739	0.402	1.883	4.635	0.929	14.41
	MCL	R^2	0.977	0.922	0.997	0.968	0.968	0.995
		SSE	0.083	3.475	0.485	1.212	1.561	1.388
	EF	R^2	0.933	0.954	0.991	0.973	0.946	0.994
		SSE	2.025	2.076	1.891	1.014	2.672	1.014
	SRS	R^2	0.971	0.996	0.999	0.985	0.991	0.997
		SSE	1.049	0.201	0.178	0.985	0.459	0.877

Table 5.3: Equilibrium parameters obtained from the multiple component isotherm models when $Ni_{(10\%)}O$/AC and unmodified AC were used (model diesel M2 at 30°C).

Adsorbent			**AC**			**$Ni_{(10\%)}O$/AC**		
Compound			DBT	4-MDBT	4,6-DMDBT	DBT	4-MDBT	4,6-DMDBT
Extended Isotherm Model Constants	**EL**	q_m (mg/g)	0.8	4.68	2.48	1.1	1.5	2.82
		K_L (kg/mg)	2.5×10^{10}	5×10^{10}	3.9×10^{10}	1.1×10^{13}	9.6×10^{14}	1.4×10^{14}
	MCL	η	7.5×10^{-10}	6.6×10^{-7}	17	0.27	7.47	0.85
	EF	x	50	0.1	23.25	10	0.1	0
		y	2.5×10^{-5}	1.2×10^{-10}	9.70	2.5×10^{-5}	1.2×10^{-10}	1.3×10^{-1}
		z	1.93	4.17	0	1.93	4.17	0
	SRS	α_{DMDBT}	0	0.29	-	0	0	-
		α_{MDBT}	0	-	4.11	0	-	0
		α_{DBT}	-	1.05	1.1	-	0.49	0.74
Interaction ratio		q_m/q_i	0.63	0.67	0.77	0.83	0.84	1.01

5.3.7 Adsorption kinetics

5.3.7.1 Pseudo-first-order model

The pseudo first-order kinetic parameters q_e and k_1 for the ADS of model diesel M1 using the $Ni_{(10\%)}O$/AC and AC adsorbent were derived from the linear plots shown in **Figure. 5.13**, where the values are listed in **Table C.1** (see. Appendices). The calculated values of q_e were lower than those obtained experimentally. Moreover, by comparison the squared regressions obtained in the pseudo-first order model were lower than those of the pseudo-second order model **(Table C.1** and **Table C.2**). Which suggested that in both instances where $Ni_{(10\%)}O$/AC and AC adsorbents were used, physisorption was not the rate limiting step.

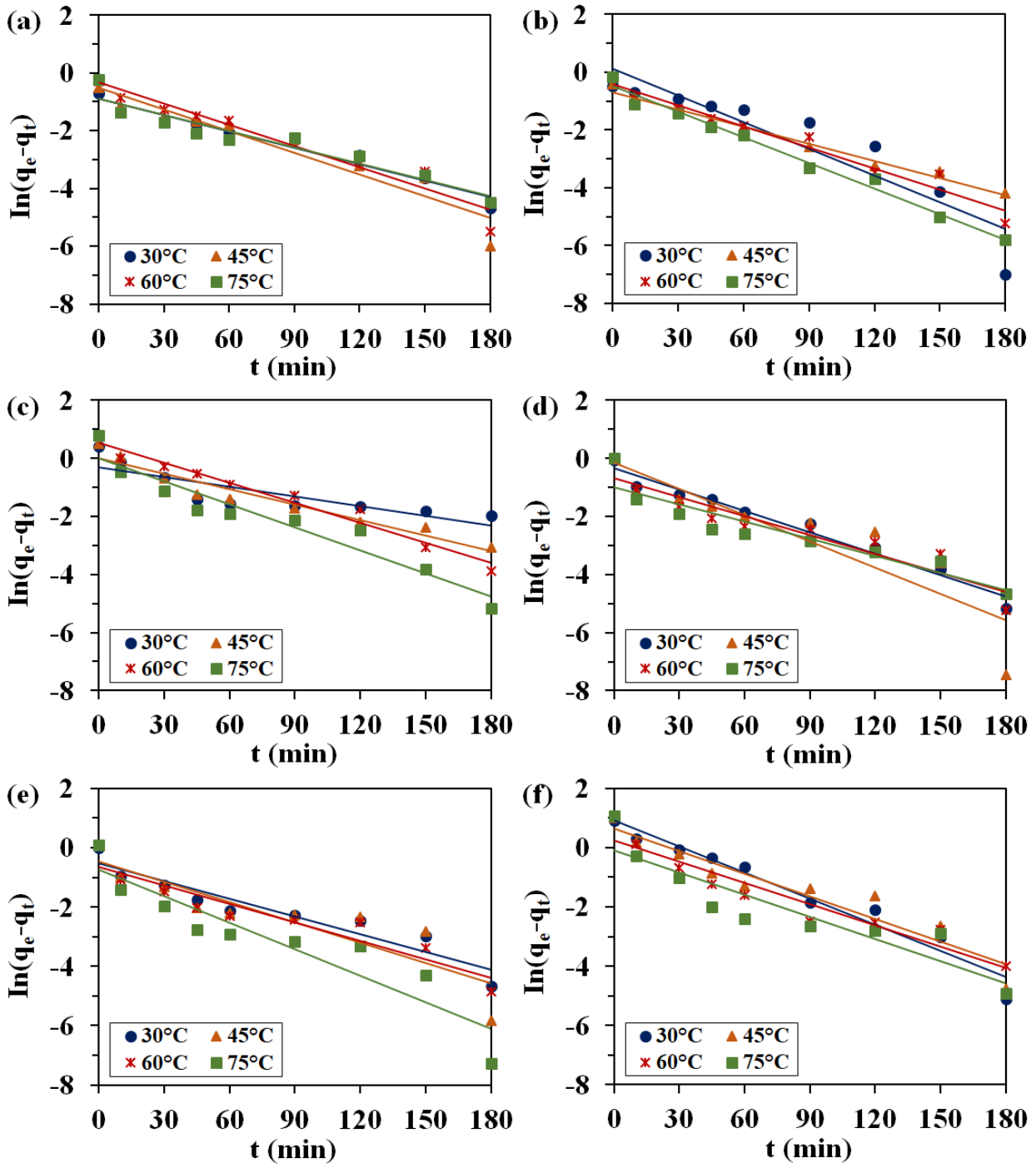

Figure 5.13: Comparison of the best fit straight line (corresponding to the pseudo-first order model) versus experimental data at varying temperatures for a) DBT, b) 4-MDBT, c) 4,6-DMDBT using unmodified AC adsorbent, and d) DBT, e) 4-MDBT f) 4,6-DMDBT using the $Ni_{(10\%)}O$/AC adsorbent (3 g adsorbent and 30g model diesel M1).

5.3.7.2 Pseudo-second-order model

The pseudo second-order kinetic parameters q_e and k_2 for the desulfurization of model diesel M1 using both $Ni_{(10\%)}O$/AC and AC adsorbent were calculated from the intercepts and slopes in **Figure. 5.14**. The calculated equilibrium capacity (q_e) values shown in **Table C.2** (see. Appendices) were almost equal to those obtained experimentally. Moreover, the values of R^2 were almost equal to 1. Therefore, the adsorption rate was limited by chemical interactions in both AC and $Ni_{(10\%)}O$/AC adsorbents. The calculated equilibrium adsorption capacities $q_{e,cal}$ and rate constant k_2 increased with temperature (**Table C.2**), which implied that adsorption became more favorable as temperature was increased [63]. These results were comparable to those obtained by other researchers, who reported that adsorption kinetics of model diesel using AC loaded with transition metal/transition metal oxide was best described by the pseudo second-order model [65, 86, 169].

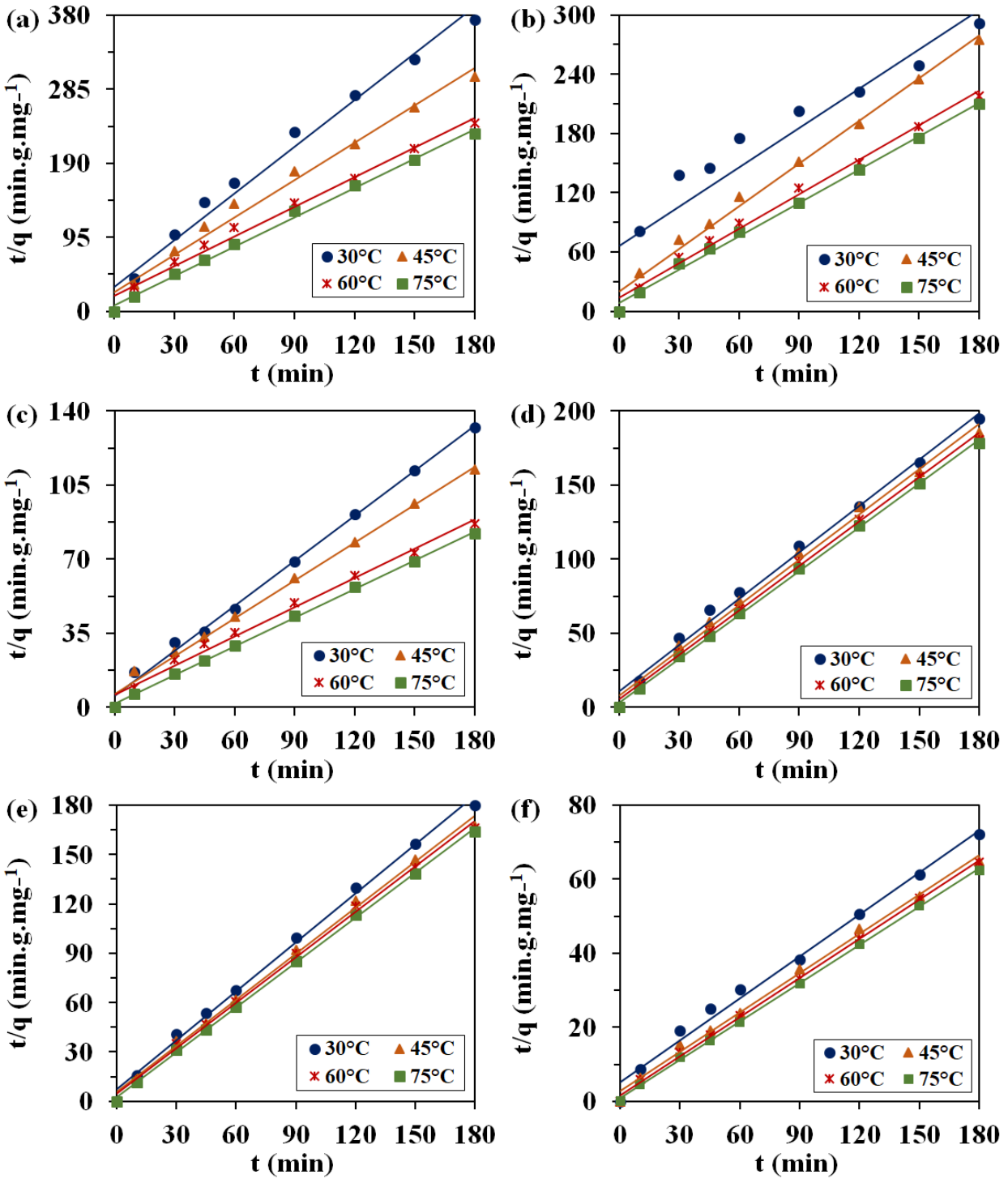

Figure 5.14: Comparison of the best fit straight lines for pseudo-second order plots at varying temperatures for a) DBT, b) 4-MDBT, c) 4,6-DMDBT using unmodified AC adsorbent, and d) DBT, e) 4-MDBT f) 4,6-DMDBT using the $Ni_{(10\%)}O$/AC adsorbent (3 g adsorbent and 30 g model diesel M1).

5.3.7.3 Intra-particle diffusion

As shown in **Figure. 5.15**, the data points in each plot at different temperatures were related by three different straight lines for all three sulfur compounds, for both $Ni_{(10\%)}O$/AC and unmodified AC adsorbents. This indicated that adsorption of all three compounds in the temperature range was controlled by three processes. The initial stage was external surface adsorption, which was completed within the initial 30 and 45 minutes of adsorption in all three compounds, for AC and $Ni_{(10\%)}O$/AC respectively. In the second stage, intra-particle diffusion controlled the adsorption rate [138], and it occurred between 30-90 minutes and 45-120 minutes in all three compounds for AC and $Ni_{(10\%)}O$/AC, respectively. The linear plots of the second stage did not pass through the origin, which indicated that additional mechanisms were involved in controlling the rate of adsorption [86]. The third stage is when intra-particle diffusion lessens and adsorption equilibrium is reached [139]. These results were also consistent with the work done by Saleh [138], where adsorption kinetics occurred in three stages for all thiophenic compounds in model diesel, using AC loaded with Co and Cu.

A sharp increase was observed in the adsorption capacity rate during external surface adsorption when $Ni_{(10\%)}O$/AC was used. These findings further validated the results in **section 5.3.2**, which showed that although the surface area and porosity of adsorbent decreased with NiO loading, there was an increase in the adsorption capacity of the adsorbents. This could be explained through adsorption interactions which occurred through NiO active sites via Ni-S acid-base interaction and π-interactions. Similarly to the kinetic results obtained for the ADS of commercial diesel using AC in **Chapter 4**, there was a sharp increase in the adsorption capacity rate during intra-particle diffusion stage, and the rate constants k_i shown in **Table C.3** (see. Appendices) obtained from the slopes of the second stage were higher when unmodified AC was used. Which implied that adsorption of the sulfur compounds occurred predominately in the pores of the AC. Comparison of the rate constants C ($mg.g^{-1}$) in **Table C.3**, showed that for all three sulfur compounds, the boundary layer effect increased with temperature, irrespective of the adsorbent used.

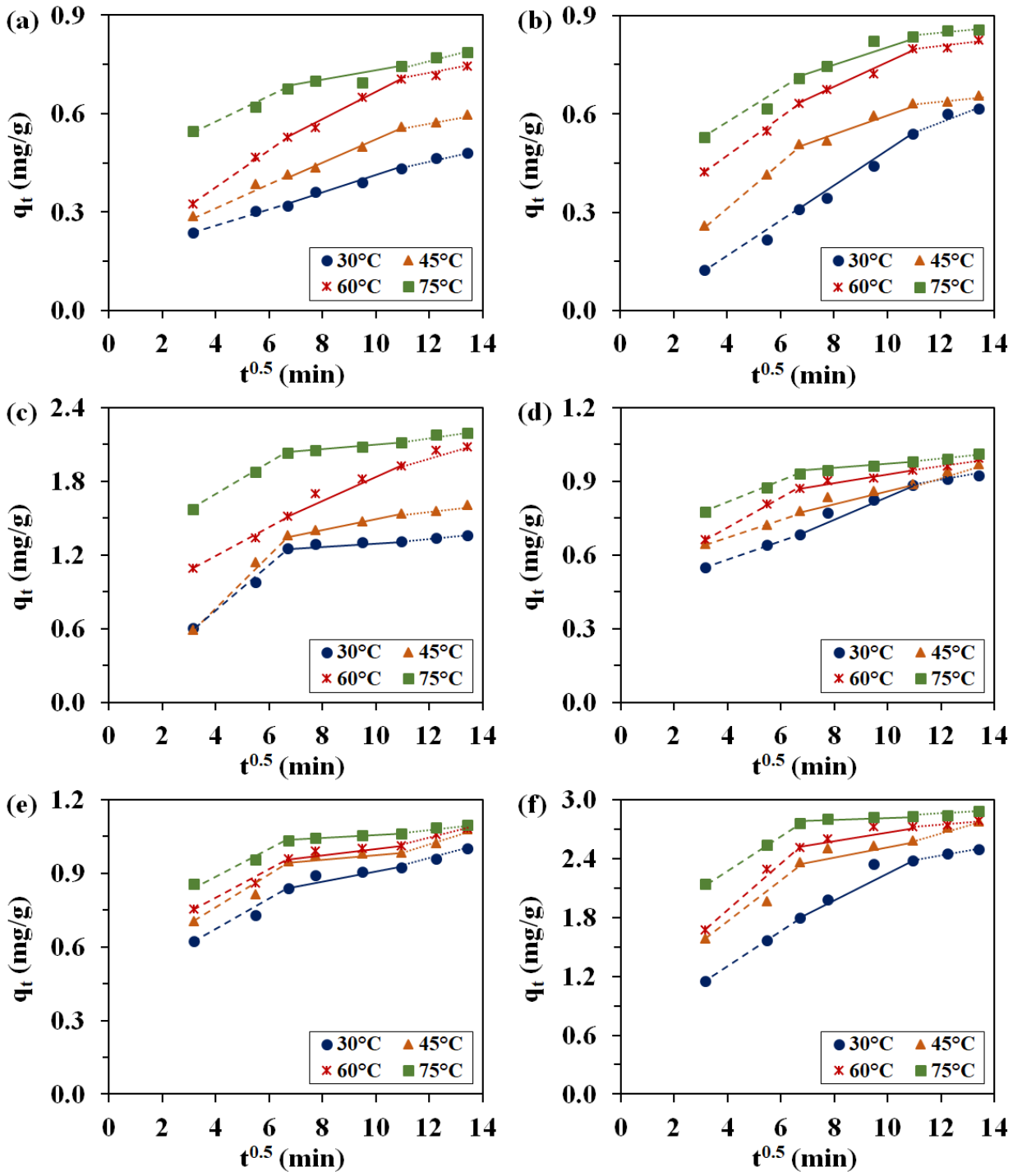

Figure 5.15: Weber-Morris plots obtained at varying temperatures for a) DBT, b) 4-MDBT, c) 4,6-DMDBT using unmodified AC adsorbent, and d) DBT, e) 4-MDBT f) 4,6-DMDBT using the $Ni_{(10\%)}O$/AC adsorbent (3 g adsorbent and 30 g model diesel M1).

5.3.7.4 The effect of temperature on adsorption kinetics

The E_a values obtained using the unmodified AC were 28.67, 26.76 and 23.48 kJ/mol for 4,6-DMDBT, MDBT and DBT, respectively (see. **Figure 5.16a**). These results suggested that the rate of adsorption was controlled by chemical bonding in all three compounds. Similarly, when the $Ni_{(10\%)}O$/AC adsorbent was used (see. **Figure 5.16b**) chemical adsorption occurred, where E_a values of 32.69, 30.75 and 29.86 kJ/mol were obtained in adsorption of 4,6-DMDBT, MDBT and DBT, respectively. The higher activation energies obtained with the $Ni_{(10\%)}O$/AC were consistent with proposed adsorption mechanisms of Ni-S acid-base interactions in addition to π-complexation.

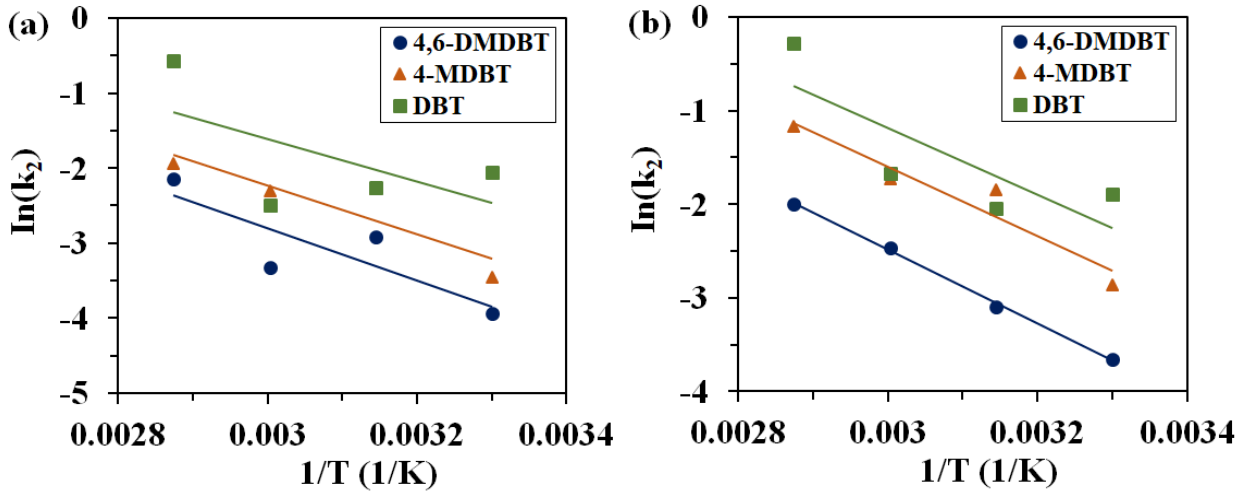

Figure 5.16: Arrhenius plots using pseudo-second order kinetic model constants using a) unmodified AC and b) $Ni_{(10\%)}O$/AC adsorbents (3 g adsorbent and 30 g model diesel M1).

5.3.8 Adsorption thermodynamics

The thermodynamic parameters that were obtained for ADS of model diesel M1 using the $Ni_{(10\%)}O$/AC and unmodified AC adsorbents are listed in **Table 5.4**. The negative values of ΔG were an indication that the adsorption of all three compounds on both $Ni_{(10\%)}O$/AC and AC was a spontaneous and thermodynamically favorable process. Moreover, as the adsorption temperature increased, the value of ΔG decreased, which further validated the results of the kinetic analysis that adsorption became more favorable as the temperature increased. The change in enthalpy ΔH of the adsorption process and ΔS is the change in entropy were obtained from the slope and intercept of the Van't Hoff plots as depicted in **Figure 5.17** [161]. The positive ΔH values

confirmed that adsorption of all three compounds was endothermic. The higher values of ΔH for AC were due to adsorption which occurred predominately in the pores and on the surface of AC, via π-π interactions between the aromatic sulfur compounds and the aromatic sheets of the AC [172]. Rheinberg et al.[173] reported that in Ni based adsorbents, predominate interactions occurred through Ni-S bonding, and AC had a higher adsorption selectivity for aromatics than Ni based adsorbents. Therefore, the sulfur compounds had to displace the toluene molecules in the model diesel solvent before they adsorbed onto the AC, which resulted in a more endothermic process. The positive ΔS values indicated that there was an increase in randomness at the diesel/adsorbent interface, with structural changes that occurred in both the adsorbent and sulfur compounds [174]. A comparison of the parameters in **Table 5.4** showed that when the $Ni_{(10\%)}O$/AC adsorbent was used, both ΔG and ΔH decreased, which indicated that the adsorption of all three sulfur compounds became more energetically favorable when NiO was loaded onto the AC. The decrease in ΔH was a result of decreased toluene adsorption and controlled chemisorption interaction occurring on the surface of the $Ni_{(10\%)}O$/AC which was consistent with slight decrease in randomness (ΔS), the chemisorption kinetics observed in **section 5.3.7** and the lower effect of toluene on $Ni_{(10\%)}O$/AC activity observed in **section 5.3.5**.

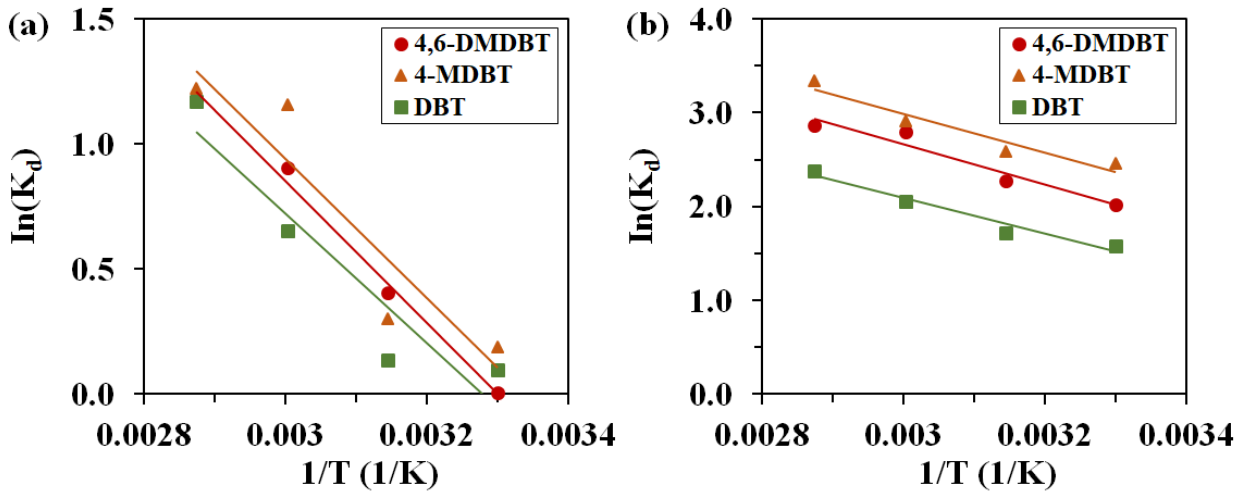

Figure 5.17: Van't Hoff plots for sulfur compounds in model diesel M1 for a) unmodified AC and b) $Ni_{(10\%)}O$/AC.

Table 5.4: Thermodynamic parameters obtained in the ADS of 4,6-DMDBT, 4-MDBT and DBT using unmodified AC and the $Ni_{(10\%)}O$/AC adsorbent.

Adsorbent	Compound	ΔG (kJ.mol^{-1})				ΔH (kJ.mol^{-1})	ΔS (J.mol^{-1}.K^{-1})
		30°C	45°C	60°C	75°C		
AC	DBT	-0.25	-0.36	-1.81	-3.38	21.51	70.54
	MDBT	-0.48	-0.79	-3.20	-3.54	23.11	77.14
	DMDBT	-0.01	-1.07	-2.51	-3.41	23.56	77.74
Ni(10%)O/AC	DBT	-3.99	-4.56	-5.71	-6.89	15.84	64.89
	MDBT	-6.19	-6.86	-8.07	-9.66	17.11	76.21
	DMDBT	-5.11	-6.01	-7.76	-8.29	17.88	75.78

5.3.9 Analysis of spent adsorbents

The FTIR analysis of the spent adsorbents (**Figure 5.18**) was performed in order to obtain a more detailed understanding of the mechanism of ADS and to show the effects of loading NiO onto AC. The bands at 721 cm^{-1} were attributed to the π- interactions between the aromatic sulfur compounds and aromatic sheets of the AC [172]. The symmetrical stretching vibrations of the aromatic rings C=C-C=C bonds when sulfur was adsorbed onto the Ni^{2+} metal sites [124] or directly onto the surface of the AC [9], were ascribed to the bands appearing at 1451 cm^{-1} and 1467 cm^{-1}. Certain bands only appeared in the spent $Ni_{(10\%)}O$/AC adsorbent. The band at 1395 cm^{-1} was attributed to π interactions, where the sulfur compounds selectively formed π complexes between their aromatic rings and Ni^{2+} metal sites. The sigma component of the bond formed via the overlap of the π orbital of the sulfur compounds aromatic rings and the vacant 4s orbital of the Ni^{2+} metal sites. The π-component of the bond formed simultaneously via the back donation of electrons from the 3d atomic orbitals of the Ni^{2+} to the vacant antibonding π*-orbitals of the sulfur compound [64]. The band which appeared at 1400 cm^{-1} represented the bonding between the aromatic rings hydrogen atoms and the hydroxyl groups on the adsorbent surface, which were formed after dehydroxylation [170]. The larger band at 1418 cm^{-1} showed the bonding of sulfur and the Ni^{2+} metal sites [138]. Finally, the bands at 2921 cm^{-1} and 2853 cm^{-1} suggested that the aromatic rings of the sulfur compounds opened or stretched during adsorption when the $Ni_{(10\%)}O$/AC adsorbent was used [123].

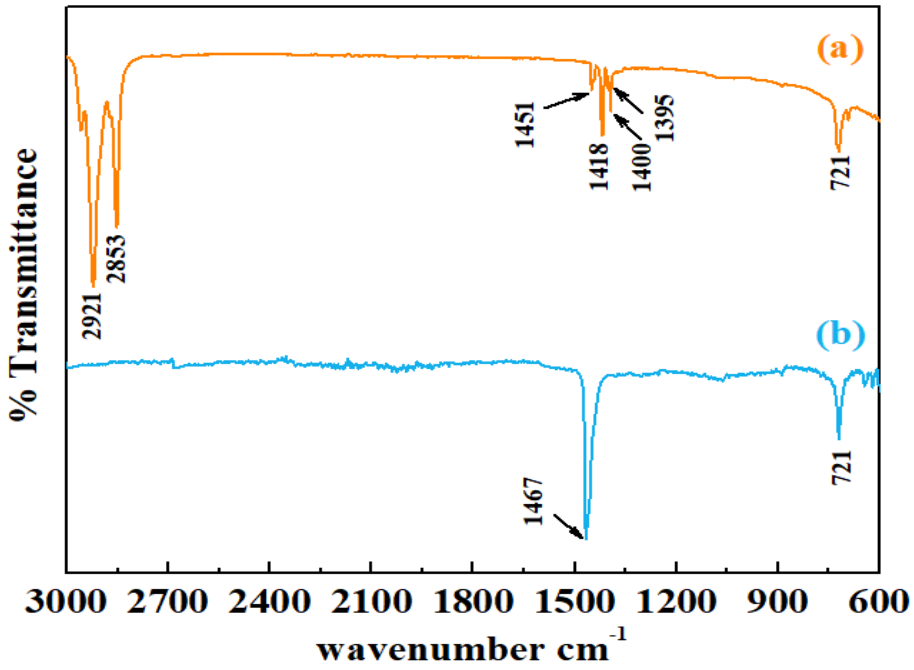

Figure 5.18: FT-IR spectrum for a) $Ni_{(10\%)}O$/AC and b) AC, after adsorption experiments using (3 g adsorbent in 30 g of model diesel M2 at 30 °C).

5.4 Conclusion

The present study showed that the incorporation of NiO onto the surface of relatively low-cost AC enhanced its sulfur adsorption capacity. The NiO/AC adsorbents were successfully prepared using the well-established incipient wetness impregnation method and were used in the removal of refractory 4,6-DMDBT, 4-MDBT and DBT. The results obtained confirmed that the incorporation of NiO onto the surface of AC, led to an increase in percentage sulfur removal, higher adsorption capacities and increased selectivity of the larger more steric 4,6-DMDBT sulfur compound. The observed trend of adsorption capacities was 4,6-DMDBT > 4-MDBT > DBT, where the total sulfur adsorption capacity increased from 2.46 to 4.42 mg/g, and the total sulfur removal increased from 46.8 % to 84.5 %, using the unmodified AC and $Ni_{(10\%)}O$/AC adsorbent, respectively. Moreover, process temperature played a significant role in the uptake of the sulfur compounds in model diesel, where increasing the ADS temperature to 75 °C increased the total sulfur removal to 95.8 %, in the $Ni_{(10\%)}O$/AC adsorbent.

Results from the extended equilibrium isotherms study showed that the adsorption process was best described using the Sheindorf-Rebuhn-Sheintuch equation, where NiO incorporation mitigated competitive interaction between steric 4,6-DMDBT and 4-MDBT. Kinetic analysis indicated that chemical interactions governed the adsorption process for both adsorbents, where experimental data best correlated with the pseudo-second order model and equilibrium adsorption capacities of the compounds increase with temperature. Thermodynamic analysis suggested that the adsorption of all three sulfur compounds was spontaneous and endothermic. The higher desulfurization performance of the $Ni_{(10\%)}O$/AC was attributed to the increased intermediate Lewis acidity of the adsorbent where the Ni^{2+} ions acted as an electron pair acceptors, while the sulfur compounds in model diesel were intermediate Lewis bases which acted as electron pair donors. This led to increased Ni-S acid-base interactions. In addition, π-complexation occurred between the sulfur compounds and the vacant orbitals of the Ni^{2+} as well as the aromatic AC matrix. The breakage in sulfur compounds aromatic rings was observed during adsorption using the $Ni_{(10\%)}O$/AC adsorbent. Which led to increased synergistic interactions and the mitigation of competitive adsorption between the larger more steric 4,6-DMDBT and 4-MDBT sulfur compounds.

Chapter 6

Conclusions and Recommendations

This study looked at synthesizing AC adsorbents loaded with transition metal oxides from the fourth period (Zn, Cr, Mn, Co, Fe, Cu, Ni) in order to identify a trend in their desulfurization performance in both commercial and model diesel, while improving the desulfurization activity and selectivity of the AC. The adsorbents were prepared using incipient wetness impregnation of transition metal acetates onto the AC, followed by calcination in a N_2 atmosphere. Adsorbent characterization techniques (including BET, PXRD, TEM, SEM/EDS, TGA/DTG and FTIR) confirmed that the metal oxides (Co_3O_4, CoO, Cr_2O_3, CuO, Cu_2O, γ-Fe_2O_3, Mn_3O_4, α-MnO_2, NiO and ZnO) were successfully loaded on the surface of the AC, with different crystal structures and metal geometries.

Initially, the study focused on investigating the desulfurization performance of the metal oxide/ AC, in the adsorption of refractory sulfur compounds in both model and commercial diesel. The Ni- oxide/AC adsorbent had the highest adsorption performance with 84.49 % and 92.99 % sulfur removal at 30 °C and 60 °C, respectively. The desulfurization activity of the adsorbents in model diesel followed a trend of: Ni-oxide/AC > Cu-oxide/AC > Co-oxide/AC > Fe-oxide/AC > Mn-oxide/AC > Cr-oxide/AC > Zn-oxide/AC > AC. Similar results were obtained in ADS of model diesel, the desulfurization of commercial diesel the Ni-oxide/AC adsorbent had superior desulfurization performance at 95.17 % sulfur removal. The activity followed the same order of Ni-oxide/AC > Cu-oxide/AC > Co-oxide/AC > Fe-oxide/AC > Mn-oxide/AC > Cr-oxide/AC > Zn-oxide/AC > AC. The Ni-oxide/AC, Cu-oxide/AC, Co-oxide/AC and Fe-oxide/AC adsorbents had equal selectivity for the 4-MDBT and 1,4,6 –TMDBT sulfur compounds in the commercial diesel. In comparison to the metal oxide adsorbents, the unmodified AC adsorbent had a lower selectivity for all the steric sulfur compounds, with the lowest being 4-E,6 –MDBT. However, the metal oxides/AC adsorbents had a higher selectivity for the sulfur compound, in the order of 4-E,6 -MDBT > 2,4,6 -TMDBT > 4,6-DMDBT. Steric sulfur compounds with alkyl group in both the 4 and 6 positions contributed to 73 % of the total sulfur in the commercial diesel used. The adsorption conversions of these compounds were between 75.19 % - 100 % when the metal oxide/AC adsorbents were used.

To further elucidate on Pearson's HSAB theory, the concentration of Lewis acid sites in the adsorbents were identified, followed by the ADS of model diesel at high and low temperatures. A trend was observed, where the desulfurization activity in model diesel increased proportionally with the concentration of adsorbent Lewis acid sites, diesel at both low and high temperatures. Further investigations showed that no correlation existed between the Pearson Lewis acidity hardness of the metal oxides and their sulfur adsorption abilities ($r \geq -0.477$ and $R^2 \leq 0.227$). However, in correlation with Portier's ICP theory, the adsorption of intermediate Lewis acid sulfur compounds became more favourable, as the ICP and subsequent Lewis acidity hardness of the adsorbents decreased. A strong inverse linear relationship ($r \leq -0.955$ and $R^2 \geq 0.912$) was observed between the adsorption of sulfur in model diesel and the ionic covalent parameter (ICP_{th}) of the metal oxide adsorbents. There was also a trend in adsorbent selectivity, where the selectivity of steric sulfur compounds in the commercial diesel increased inversely with the ICP_{th} of the metal oxide adsorbents. Therefore, a novel concept was introduced in terms of ADS, which is that the ICP was a more accurate measure of the Lewis acid strength of transition metal oxides with different crystal structures and metal geometries and their subsequent desulfurization performance.

Adsorption kinetics in the desulfurization of commercial diesel was best described by the pseudo-second order and Elovich model for all the adsorbents used, where chemisorption was the controlling mechanism and the metal oxides on the AC surface acted as active adsorption sites. An investigation of the role of diffusion on the sulfur adsorption process showed that intra-particle diffusion was not the only factor that controlled the adsorption rate. However, adsorption occurring in the pores of the unmodified AC played a significant role in controlling the adsorption rate. The evaluation of fixed-bed breakthrough curves showed that the addition of NiO supported on the AC led to the breakthrough time increasing for the adsorption of 4-MDBT, 4,6-DMDBT, 4-E,6-MDBT and 2,4,6 -TMDBT 4-MDBT in commercial diesel. The breakthrough of 4,6-DMDBT, 4-E,6-MDBT and 2,4,6 -TMDBT increased from 1.476 g-diesel/g-adsorbent to 1.968 g-diesel/g-adsorbent. Similarly, the breakthrough of 4-MDBT increased from 1.968 g-diesel/g-adsorbent using un-promoted AC to 3.936 g-diesel/g-adsorbent when using the NiO/AC adsorbent. The Thomas and Yoon-Nelson models best described the fixed-bed desulfurization of commercial diesel using AC. However, the fixed-bed desulfurization using the Ni-oxide/AC was best described by the filtration advection-dispersion equation. This kind of adsorption was kinetic driven, in which irreversible interactions (strong van der Waals, steric, Lewis acid-base) occurred between

the adsorbent and sulfur compounds; and competitive adsorption interactions between the sulfur compounds were mitigated.

Further investigation looked at the competitive adsorption interactions occurring in the multi-component diesel system using NiO/AC adsorbent, which displayed the highest desulfurization performance of all the adsorbents used. Experimental data was fitted into multi-component isotherm models. The Sheindorf-Rebuhn-Sheintuch equation best described the adsorption of all three sulfur compounds when using both NiO/AC and unmodified AC. The competition coefficients (α) of 4,6-DMDBT and 4-MDBT ranged between 0.296 - 0.411 when unmodified AC was used. In the NiO/AC adsorbent the. For the unmodified AC adsorbent, competitive interactions occurred between 4,6-DMDBT and 4-MDBT, where the competition coefficients (α) 0.296 and 0.411 were obtained, respectively. This indicated that the adsorption of 4-MDBT was noticeably hindered by the presence of 4,6-DMDBT in the diesel. Moreover, the presence of the two larger steric compounds affected the adsorption of DBT markedly. However, the loading of NiO onto AC increased the synergistic interactions between all three sulfur compounds, and mitigated the competitive interaction between 4,6-DMDBT and 4-MDBT, as the competition coefficients between the compounds were both equal to zero.

Analysis of the spent adsorbents suggested that the breakage in the aromatic rings of the sulfur compounds occured during adsorption using the $Ni_{(10\%)}O$/AC adsorbent. This led to increased synergistic interactions and the mitigation of competitive adsorption between the larger more steric 4,6-DMDBT and 4-MDBT sulfur compounds. The enhanced desulfurization performance of the $Ni_{(10\%)}O$/AC was also the result of the intermediate Lewis acidity of the adsorbent, where the Ni^{2+} ions acted as an electron pair acceptors. The sulfur atoms in model diesel were intermediate Lewis bases acting as electron pair donors, leading to increased Ni-S acid-base interactions. Adsorption also occurred via π-complexation through the bonding of the aromatic rings of the sulfur compounds with the vacant orbitals of the Ni^{2+} and the aromatic AC matrix.

The ADS kinetics of the model diesel correlated best with the pseudo-second order model, which further validates the kinetics results obtained in the ADS of commercial diesel. The equilibrium adsorption capacities of all three sulfur compounds increased proportionally with temperature. This observation was further supported by thermodynamic analysis, which suggested that the adsorption of all three sulfur compounds was endothermic and spontaneous.

Based on the results of this study, the following recommendations should be considered when developing carbon supported and period four transition metal oxide adsorbents for the ADS of diesel:

- Further consideration should be given in regards to mitigating the challenges associated with the high cost of utilizing various transition metals.
- In a bid to increase the process efficiency and economic feasibility, adsorbent regeneration methods should be developed for ADS adsorbents containing AC and transition metals.
- Studies on the preparation of ADS adsorbents are predominately based on Pearson's HSAB theory. Further research should be conducted to elaborate on the relationship between ICP and desulfurization performance of transmission metal adsorbents.
- Multi-component isotherm models should be utilized in future studies to identify the adsorption interaction occurring between sulfur compounds and other aromatics in diesel, with a focus on the nitrogen heterocycle
- The adsorption of sulfur compounds onto the adsorbents was chemisorption. For economic viability of the process, reusability of the adsorbents is very important. How economically viable will the process be, considering the energy that will be required in desorbing and regenerating the spent adsorbents for re-use since the adsorption is chemisorption? More research work is highly recommended to regenerate the spend adsorbents for re-use.

References

[1] N. N. Darwish, "Adsorption Study of Desulfurization of Diesel Oil Using Activated Charcoal," American University of Sharjah, 2015.

[2] B. R. Fox, A. W. Sun, H. B. Dauer, J. L. Male, M. L. Stewart, and D. R. Tyler, "Enhanced oxidative desulfurization of model fuels using a film-shear reactor," *Fuel*, vol. 90, no. 2, pp. 898–901, 2011.

[3] A. S. Ogunlaja, S. Khene, E. Antunes, T. Nyokong, N. Torto, and Z. R. Tshentu, "The development of catalytic oxovanadium(IV)-containing microspheres for the oxidation of various organosulfur compounds," *Appl. Catal. A Gen.*, vol. 462–463, pp. 157–167, 2013.

[4] M. Williams and R. Minjares, "A technical summary of Euro 6 / VI vehicle emission standards," no. June. pp. 1–12, 2016, [Online]. Available: https://theicct.org/sites/default/files/publications/ICCT_Euro6-VI_briefing_june2016.pdf.

[5] V. Mahotas, "Petroleum Regulation Hydrocarbons Policy Cleaner Fuel Strategy," in *South African National Workshop on Implementation of Marpol VI on 0.50% Sulphur Limit*, 2019, pp. 1–15, [Online]. Available: http://www.samsa.org.za/Documents/Marpol 2019/South Africa%27s Clean Fuels Strategy.pdf.

[6] J. M. Campos-Matin, M. C. Capel-Sanchez, P. Perez-Presas, and J. L. G. Fierro, "Oxidative Processes of Desulfurization of Liquid Fuels," *J. Chem. Technol. Biotechnol.*, vol. 85, no. 7, pp. 879–890, 2010.

[7] Z. Khan and S. Ali, "Oxidative desulphurization followed by catalytic adsorption method," *Southa African J. Chem. Eng.*, vol. 18, no. 2, pp. 14–28, 2010.

[8] A. M. Siefers, "A novel and cost-effective hydrogen sulfide removal technology using tire derived rubber particles," 2010.

[9] X. Han, H. Lin, and Y. Zheng, "Understanding capacity loss of activated carbons in the adsorption and regeneration process for denitrogenation and desulfurization of diesel fuels,"

Sep. Purif. Technol., vol. 133, pp. 194–203, 2014.

[10] S. Zhao, C. Ge, Z. Yan, J. Zhang, S. Ren, and H. Liang, "One-pot microwave-assisted combustion synthesis of NiFe2O4 -reduced graphene oxide composite for adsorptive desulfurization of diesel fuel," *Mater. Chem. Phys.*, vol. 229, no. March, pp. 294–302, 2019.

[11] L. Dong *et al.*, "Desulfurization Kinetics and Regeneration of Silica Gel-Supported TiO 2 Extrudates for Reactive Adsorptive Desulfurization of Real Diesel," *Ind. Eng. Chem. Res.*, vol. 59, p. 10130−10141, 2020.

[12] C. Song, "An overview of new approaches to deep desulfurization for ultra-clean gasoline, diesel fuel and jet fuel," *Catal. Today*, vol. 86, no. 1–4, pp. 211–263, 2003.

[13] H. S. Bamufleh, "Single and binary sulfur removal components from model diesel fuel using granular activated carbon from dates ' stones activated by ZnCl 2," *Appl. Catal. A, Gen.*, vol. 365, pp. 153–158, 2009.

[14] S. Bagheri, N. Muhd, and I. Á. Green, "Effect of hybridization on the value-added activated carbon materials," *Int. J. Ind. Chem.*, vol. 7, no. 3, pp. 249–264, 2016.

[15] R. N. Fallah, S. Azizian, G. Reggers, S. Schreurs, R. Carleer, and J. Yperman, "Selective Desulfurization of Model Diesel Fuel by Carbon Nanoparticles as Adsorbent," *Ind. Eng. Chem. Res.*, vol. 51, no. 44, pp. 14419–14427, 2012.

[16] J. Xiao, Z. Li, B. Liu, Q. Xia, and M. Yu, "Adsorption of Benzothiophene and Dibenzothiophene on Ion-Impregnated Activated Carbons and Ion-Exchanged Y Zeolites," *Energy and Fuels*, vol. 22, pp. 3858–3863, 2008.

[17] J. Lison, "Selective Adsorption of Dibenzothiophenes on Activated Carbons with Metal Species," City College of New York, 2010.

[18] S. S. Cheng, "Ultra Clean Fuels via Modified UAOD Process with Room Temperature Ionic Liquid (RTIL) & Solid Catalyst Polishing," University of Southern California, 2008.

[19] B. Fox, "Investigations into the oxidative desulfurization activity in a film-shear reactor, the

source of enhanced reactivity, and other potential applications," Univesity of Oregon, 2011.

[20] J. Speight, "Hydrogen in Refineries," in *Hydrogen Science and Engineering: Materials, Processes, Systems and Technology*, 1st ed., P. D. Stolten and D. B. Emonts, Eds. John Wiley and Sons, 2016, pp. 1–18.

[21] E. J. M. Hensen, "Hydrodesulfurization catalysis and mechanism of supported transition metal sulfides," Eindhoven University of Technology., 2000.

[22] A. Bodin *et al.*, "Engineering Ni-Mo-S Nanoparticles for Hydrodesulfurization," *ACS Nano Lett.*, vol. 18, no. 6, pp. 3454–3460, 2018.

[23] J. Liang *et al.*, "A new approach to construct a hydrodesulfurization catalyst from a crystalline precursor: ligandinduced self-assembly, sulfidation and hydrodesulfurization," *RSC Catal. Sci. Technol.*, vol. 8, pp. 6330–6345, 2018.

[24] M. Gupta *et al.*, "'Nanowire catalysts for ultra-deep hydro-desulfurization and aromatic hydrogenation,'" *Appl. Catal. B, Environ.*, vol. 180, pp. 246–254, 2016.

[25] R. Moonen, J. Alles, E. Ras, C. Harvey, and J. Moulijn, "Performance Testing of Hydrodesulfurization Catalysts Using a Single-Pellet-String Reactor," *Chem. Eng. Technol.*, vol. 40, no. 11, pp. 2025–2034, 2017.

[26] J. . García-Martínez, A. Dutta, G. Chávez, J. . De los Reyes, and C. . Castillo-Araiza, "Hydrodesulfurization of Dibenzotiophene in a Micro Trickle Bed Catalytic Reactor under Operating Conditions from Reactive Distillation," *Int. J. Chem. React. Eng.*, no. December, pp. 1–15, 2015.

[27] Z. Deng, T. Wang, and Z. Wang, "Hydrodesulfurization of diesel in a slurry reactor," *Chem. Eng. Sci.*, vol. 65, pp. 480–486, 2010.

[28] R. Gatan, P. Barger, V. Gembicki, A. Cavanna, D. Molinari, and S. A. Enitecnologie, "Oxidative desulfurization : A new technology for ULSD," *ACS Div. Fuel Chem. Prepr.*, vol. 49, pp. 577–579, 2004.

[29] W. Zhang, H. Zhang, J. Xiao, Z. Zhao, M. Yu, and Z. Li, "Carbon nanotube catalysts for oxidative desulfurization of a model diesel fuel using molecular oxygen," *RSC Green Chem.*, vol. 16, pp. 211–220, 2014.

[30] S. Chen, W. Lu, Y. Yao, H. Chen, and W. Chen, "Oxidative desulfurization of dibenzothiophene with molecular oxygen catalyzed by carbon fiber- supported iron phthalocyanine," *React. Kinet. Mech. Catal.*, vol. 111, pp. 535–547, 2014.

[31] S. Murata, K. Murata, K. Kidena, and M. Nomura, "A Novel Oxidative Desulfurization System for Diesel Fuels with Molecular Oxygen in the Presence of Cobalt Catalysts and Aldehydes," *Energy and Fuels*, vol. 18, no. 1, pp. 116–121, 2004.

[32] T. V. Rao *et al.*, "Oxidative Desulfurization of HDS Diesel Using the Aldehyde / Molecular Oxygen Oxidation System," *Energy and Fuels*, vol. 21, no. 6, pp. 3420–3424, 2007.

[33] N. Palaić, K. Sertić-bionda, D. Margeta, and Š. Podolski, "Oxidative Desulphurization of Diesel Fuels," *Chem. Biochem. Eng. Q.*, vol. 29, no. 3, pp. 323–327, 2015.

[34] V. V. D. N. Prasad, K. Jeong, H. Chae, C. Kim, and S. Jeong, "Oxidative desulfurization of 4 , 6-dimethyl dibenzothiophene and light cycle oil over supported molybdenum oxide catalysts," *Catal. Commun.*, vol. 9, pp. 1966–1969, 2008.

[35] W. Azelee *et al.*, "Effect of transition metal oxides catalysts on oxidative desulfurization of model diesel," *Fuel Process. Technol.*, vol. 101, pp. 78–84, 2012.

[36] K. M. Dooley, D. Liu, A. M. Madrid, and F. C. Knopf, "Oxidative desulfurization of diesel with oxygen : Reaction pathways on supported metal and metal oxide catalysts," *"Applied Catal. A, Gen.*, vol. 468, pp. 143–149, 2013.

[37] C. Ma, D. Chen, F. Liu, X. Sun, F. Xiao, and B. Dai, "Oxidative desulfurization of a model fuel using ozone oxidation generated by dielectric barrier catalysis," *RSC Adv.*, vol. 5, pp. 96945–96952, 2015.

[38] A. V Anisimov *et al.*, "Vanadium peroxocomplexes as oxidation catalysts of sulfur organic compounds by hydrogen peroxide in bi-phase systems," *Catal. Today*, vol. 78, pp. 319–325,

2003.

[39] C. Komintarachat and W. Trakarnpruk, "Oxidative Desulfurization Using Polyoxometalates," *Ind. Eng. Chem. Res.*, vol. 45, pp. 1853–1856, 2006.

[40] W. Trakarnpruk and K. Rujiraworawut, "Oxidative desulfurization of Gas oil by polyoxometalates catalysts," *Fuel Process. Technol.*, vol. 90, no. 3, pp. 411–414, 2009.

[41] J. A. Kadijani, E. Narimani, and H. A. Kadijani, "Oxidative Desulfurization of Organic Sulfur Compounds in the Presence of Molybdenum Complex and Acetone as Catalysts," *Pet. Coal*, vol. 56, no. 1, pp. 116–123, 2014.

[42] M. Tao, H. Zheng, J. Shi, S. Wang, X. Wang, and P. Á. R. Á. Oxidation, "Oxidative Desulfurization by Oxygen Using Amphiphilic Quaternary Ammonium Peroxovanadium Polyoxometalates," *Catal. Surv. from Asia*, vol. 19, no. 4, pp. 257–264, 2015.

[43] P. De Filippis and M. Scarsella, "Functionalized Hexagonal Mesoporous Silica as an Oxidizing Agent for the Oxidative Desulfurization of Organosulfur Compounds," *Ind. Eng. Chem. Res.*, vol. 47, pp. 973–975, 2008.

[44] J. Gao, W. Ma, L. Yuan, Y. Dai, and C. Li, "Catalytic oxidative desulfurization mechanism in Lewis – Brønsted complex acid," *Appl. Catal. A, Gen.*, vol. 467, pp. 187–195, 2013.

[45] D. Liu, "Catalytic Oxidative Desulfurization of a Model Diesel," Louisiana State University and Agricultural and Mechanical College, 2010.

[46] W. Li, J. Xing, X. Xiong, J. Huang, and H. Liu, "Feasibility Study on the Integration of Adsorption / Bioregeneration of π -Complexation Adsorbent for Desulfurization," *Ind. Eng. Chem. Res.*, vol. 45, pp. 2845–2849, 2006.

[47] D. . Aribike, A. . Susu, S. C. . Nwachukwu, and S. . Kareem, "Microbial Desulfurization of Diesel by Desulfobacterium anilini," *Acad. Arena*, vol. 1, no. 4, pp. 11–17, 2009.

[48] G. Mohebali and A. S. Ball, "Biodesulfurization of diesel fuels – Past, present and future perspectives," *Int. Biodeterior. Biodegradation*, vol. 110, pp. 163–180, 2016.

[49] J. Wang, R. R. Butler, F. Wu, J. J. Kilbane, and B. C. Stark, "Enhancement of Microbial Biodesulfurization via Genetic Engineering and Adaptive Evolution," *PLoS One*, vol. 12, no. 1, pp. 1–20, 2017.

[50] B. Yu, P. Xu, Q. Shi, and C. Ma, "Deep Desulfurization of Diesel Oil and Crude Oils by a Newly Isolated Rhodococcus erythropolis Strain," *Appl. Environ. Microbiol.*, vol. 72, no. 1, pp. 54–58, 2006.

[51] M. Mukhopadhyaya, R. Chowdhury, and P. Bhattacharya, "Biodesulfurization of hydrodesulfurized diesel in a trickle bed reactor — Experiments and modeling," *J. Sci. Ind. Res. (India).*, vol. 65, no. May, pp. 432–436, 2006.

[52] D. Karayilan, "Removal of Hydrogen Sulfide by Regenerable Metal Oxide Sorbents," Middel East Technical University, 2004.

[53] W. M. T. M. Reimerink, *The use of activated carbon as catalyst and catalyst carrier in industrial applications*, vol. 120. Elsevier Masson SAS, 1998.

[54] A. Barroso-Bogeat, M. Alexandre-Franco, C. Ferndez-Gonzaez, and V. Gomez-Serrano, "Activated carbon surface chemistry : Changes upon impregnation with Al (III), Fe (III) and Zn (II) -metal oxide catalyst precursors from NO3 aqueous solutions," *Arab. J. Chem.*, vol. 12, no. 8, pp. 3963–3976, 2019.

[55] S. Binti, I. Anthonysamy, S. B. Afandi, M. Khavarian, A. Rahman, and B. Mohamed, "A review of carbon-based and non-carbon-based catalyst supports for the selective catalytic reduction of nitric oxide," *Beilstein J. Nanotechnol.*, vol. 9, pp. 740–761, 2018.

[56] I. Al Zubaidi, N. N. Darwish, Y. El Sayed, Z. Shareefdeen, and Z. Sara, "Adsorptive Desulfurization of Commercial Diesel oil Using Granular Activated Charcoal," *Int. J. Adv. Chem. Eng. Biol. Sci.*, vol. 2, no. 1, pp. 15–18, 2015.

[57] S. Velu, S. Watanabe, X. Ma, and C. Song, "Regenerable Adsorbents for the Adsorptive Desulfurization of Transportation Fuels for Fuel Cell Applications," *ACS Div. Fuel Chem. Prepr.*, vol. 48, no. 2, pp. 526–528, 2003.

[58] M. Muzic, K. Sertic-bionda, Z. Gomzi, S. Podolski, and S. Telen, "Chemical Engineering Research and Design Study of diesel fuel desulfurization by adsorption," *Chem. Eng. Res. Des.*, vol. 88, no. 4, pp. 487–495, 2009.

[59] J. H. Kim, X. Ma, A. Zhou, and C. Song, "Ultra-deep desulfurization and denitrogenation of diesel fuel by selective adsorption over three different adsorbents : A study on adsorptive selectivity and mechanism," *Catal. Today*, vol. 111, pp. 74–83, 2006.

[60] P. Baltzopoulou, K. X. Kallis, G. Karagiannakis, and A. G. Konstandopoulos, "Diesel Fuel Desulfurization via Adsorption with the Aid of Activated Carbon : Laboratory- and Pilot-Scale Studies," *Energy and Fuels*, vol. 29, pp. 5640–5648, 2015.

[61] E. Vilarrasa-Garcı´a *et al.*, "Thiophene Adsorption on Microporous Activated Carbons Impregnated with PdCl 2 †," *Energy and Fuels*, vol. 24, no. 8, pp. 3436–3442, 2010.

[62] M. Seredych and T. J. Bandosz, "Adsorption of dibenzothiophenes on activated carbons with copper and iron deposited on their surfaces," *Fuel Process. Technol.*, vol. 91, no. 6, pp. 693–701, 2010.

[63] A. Saleh, K. O. Sulaiman, S. A. Al-hammadi, H. Dafalla, and I. Danmaliki, "Adsorptive desulfurization of thiophene , benzothiophene and dibenzothiophene over activated carbon manganese oxide nanocomposite : with column system evaluation," *J. Clean. Prod.*, vol. 154, pp. 401–412, 2017.

[64] N. A. Khan and S. H. Jhung, "Adsorptive removal and separation of chemicals with metal-organic frameworks : Contribution of □ -complexation," *J. Hazard. Mater.*, vol. 325, pp. 198–213, 2017.

[65] N. Khan, Z. Hasan, K. Sik, S. Paek, and S. Hwa, "Facile introduction of Cu + on activated carbon at ambient conditions and adsorption of benzothiophene over Cu + / activated carbon," *Fuel Process. Technol.*, vol. 116, pp. 265–270, 2013.

[66] L. Wang, B. Sun, F. H. Yang, and R. T. Yang, "Effects of aromatics on desulfurization of liquid fuel by p -complexation and carbon adsorbents," *Chem. Eng. Sci.*, vol. 73, pp. 208–217, 2012.

[67] Y. Wang, R. T. Yang, and J. M. Heinzel, "Desulfurization of jet fuel by -complexation adsorption with metal halides supported on MCM-41 and SBA-15 mesoporous materials," *Chem. Eng. Sci.*, vol. 63, pp. 356–365, 2008.

[68] G. Herna´ndez-Maldonado, Arturo J. Qi and R. T. Yang, "Desulfurization of commercial fuels by pi -complexation : Monolayer CuCl/g-Al2O3," *Appl. Catal. B, Environ.*, vol. 61, pp. 212–218, 2005.

[69] T. A. Saleh, M. N. Siddiqui, and A. A. Al-arfaj, "Synthesis of Multiwalled Carbon Nanotubes-Titania Nanomaterial for Desulfurization of Model Fuel," *J. Nanomater.*, vol. 2, pp. 1–6, 2014.

[70] W. Ahmad, I. Ahmad, M. Ishaq, and K. Ihsan, "Adsorptive desulfurization of kerosene and diesel oil by Zn impregnated montmorollonite clay," *Arab. J. Chem.*, vol. 10, no. S2, pp. S3263–S3269, 2017.

[71] Z. C. Kampouraki, D. A. Giannakoudakis, and V. Nair, "Metal Organic Frameworks as Desulfurization Adsorbents of DBT and 4 , 6- DMDBT from Fuels Metal Organic Frameworks as Desulfurization Adsorbents of DBT and 4 , 6 - DMDBT from Fuels," *Molecules*, vol. 24, no. December, p. 4525, 2019.

[72] D. Peralta, G. Chaplais, A. Simon-Masseron, K. Barthelet, and G. Pirngruber, "Metal–Organic Framework Materials for Desulfurization by Adsorption," *Energy & Fuels*, vol. 26, pp. 4953–4960, Jul. 2012.

[73] B. Van de Voorde *et al.*, "Adsorptive desulfurization with CPO-27/MOF-74: an experimental and computational investigation.," *Phys. Chem. Chem. Phys.*, vol. 17, pp. 10759–10766, 2015.

[74] N. A. Khan and S. H. Jhung, "Effect of central metal ions of analogous metal-organic frameworks on the adsorptive removal of benzothiophene from a model fuel," *J. Hazard. Mater.*, vol. 260, pp. 1050–1056, 2013.

[75] H.-X. Zhang *et al.*, "Adsorption Behavior of Metal–Organic Frameworks for Thiophenic

Sulfur from Diesel Oil," *Ind. Eng. Chem. Res.*, vol. 51, no. 38, pp. 12449–12455, Sep. 2012.

[76] Y. Han *et al.*, "Desulfurization Efficiency Preserved in a Heterometallic MOF : Synthesis and Thermodynamically Controlled Phase Transition," *Adv. Sci. News*, vol. 101, pp. 1–8, 2019.

[77] R. Zhang, C. Tao, R. Chen, L. Wu, and X. Zou, "Ultrafast Synthesis of Ni-MOF in One Minute by Ball Milling," *Nanomaterials*, vol. 8, pp. 1–12, 2018.

[78] J. Liao, Y. Zhang, L. Fan, L. Chang, and W. Bao, "Insight into the Acid Sites over Modified NaY Zeolite and Their Adsorption Mechanisms for Thiophene and Benzene," *Ind. Eng. Chem. Res.*, vol. 58, pp. 4572–4580, 2019.

[79] J. Liao, W. Bao, Y. Chen, Y. Zhang, and L. Chang, "The Adsorptive Removal of Thiophene from Benzene over ZSM-5 Zeolite," *Energy Sources, Part A*, vol. 34, no. November 2014, pp. 618–625, 2012.

[80] T. A. Saleh and G. I. Danmaliki, "Influence of acidic and basic treatments of activated carbon derived from waste rubber tires on adsorptive desulfurization of thiophenes," *J. Taiwan Inst. Chem. Eng.*, vol. 60, pp. 460–468, 2016.

[81] S. S. Shah, I. Ahmad, W. Ahmad, M. Ishaq, and H. Khan, "Deep Desulphurization Study of Liquid Fuels Using Acid Treated Activated Charcoal as Adsorbent," *Energy and Fuels*, vol. 31, pp. 7867–7873, 2017.

[82] J. Bu, G. Loh, C. G. Gwie, S. Dewiyanti, M. Tasrif, and A. Borgna, "Desulfurization of diesel fuels by selective adsorption on activated carbons : Competitive adsorption of polycyclic aromatic sulfur heterocycles and polycyclic aromatic hydrocarbons," *Chem. Eng. J.*, vol. 166, pp. 207–217, 2011.

[83] J. Luo *et al.*, "Design of Lewis Acid Centers in Bundlelike Boron Nitride for Boosting Adsorptive Desulfurization Performance," *Ind. Eng. Chem. Res.*, vol. 58, no. 29, pp. 13303–13312, 2019.

[84] S. Nair and B. J. Tatarchuk, "Characteristics of sulfur removal by silver-titania adsorbents

at ambient conditions," *Adsorption*, vol. 17, pp. 663–673, 2011.

[85] S. Nair, A. H. M. S. Hussain, and B. J. Tatarchuk, "The role of surface acidity in adsorption of aromatic sulfur heterocycles from fuels," *Fuel*, vol. 105, pp. 695–704, 2013.

[86] A. A. Swat, A. Saleh, S. A. Ganiyu, and M. N. Siddiqui, "Preparation of activated carbon , zinc oxide and nickel oxide composites for potential application in the desulfurization of model diesel fuels," *J. Anal. Appl. Pyrolysis*, vol. 128, pp. 246–256, 2017.

[87] V. S. Marakatti, G. V Shanbhag, and A. B. Halgeri, "Applied Catalysis A : General Sulfated zirconia ; an efficient and reusable acid catalyst for the selective synthesis of 4-phenyl-1 , 3-dioxane by Prins cyclization of styrene," *Appl. Catal. A Gen.*, vol. 451, pp. 71–78, 2013.

[88] Y. Toida, K. Nakamura, and K. Matsumoto, "Adsorptive Desulfurization of Commercial Kerosene with Sulfated Alumina Producing Heavier Organic Sulfur Compounds," *J. Japan Pet. Inst.*, vol. 53, no. 6, pp. 342–350, 2010.

[89] M. K. Nazal, M. Khaled, M. A. Atieh, I. H. Aljundi, G. A. Oweimreen, and A. M. Abulkibash, "The nature and kinetics of the adsorption of dibenzothiophene in model diesel fuel on carbonaceous materials loaded with aluminum oxide particles," *Arab. J. Chem.*, vol. 12, no. 8, pp. 3678–3691, 2019.

[90] S. Kumar, V. Chandra, and R. P. Badoni, "Studies on adsorptive desulfurization by zirconia based adsorbents," *Fuel*, vol. 90, no. 11, pp. 3209–3216, 2011.

[91] A. Srivastav and V. C. Srivastava, "Adsorptive desulfurization by activated alumina," vol. 170, pp. 1133–1140, 2009.

[92] X. U. Cheng-zhi, Z. Mei-qin, C. Keng, H. U. Hui, and C. Xiao-hui, "CeO x doping on a TiO 2 -SiO 2 supporter enhances Ag based adsorptive desulfurization for diesel," *J. Fuel Chem. Technol.*, vol. 44, no. 8, pp. 943–953, 2016.

[93] K. X. Lee and J. A. Valla, "Investigation of metal-exchanged mesoporous Y zeolites for the adsorptive desulfurization of liquid fuels," *Appl. Catal. B, Environ.*, vol. 201, pp. 359–369, 2017.

[94] R. V. Sales *et al.*, "Experimental and theoretical study of adsorptive interactions in diesel fuel Experimental and theoretical study of adsorptive interactions in diesel fuel desulfurization over Ag / MCM ‑ 41 adsorbent," *Adsorption*, no. November, pp. 1–14, 2019.

[95] X. Zhang, Z. Wang, Y. Feng, Y. Zhong, J. Liao, and Y. Wang, "Adsorptive desulfurization from the model fuels by functionalized UiO- 66 (Zr)," *Fuel*, vol. 234, no. February, pp. 256–262, 2018.

[96] D. Iruretagoyena *et al.*, "Enhanced selective adsorption desulfurization on CO2 and steam treated activated carbons : Equilibria and kinetics," *Chem. Eng. J.*, vol. 379, no. March 2019, p. 122356, 2020.

[97] A. A. Olajire, J. J. Abidemi, A. Lateef, and N. U. Benson, "Adsorptive desulphuirization of model oil by Ag nanoparticles-modified activated carbon prepared from brewer's spent grains," *J. Environ. Chem. Eng.*, vol. 5, no. 1, pp. 147–159, 2017.

[98] L. Fan, X. Jiang, W. Jiang, J. Guo, and J. Chen, "Physicochemical properties and desulfurization activities of metal oxide / biomass-based activated carbons prepared by blending method," *Adsorption*, vol. Published, pp. 1–10, 2014.

[99] D. S. Aribike, M. A. Usman, and M. M. Oloruntoba, "Adsorptive desulfurization of diesel using activated sewage sludge : kinetics , equilibrium and thermodynamics studies," *Appl. Petrochemical Res.*, vol. 10, no. 1, pp. 1–12, 2020.

[100] L. Duan *et al.*, "Adsorption , Co-adsorption , and Reactions of Sulfur Compounds , Aromatics , Ole fi ns over Ce-Exchanged Y Zeolite," *ACS J. Phys. Chem.*, vol. 116, p. 25748−25756, 2012.

[101] M. Maes *et al.*, "Selective Removal of N-Heterocyclic Aromatic Contaminants from Fuels by Lewis Acidic Metal – Organic Frameworks **," *Commun. Angew. Chemie Int. Ed.*, vol. 50, pp. 4210–4214, 2011.

[102] R. G. Pearson, "Hard and Soft Acids and Bases," *J. Am. Chem. Soc.*, vol. 265, no. 3, 1963.

[103] R. G. Pearson, "Absolute Electronegativity and Hardness: Application to Inorganic Chemistry," *ACS Inorg. Chem.*, vol. 27, pp. 734–740, 1988.

[104] J. Portier, G. Campet, and J. Etourneau, "A simple model for the estimation of electronegativities of cations in different electronic states and coordinations," *J. Alloys Compd.*, vol. 209, pp. 285–289, 1994.

[105] J. Portier, "A simple approach to materials design: role played by an ionic-covalent parameter based on polarizing power and electronegativity," *J. Alloys Compd.*, vol. 209, pp. 59–64, 1994.

[106] E. Bordes-Richard and P. Courtine, "Optical basicity: a scale of acidity/basicity of solids and its application to oxidation catalysis.," *Met. Oxides Chem. Appl.*, vol. 108, no. January, pp. 319–352, 2006.

[107] A. Lebouteiller and P. Courtine, "Improvement of a Bulk Optical Basicity Table for Oxidic Systems to give stable combinations according to the reaction," *J. Solid State Chem.*, vol. 103, no. 137, pp. 94–103, 1998.

[108] M. Lenglet and F. Hochu, "Correlation Between Ionic-Covalent Parameters and Infrared Spectroscopic Data in II-III Transition Metal Spinel-Type Oxides," *Mater. Res. Bull.*, vol. 32, no. 7, pp. 863–872, 1997.

[109] V. Fierro, V. Torne-Ferna´ndez, D. Montane, and A. Celzard, "Adsorption of phenol onto activated carbons having different textural and surface properties," *Microporous Mesoporous Mater.*, vol. 111, pp. 276–284, 2008.

[110] W. . Weber and J. . Morris, "Kinetics of adsorption on carbon from solution," *J. Sanit. Eng. Div.*, vol. 89, no. 2, pp. 31–60, 1963.

[111] L. Fei, J. Rui, R. Wang, Y. Lu, and X. Yang, "Equilibrium and kinetic studies on the adsorption of thiophene and benzothiophene onto NiCeY zeolites," *RSC Adv.*, no. 7, pp. 23011–23020, 2017.

[112] R. G. Parr and R. G. Pearson, "Absolute Hardness : Companion Parameter to Absolute

Electronegativity," *J. Am. Chem. Soc.*, vol. 105, pp. 7512–7516, 1983.

[113] E. Bordes-Richard and P. Courtine, "Optical basicity: a scale of acidity/basicity of solids and its application to oxidation catalysis.," *Met. Oxides Chem. Appl.*, vol. 108, no. January 2006, pp. 319–352, 2006.

[114] B. Y. R. D. Shannon, M. H, N. H. Baur, O. H. Gibbs, M. Eu, and V. Cu, "Revised Effective Ionic Radii and Systematic Studies of Interatomie Distances in Halides and Chaleogenides," *Acta Crystallogr. A*, vol. 32, no. 5, pp. 751–767, 1976.

[115] H. Patel, "Fixed-bed column adsorption study: a comprehensive review," *Appl. Water Sci.*, vol. 9, no. 3, pp. 1–17, 2019.

[116] R. J. Hunt and W. P. Johnson, "Pathogen transport in groundwater systems : contrasts with traditional solute transport," *Hydrogeol. Hum. Heal.*, no. December, pp. 1–11, 2016.

[117] L. I. Li-da, X. U. Cheng-zhi, Z. Mei-qin, and C. Xiao-hui, "Effect of B 2 O 3 modified Ag / TiO 2 -Al 2 O 3 adsorbents on the adsorption desulfurization of diesel," *J. Fuel Chem. Technol.*, vol. 43, no. 8, pp. 990–997, 2015.

[118] V. Ramakrishnan, H. Kim, J. Park, and B. Yang, "RSC Advances as a photoanode with enhanced visible light," *RSC Adv.*, no. 3, pp. 9789–9795, 2016.

[119] B. Sone, M. Elayaperumal, A. Gurib-Fakim, and M. Maaza, "Single-phase α -Cr 2 O 3 nanoparticles ' green synthesis using Callistemon viminalis ' red flower extract," *Green Chem. Lett. Rev.*, vol. 9, no. 2, pp. 85–90, 2016.

[120] Z. Lin, D. Han, and S. Li, "Study on thermal decomposition of copper (II) acetate monohydrate in air," *J. Therm. Anal. Calorim.*, vol. 107, pp. 471–475, 2012.

[121] M. R. Bodke, Y. Purushotham, B. N. Dole, and A. Materials, "Comparative study on zinc oxide nanocrystals synthesized by two precipitation methods," *Ceramica*, vol. 64, pp. 91–96, 2018.

[122] I. E. Wachs, "Raman and IR studies of surface metal oxide species on oxide supports:

Supported metal oxide catalysts," 1996.

[123] H. Song, Y. Chang, and H. Song, "Deep adsorptive desulfurization over Cu , Ce bimetal ion-exchanged Y-typed molecule sieve," *Adsorption*, no. December, pp. 139–150, 2015.

[124] H. Song, X. Wan, M. Dai, J. Zhang, F. Li, and H. Song, "Deep desulfurization of model gasoline by selective adsorption over Cu – Ce bimetal ion-exchanged Y zeolite," *Fuel Process. Technol.*, vol. 116, pp. 52–62, 2013.

[125] L. L. Mguni, Y. Yao, T. Nkomzwayo, X. Liu, and D. Glasser, "Desulphurization of diesel fuels using intermediate Lewis acids loaded on activated charcoal and alumina activated charcoal and alumina," *Chem. Eng. Commun.*, vol. 206, no. 5, pp. 572–580, 2018.

[126] F. C. Jentoft, "Solid Acids and Bases," in *Comprehensive Inorganic Chemistry II*, Elsevier Ltd., 2013, pp. 205–230.

[127] H. H. Kung, *TRANSITION METAL OXIDES: Surface Chemistry and Catalysis*, 45th ed. E LS EVI E R, 1989.

[128] J. R. Smyth and D. L. Bish, *Crystal Structures and Cation Sites of the Rock-Forming Minerals*, 1st ed., no. May. Boston, 2014.

[129] D. A. Tompsett, S. C. Parker, and M. S. Islam, "Surface properties of a-MnO2: relevance to catalytic and supercapacitor behaviour," *J. Mater. Chem. A Mater. energy Sustain.*, pp. 1–10, 2014.

[130] R. P. G. Gonçalves, H. A. De Abreu, and H. A. Duarte, "Stability , Structural and Electronic Properties of Hausmannite (Mn3 O4) Surfaces and Their Interaction with Water," *ACS J. Phys. Chem.*, vol. 122, no. 36, pp. 20841–20849, 2018.

[131] R. M. Cornell and U. Schwertmann, *The Iron Oxides: Structure, Properties, Reactions, Occurances and Uses*, 2nd ed. Wiley-VCH, 2003.

[132] R. A. P. Ribeiro, S. R. De Lazaro, L. Gracia, E. Longo, and J. Andrés, "Theoretical approach for determining the relation between the morphology and surface magnetism of Co3O4," *J.*

Magn. Magn. Mater., vol. 453, pp. 262–267, 2018.

[133] Y. F. Nishimura, Y. Kondo, and H. Oka, "Estimation of the average oxidation number of nickel in a nickel oxide based on local structural information," *J. Power Sources*, vol. 446, no. September 2019, p. 227351, 2020.

[134] P. N. . Amaniampong, Q. T. Trinh, B. Wang, A. Borgna, Y. Yang, and S. H. Mushrif, "Supporting Information Biomass Oxidation : Formyl C À H Bond Activation by the Surface Lattice Oxygen of Regenerative CuO Nanoleaves," *Angew. Chemie Int. Ed.*, no. June, pp. 1–17, 2015.

[135] M. A. Safa, R. Bouresli, R. Al-majren, T. Al-shamary, and X. Ma, "Oxidative desulfurization kinetics of refractory sulfur compounds in hydrotreated middle distillates," *Fuel*, vol. 239, no. September 2018, pp. 24–31, 2019.

[136] G. Estephane, C. Lancelot, P. Blanchard, J. Toufaily, T. Hamiyeb, and C. Lamonier, "Sulfur compounds reactivity in the ODS of model and real feeds on W – SBA based catalysts †," *RSC Adv.*, vol. 8, pp. 13714–13721, 2018.

[137] K. A. Abu Safieh, Y. S. Al-Degs, M. S. Sunjuk, A. I. Saleh, and M. A. Al-Ghouti, "Selective removal of dibenzothiophene from commercial diesel using manganese dioxide-modified activated carbon: A kinetic study," *Environ. Technol. (United Kingdom)*, vol. 36, no. 1, pp. 98–105, 2015.

[138] A. Saleh, "Simultaneous adsorptive desulfurization of diesel fuel over bimetallic nanoparticles loaded on activated carbon," *J. Clean. Prod.*, vol. 172, pp. 2123–2132, 2018.

[139] B. I. Olu-owolabi, P. N. Diagboya, and K. O. Adebowale, "Evaluation of pyrene sorption e desorption on tropical soils," *J. Environ. Manage.*, vol. 137, pp. 1–9, 2014.

[140] R. Yang, R. Gao, Z. Qian, and Y. Wang, "Batch and fixed bed column selective adsorption of C6 , C8 and C10 linear α - olefins from binary liquid olefin / paraffin mixtures onto 5A and 13X microporous molecular sieves," *Sep. Purif. Technol.*, vol. 230, no. July 2019, p. 115884, 2020.

[141] M. Trgo, N. Vukojevi, and J. Peri, "Application of mathematical empirical models to dynamic removal of lead on natural zeolite clinoptilolite in a fixed bed column," *Indian J. Chem. Technol.*, vol. 18, no. March, pp. 123–131, 2011.

[142] J. Xiao, X. Wang, M. Fujii, Q. Yang, and C. Song, "A Novel Approach for Ultra-Deep Adsorptive Desulfurization of Diesel Fuel over TiO 2 – CeO 2 /MCM-48 under Ambient Conditions," *AIChE Lett. Sep. Mater. Devices Process.*, vol. 59, no. 5, pp. 1441–1445, 2013.

[143] X. Ren, G. Miao, Z. Xiao, F. Ye, and Z. Li, "Catalytic adsorptive desulfurization of model diesel fuel using TiO 2 / SBA-15 under mild conditions," *FUEL*, vol. 174, pp. 118–125, 2016.

[144] J. Zhang, G. Wang, and W. Wang, "Effect of calcination temperature on desulfurization performance over Mn x O y supported on MCM-41 at low temperatures," *Res. Chem. Intermed.*, vol. 42, no. 6, pp. 6003–6012, 2016.

[145] G. I. Danmaliki, T. A. Saleh, and A. A. Shamsuddeen, "Response Surface Methodology Optimization of Adsorptive Desulfurization on Nickel / Activated Carbon," *Chem. Eng. J.*, no. February, 2017.

[146] X. Ma, M. Sprague, and C. Song, "Deep Desulfurization of Gasoline by Selective Adsorption over Nickel-Based Adsorbent for Fuel Cell Applications," *Ind. Eng. Chem. Res.*, vol. 44, no. 15, pp. 5768–5775, 2005.

[147] S. Aslam, F. Subhan, Z. Yan, U. J. Etim, and J. Zeng, "Dispersion of nickel nanoparticles in the cages of metal-organic framework : An efficient sorbent for adsorptive removal of thiophene," *Chem. Eng. J.*, vol. 315, pp. 469–480, 2017.

[148] H. Li *et al.*, "Competitive adsorption desulfurization performance over K – Doped NiY zeolite," *J. Colloid Interface Sci.*, vol. 483, pp. 102–108, 2016.

[149] R. Mahmoudi and C. Falamaki, "Ni 2 + -ion-exchanged dealuminated clinoptilolite : A superior adsorbent for deep desulfurization," *FUEL*, vol. 173, pp. 277–284, 2016.

[150] S. Rashidi, M. Reza, K. Nikou, and B. Anvaripour, "Microporous and Mesoporous

Materials Adsorptive desulfurization and denitrogenation of model fuel using HPW and NiO-HPW modi fi ed aluminosilicate mesostructures," *Microporous Mesoporous Mater.*, vol. 211, pp. 134–141, 2015.

[151] Y. Prajapati and N. Verma, "Adsorptive desulfurization of diesel oil using nickel nanoparticle-doped activated carbon beads with / without carbon nanofibers : Effects of adsorbate size and adsorbent texture," *Fuel*, vol. 189, pp. 186–194, 2017.

[152] R. Tovar-Gomez, M. R. Moreno-virgen, J. Moreno-perez, V. Hernandez-montoya, A. Bonilla-petriciolet, and C. Duran-Valle, "Analysis of synergistic and antagonistic adsorption of heavy metals and acid blue 25 on activated carbon from ternary systems of heavy metals and acid blue 25 on activated from ternary systems," *Chem. Eng. Res. Des.*, vol. 93, pp. 755–772, 2015.

[153] S. K. Thaligari, V. C. Srivastava, and B. Prasad, "Binary Isotherm Modeling for Simultaneous Desulfurization and Denitrogenation of Model Fuel by Zinc Loaded Activated Carbon," *Int. J. Chem. React. Eng.*, vol. 15, no. 3, 2017.

[154] S. A. Al-jlil and M. S. Latif, "Evaluation of equilibrium isotherm models for the adsorption of Cu and Ni from waste water on bentonite clay," *Mater. Technol.*, vol. 47, no. 4, pp. 481–486, 2013.

[155] C. R. Girish, "Various isotherm models for multicomponent adsorption: a review," *Int. J. Civ. Eng. Technol.*, vol. 8, no. 10, pp. 80–86, 2017.

[156] L. Remenárová, M. Pipíška, M. Horník, and J. Augustín, "Biosorption of cationic dyes BY1, BY2 from binary solutions," *Nov. Biotechnol.*, vol. 9, no. 3, pp. 239–247, 2009.

[157] T. F. Hassanein and B. Koumanova, "Binary mixture sorption of basic dyes onto wheat straw," *Bulg. Chem. Commun.*, vol. 44, no. 2, pp. 131–138, 2012.

[158] P. Saha and S. Chowdhury, "Insight Into Adsorption Thermodynamics," in *Thermodynamics*, P. M. Tadashi, Ed. InTech, 2011, pp. 349–364.

[159] M. L. Samaniego, M. D. G. De Luna, D. C. Ong, M. Wan, and M. Lu, "Isotherm and

Thermodynamic Studies on the Removal of Sulfur from Diesel Fuel by Mixing-Assisted Oxidative − Adsorptive Desulfurization Technology," *Energy & Fuels*, vol. 33, pp. 1098–1105, 2019.

[160] M. Mafra, L. Igarashi-Mafra, D. Zuim, E. Vasques, and M. Ferreira, "Adsorption of Remazol Brilliant Blue on an orange peel adsorbent," *Brazilian J. Chem. Eng.*, vol. 30, no. 03, pp. 657–665, 2013.

[161] B. Adane, K. Siraj, and N. Meka, "Kinetic , equilibrium and thermodynamic study of 2-chlorophenol adsorption onto Ricinus communis pericarp activated carbon from aqueous solutions," *Green Chem. Lett. Rev.*, vol. 8, no. 3–4, pp. 1–12, 2015.

[162] A. Rahdar, M. Aliahmad, and Y. Azizi, "NiO Nanoparticles: Synthesis and Characterization," *J. Nanostructures*, vol. 5, pp. 145–151, 2015.

[163] W. Y. Dan, J. F. Li, X. C. Tu, and K. Le Jia, "Preparation and Characterization of NiO Nanoparticles through Thermal Decomposition of Bis(glycinato)Nickel(II)dihydrate," *Adv. Mater. Res.*, vol. 601, pp. 21–25, 2012.

[164] T. Thanh, L. Dang, and M. Tonezzer, "Polycrystalline NiO nanowires : scalable growth and ethanol sensing," *Procedia Eng.*, vol. 120, pp. 427–434, 2015.

[165] Y. Zhu *et al.*, "Self-assembled Ni/NiO/RGO heterostructures for high-performance supercapacitor," *RSC Adv.*, vol. 5, no. September, pp. 77958–77964, 2015.

[166] B. Stuart, *Infared Spectroscopy: Fundametals and Applications*. Wiley, 2004.

[167] G. Korotcenkov, S. Do Han, B. Cho, and V. Tolstoy, "Structural characterization and phase transformations in metal oxide films synthesized by Successive Ionic Layer Deposition (SILD) method," *Process. Appl. Ceram.*, vol. 3, pp. 1–10, 2009.

[168] I. E. Wachs, "Infrared spectroscopy of supported metal oxide catalysts," *Colloids Surfaces A Physicochem. Engineeering Asp.*, vol. 105, no. 1, pp. 143–149, 1995.

[169] S. A. Ganiyu *et al.*, "Influence of aluminium impregnation on activated carbon for enhanced

desulfurization of DBT at ambient temperature : Role of surface acidity and textural properties," *Chem. Eng. J.*, vol. 303, pp. 489–500, 2016.

[170] G. I. Danmaliki and T. A. Saleh, "Effects of bimetallic Ce / Fe nanoparticles on the desulfurization of thiophenes using activated carbon," *Chem. Eng. J.*, vol. 307, pp. 914–927, 2017.

[171] S. S. Shah, I. Ahmad, and W. Ahmad, "Adsorptive desulphurization study of liquid fuels using Tin (Sn) impregnated activated charcoal," *J. Hazard. Mater.*, vol. 304, pp. 205–213, 2016.

[172] M. A. Al-ghouti, Y. S. Al-degs, and F. I. Khalili, "Minimisation of organosulphur compounds by activated carbon from commercial diesel fuel : Mechanistic study," *Chem. Eng. J.*, vol. 162, no. 2, pp. 669–676, 2010.

[173] O. Van Rheinberg, K. Lucka, and H. Köhne, "About the process improvement of adsorptive desulphurisation by adding hydrogen donators as additives in liquid fuels," *J. Power Sources*, vol. 196, no. 21, pp. 8983–8993, 2011.

[174] J. He, S. Hong, L. Zhang, F. Gan, and Y. Ho, "Equilibrium and thermodyamic parameters of adsorption of methylene blue onto rectorite," *Fresenius Environ. Bull.*, vol. 19, no. 11, pp. 2651–2656, 2010.

Appendices

A detailed description of the experimental methods used in Chapters 4 and 5 is provided in this section. In addition, the supplementary data for these chapters is also provided.

A. Experimental design

A.1 Adsorbent metal loading

An illustration of the calculation used to obtain 10 weight % metal loading Ni is shown below:

$$\frac{\text{10\% metal required}}{\text{100\% total adsorbent}} \times 30\text{g total adsorbent} = 3\text{g Ni (required)} \qquad \text{(A-1)}$$

$$\text{Ni}(CH_3CO_2)_2 \cdot 4H_2O \text{ required (g)} = 3\text{g Ni} \times \frac{\text{Mm Ni}(CH_3CO_2)_2 \cdot 4H_2O}{\text{Mm Ni}}$$

$$= 3\text{g Ni} \times \frac{248.84 \ \frac{\text{g}}{\text{mol}}}{58.6934 \ \frac{\text{g}}{\text{mol}}}$$

$$\text{Ni}(CH_3CO_2)_2 \cdot 4H_2O \text{ required} = 12.7189 \text{ (g)}$$

A.2 Experimental Layout Group 1: ADS of model and commercial diesel using AC loaded with metal oxides

In the first set of experiments (Group 1) the ADS of model diesel M1 was carried out using unmodified AC as well as the AC loaded with metal oxides (Ni-oxide, Cu-oxide, Fe-oxide, Zn-oxide, Co-oxide, Mn-oxide, Cr-oxide). Thereafter, the ADS of commercial diesel was carried out using unmodified AC as well as the AC loaded with metal oxides (Ni-oxide, Cu-oxide, Fe-oxide, Zn-oxide, Co-oxide, Mn-oxide, Cr-oxide) to investigate the effects of contact time and adsorption kinetics. Finally, fixed bed desulfurization experiment of diesel were carried out using unmodified AC and metal oxide/AC that had the highest desulfurization performance, in order to compare how the incorporation of the metal oxide effected the breakthrough and saturation points of steric sulfur compounds in the commercial diesel.

Run 1: ADS of model diesel M1 at high and low temperatures.

1. Firstly, 30 g of either model diesel M1 was added into a 3-neck round-bottom flask that as submerged in a water bath and heated to the desired temperature of either 30 °C or 60 °C using a heated magnetic stirrer, equip with a temperature controlling thermocouple.

2. Then 3 g of adsorbent, either unmodified AC or AC loaded with metal oxides of Ni, Cu, Fe, Zn, Co, Mn, Cr (10 wt. % metal) were carefully added into the diesel.

3. The adsorbent/fuel mixture was stirred at 1200 rpm for 3 hours experiments.

4. Treated diesel samples were collected at the following time intervals: 0, 15, 30, 45, 60, 90, 120, 150 and 180 minutes.

5. Each sample was centrifuged to remove any residual adsorbent suspended in the diesel, and placed in a labeled sample vial.

6. Each samples was then injected into GC into a GC to analyse its sulfur concentration.

Run 2: ADS of commercial diesel at low temperatures.

1. Firstly, 30 g of commercial diesel fuel was added into a 3-neck round-bottom flask that as submerged in a water bath and heated to 30 °C using a heated magnetic stirrer, equip with a temperature controlling thermocouple.

2. Then 3 g of adsorbent, either unmodified AC or AC loaded with metal oxides of Ni, Cu, Fe, Zn, Co, Mn, Cr (10 wt. % metal) were carefully added into the diesel.

3. The adsorbent/fuel mixture was stirred at 1200 rpm for 3 hours experiments.

4. Treated diesel samples were collected at the following time intervals: 0, 15, 30, 45, 60, 90, 120, 150 and 180 minutes.

5. Each sample was centrifuged to remove any residual adsorbent suspended in the diesel, and placed in a labeled sample vial.

6. Each samples was then injected into GC into a GC to analyse its sulfur concentration.

Run 4: ADS of commercial diesel using fixed-bed system

1. The ADS of the model diesel M1 and commercial diesel using unmodified AC and metal oxide/AC that had the highest desulfurization performance in the previous experiments was carried out at ambient temperature and pressure.

2. Each adsorbent was packed in a glass column having a bed dimension of 1.5 mm I.D. and 400 mm length. Where the adsorbent bed length was fixed at 110 mm.

3. Prior to introducing the diesel fuel into the adsorbent bed, the adsorbent bed was treated with n-hexadecane.

4. The diesel fuel was pumped (it's a peristaltic pump-get model form lab) through the adsorbent bed at a liquid hourly space velocity (LHSV) of 0.617 h^{-1}.

5. The treated diesel samples were collected for analysis at time intervals of: 0, 15, 30, 45, 60, 90, 120, 150, 180, 240, 300, 360 and 420 minutes.

6. Each sample was centrifuged to remove any residual adsorbent suspended in the diesel, and placed in a labeled sample vial.

7. The residual sulfur concentration of the samples was the analysed using a G.C.

A.3 Experimental Layout Group 2: ADS of model diesel carried out using highest performance metal oxide adsorbent.

The second part of the experimental work looked at investigating how the loading a metal oxide onto AC would affect the mechanisms of adsorption process. This was achieved by comparing the desulfurization performance of AC to that of the metal oxide/AC that had the highest desulfurization performance in the previous Group 1 experiments.

A3.1 Section 1: Effects of metal loading and adsorbent dosage

Run 1: Effect of metal loading

1. Prior to each experiment the AC and AC loaded with metal oxide (2.5, 5, 10 and 15 wt. % metal) adsorbent were first heated up to 30°C.

2. 30 g of model diesel M1 was added into a 3-neck round-bottom flask that as submerged in a water bath and heated to 30 °C, using a heated magnetic stirrer, equip with a temperature controlling thermocouple.

3. Then 3 g of adsorbent was added into the diesel fuel.

4. The adsorbent/fuel mixture was stirred at 1200 rpm for 3 hours experiments.

5. Treated diesel samples were collected at the following time intervals: 0, 15, 30, 45, 60, 90, 120, 150 and 180 minutes.

6. Each sample was centrifuged to remove any residual adsorbent suspended in the diesel, and placed in a labeled sample vial.

7. Each samples was then injected into a GC to analyse its sulfur concentration.

Run 2: Effect of adsorbent dosage

The procedure is the same as that of run 1 was carried out, wherein this experimental run the optimum metal loading from experimental run 1 was used, keeping the mixing speed and temperature constant at 1200 rpm and 30 °C respectively, while the amount adsorbent loading was changed. Adsorbent loading of 0.75 g, 1.5 g, 2.25 g and 3 g were used.

In the remaining experiments (Sections 2 and 3) the optimum metal loading and adsorbent dosage obtained from Section 1 was used.

A3.2 Section 2: Equilibrium isothermal experiments

Run 1:

1. Individual experiments were carried out using adsorbents AC and metal-oxide/AC at dosages of 0.75, 1.5, 2.25 and 3 grams.

2. Where for each experiment 30 g of model diesel M2 containing all three sulfur compounds (DBT, 4-MDBT and 4,6-DMDBT) was added into a 3-neck round-bottom flask that as submerged in a water bath and heated to 30 °C using a heated magnetic stirrer, equip with a temperature controlling thermocouple.

3. The adsorbent was added into the model diesel and the adsorbent/fuel mixture was stirred at 1200 rpm for 3 hours experiments.

4. Treated diesel samples were collected at the following time intervals: 0, 15, 30, 45, 60, 90, 120, 150 and 180 minutes.

5. Each sample was centrifuged to remove any residual adsorbent suspended in the diesel, and placed in a labeled sample vial.

6. Each samples was then injected into GC into a GC to analyse its sulfur concentration.

Run 2:

Similar to run 1, except model diesel M3 contain only DBT was used.

Run 3:

Similar to run 1, except model diesel M4 contain only 4-MDBT was used.

Run 4:

Similar to run 1, except model diesel M5 contain only 4,6-DMDBT was used.

A3.3 Section 3: Adsorption thermodynamic and kinetic analysis

Run 1:

1. Firstly, 30 g of model diesel M1 was added into a 3-neck round-bottom flask that as submerged in a water bath and heated to 30 °C using a heated magnetic stirrer, equip with a temperature controlling thermocouple.

2. The adsorbent was added into the model diesel and the adsorbent/fuel mixture was stirred at 1200 rpm for 3 hours experiments.

3. Treated diesel samples were collected at the following time intervals: 0, 15, 30, 45, 60, 90, 120, 150 and 180 minutes.

4. Each sample was centrifuged to remove any residual adsorbent suspended in the diesel, and placed in a labeled sample vial.

5. Each samples was then injected into GC into a GC to analyse its sulfur concentration.

Run 2:

Similar to run 1, except an experimental temperature of 45 °C was used.

Run 3:

Similar to run 1, except an experimental temperature of 60 °C was used.

Run 4:

Similar to run 1, except an experimental temperature of 75 °C was used.

B. Supplementary data: Chapter 4

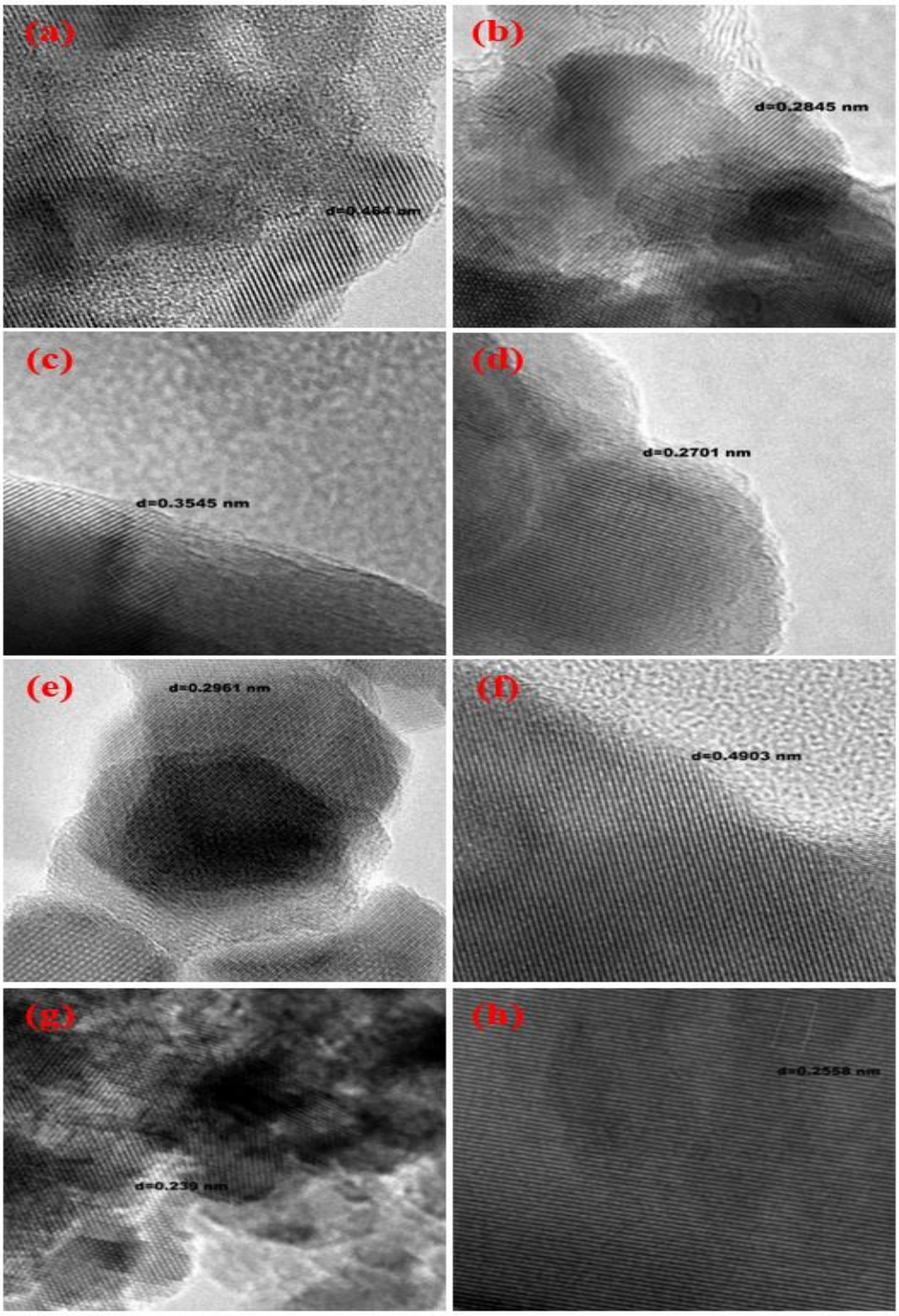

Figure B.1: Lattice-fringe HRTEM images of obtained for (a) AC, (b) Co-oxide/AC, (c) Cr-oxide/AC, (d) Cu-oxide/AC, (e) Fe-oxide/AC, (f) Mn-oxide/AC, (g) Ni-oxide/AC and (h) Zn-oxide/AC.

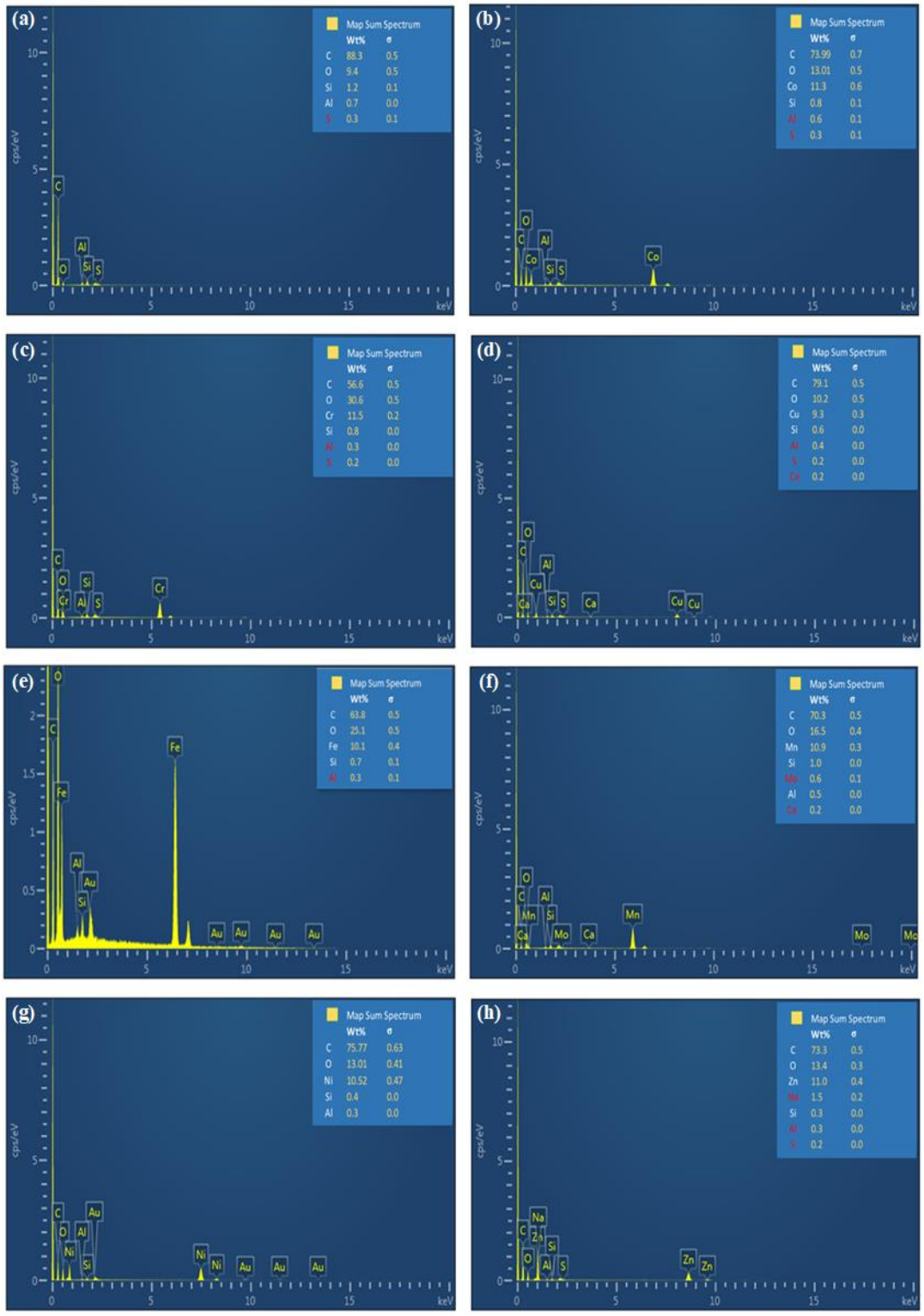

Figure B.2: The elemental analysis and EDS spectrum obtained for (a) AC, (b) Co-oxide/AC, (c) Cr-oxide/AC, (d) Cu-oxide/AC, (e) Fe-oxide/AC, (f) Mn-oxide/AC, (g) Ni-oxide/AC and (h) Zn-oxide/AC.

Table B.1: PXRD qualitative analysis results obtained for desulfurization adsorbents.

Precursor	Metal oxide product	Space group	Lattice parameters					
			a (Å)	b (Å)	c (Å)	α (°)	β (°)	γ (°)
Graphite-2H	–	194 : P63/mmc	2.47	2.47	6.67	90	90	120
Buckminster-fullerene	–	147 : P-3	10.04	10.04	16.01	90	90	120
$Co(C_2O_2H_3)_2 \cdot 4H_2O$	Co_3O_4	227 : Fd-3m	8.10	8.10	8.10	90	90	90
	CoO	12 : C12/m1	5.18	3.016	3.018	90	125.55	90
$Cr(C_2O_2H_3)_7 \cdot (OH)_2$	Cr_2O_3	167 : R-3c	4.95	4.95	13.59	90	90	120
$Cu(C_2O_2H_3)_2 \cdot H_2O$	CuO	15 : C2/c	4.68	3.42	5.13	90	99.54	90
	Cu_2O	224 : Pn-3m	4.29	4.29	4.29	90	90	90
$Fe(C_2O_2H_3)_2$	γ-Fe_2O_3	212 : P4332	8.34	8.34	8.34	90	90	90
$Mn(C_2O_2H_3)_2 \cdot 4H_2O$	Mn_3O_4	141 : I41/amd	5.76	5.76	9.43	90	90	90
	α-MnO_2	87 : I4/m	9.81	9.81	2.84	90	90	90
$Ni(C_2O_2H_3)_2 \cdot 4H_2O$	NiO	225 : Fm-3m	4.17	4.17	4.17	90	90	90
$Zn(C_2O_2H_3)_2 \cdot 2H_2O$	ZnO	186 : P63mc	3.25	3.25	5.20	90	90	120

Table B.2: Structural parameters of MeO/AC adsorbents.

Precursor	Metal oxide product	Crystallite size (nm)	Crystallite weight (%)
$Co(C_2O_2H_3)_2 \cdot 4H_2O$	Co_3O_4	11.89	72
	CoO	11.48	28
$Cr(C_2O_2H_3)_7 \cdot (OH)_2$	Cr_2O_3	30.75	100
$Cu(C_2O_2H_3)_2 \cdot H_2O$	CuO	14.94	83.5
	Cu_2O	15.61	16.5
$Fe(C_2O_2H_3)_2$	γ-Fe_2O_3	4.76	100
$Mn(C_2O_2H_3)_2 \cdot 4H_2O$	Mn_3O_4	10.23	99.91
	α-MnO_2	10.97	0.09
$Ni(C_2O_2H_3)_2 \cdot 4H_2O$	NiO	13.3	100
$Zn(C_2O_2H_3)_2 \cdot 2H_2O$	ZnO	49.2	100

Table B.3: The co-ordination number, spin state, ionic radius and atomic number corrective constant of the adsorbents used on this study.

Adsorbent	MeO	CN	SS	r_i (Å)[a]	α[b]
Zn-oxide/AC	ZnO	4	–	0.6	0.16
Cr-oxide/AC	Cr_2O_3	6	–	0.615	0.12
Mn-oxide/AC	Mn_3O_4	4	HS	0.66	0.15
		6	HS	0.645	0.15
	α-MnO_2	6	–	0.53	0.15
Fe-oxide/AC	γ-Fe_2O_3	4	HS	0.49	0.18
		6	HS	0.645	0.18
Co-oxide/AC	Co_3O_4	4	HS	0.58	0.22
		6	LS	0.545	0.22
	CoO	4	HS	0.58	0.22
Cu-oxide/AC	CuO	4	–	0.57	0.3
	Cu_2O	2	–	0.46	0.3
Ni-oxide/AC	NiO	6	–	0.69	0.24

[a] Data obtained from Shannon [114].

[b] Data obtained from Portier et al. [104], with the permission from Elsevier.

C. Supplementary data: Chapter 5

Table C.1: Pseudo-first order parameters obtained for adsorption in model diesel M1 at varying temperatures.

Compound	Parameter	AC				$Ni_{(10\%)}O$/AC			
		30°C	45°C	60°C	75°C	30°C	45°C	60°C	75°C
DBT	$q_{e\ exp}$ ($mg.g^{-1}$)	0.49	0.6	0.75	0.8	0.93	0.97	1	1.02
	$q_{e\ cal}$ ($mg.g^{-1}$)	0.41	0.59	0.71	0.41	0.71	0.85	0.51	0.36
	k_1 (min^{-1})	0.01	0.02	0.02	0.01	0.02	0.03	0.02	0.02
	R^2	0.956	0.911	0.944	0.914	0.971	0.798	0.89	0.868
4-MDBT	$q_{e\ exp}$ ($mg.g^{-1}$)	0.62	0.67	0.83	0.86	1.01	1.08	1.09	1.096
	$q_{e\ cal}$ ($mg.g^{-1}$)	1.13	0.49	0.66	0.61	0.59	0.64	0.53	0.48
	k_1 (min^{-1})	0.03	0.02	0.02	0.03	0.02	0.02	0.02	0.03
	R^2	0.851	0.979	0.961	0.986	0.898	0.794	0.887	0.856
4,6-DMDBT	$q_{e\ exp}$ ($mg.g^{-1}$)	1.5	1.65	2.1	2.2	2.5	2.78	2.8	2.89
	$q_{e\ cal}$ ($mg.g^{-1}$)	0.74	1	1.72	1.01	2.47	1.92	1.26	0.91
	k_1 (min^{-1})	0.01	0.02	0.02	0.03	0.03	0.03	0.02	0.025
	R^2	0.724	0.931	0.969	0.919	0.957	0.905	0.914	0.838

Table C.2: Pseudo-second order kinetic parameters obtained for model diesel M1 adsorption at varying temperatures.

Compound	Parameter	AC				$Ni_{(10\%)}O$/AC			
		30°C	45°C	60°C	75°C	30°C	45°C	60°C	75°C
DBT	$q_{e\ exp}$ ($mg.g^{-1}$)	0.49	0.6	0.75	0.8	0.93	0.97	1	1.02
	$q_{e\ cal}$ ($mg.g^{-1}$)	0.49	0.62	0.78	0.79	0.95	0.98	1	1.01
	k_2 (min^{-1})	0.12	0.11	0.08	0.569	0.15	0.13	0.19	0.76
	R^2	0.981	0.983	0.986	0.991	0.989	0.994	0.998	0.998
4-MDBT	$q_{e\ exp}$ ($mg.g^{-1}$)	0.618	0.67	0.83	0.86	1.01	1.08	1.09	1.096
	$q_{e\ cal}$ ($mg.g^{-1}$)	0.75	0.69	0.85	0.89	1.01	1.07	1.09	1.1
	k_2 (min^{-1})	0.03	0.1	0.11	0.14	0.06	0.16	0.18	0.31
	R^2	0.868	0.991	0.992	0.996	0.968	0.996	0.998	0.999
4,6-DMDBT	$q_{e\ exp}$ ($mg.g^{-1}$)	1.5	1.65	2.1	2.2	2.5	2.78	2.8	2.89
	$q_{e\ cal}$ ($mg.g^{-1}$)	1.41	1.68	2.17	2.21	2.64	2.82	2.82	2.91
	k_2 (min^{-1})	0.02	0.05	0.04	0.11	0.02	0.04	0.08	0.13
	R^2	0.765	0.994	0.989	0.999	0.989	0.996	0.999	0.999

Table C.3: Intra-particle diffusion parameters obtained for adsorption using model diesel M1 at varying temperatures.

Compound	Parameter	AC				$Ni_{(10\%)}O$/AC			
		30°C	45°C	60°C	75°C	30°C	45°C	60°C	75°C
DBT	k_i ($mg.g^{-1}min^{-0.5}$)	0.03	0.02	0.04	0.04	0.03	0.02	0.12	0.01
	C ($mg.g^{-1}$)	0.14	0.15	0.23	0.45	0.43	0.53	0.58	0.63
	R^2	0.915	0.999	0.975	0.964	0.998	0.994	0.998	0.999
4-MDBT	k_i ($mg.g^{-1}min^{-0.5}$)	0.06	0.05	0.06	0.06	0.01	0.004	0.006	0.006
	C (mg.g-1)	0.01	0.04	0.25	0.41	0.43	0.49	0.57	0.69
	R^2	0.954	0.858	0.979	0.961	0.971	0.946	0.975	0.989
4,6-DMDBT	k_i($mg.g^{-1}min^{-0.5}$)	0.14	0.12	0.16	0.08	0.13	0.02	0.04	0.01
	C (mg.g-1)	0.09	0.17	0.76	1.16	0.58	0.89	0.93	1.59
	R^2	0.871	0.899	0.996	0.865	0.999	0.966	0.992	0.999